INFLUENCE OF BRIDGE PARAMETERS ON FINITE ELEMENT MODELING OF SLAB ON GIRDER BRIDGES

Amey V. Bapat

Thesis submitted to the faculty of the Virginia Polytechnic Institute and State University
in partial fulfillment of the requirements for the degree of

Master of Science
In
Civil Engineering

Elisa D. Sotelino, Chairperson
Carin L.Roberts-Wollmann
Thomas E. Cousins

December 03, 2009
Blacksburg, Va

Keywords: Slab on Girder Bridge, Finite Element Analysis, Static, Dynamic

INFLUENCE OF BRIDGE PARAMETERS ON FINITE ELEMENT MODELING OF SLAB ON GIRDER BRIDGES.

Amey V. Bapat

ABSTRACT

The present study is part of the Long Term Bridge Performance Program (LTBP) funded by the Federal Highway Administration. The objectives of this program are to create a comprehensive database of quantitative information of the long-term performance of selected pilot bridges and to develop a methodology to assess bridge performance. Finite element (FE) modeling of the pilot bridges is an intrinsic part of the LTBP program and is intended to not only assist with instrumentation decisions, but also to provide further insight into the behavior of these bridges, which cannot be achieved solely from field testing of the bridges. This thesis provides a comprehensive study of a plethora of issues associated with the development of reliable and accurate FE models of bridges.

The first objective of this investigation was to develop reliable finite element models with a variety of levels of refinement and to study the effect of the inclusion of various bridge parameters in the model, such as bridge skew, degree of composite action, thermal gradient and level of support restraint, on the response of bridges. First, the suitability of different modeling techniques and of elements used to model the primary bridge components was assessed using simple models for which analytical solutions are readily available. From these studies, it was concluded that shell elements are adequate to model the bridge deck, and beam and shell elements are both satisfactory to model the bridge girders. From the dynamic analyses of theWildcat Creek River Bridge and the Colquitz River Bridge, flexural modes of vibration were found to be highly sensitive to support restraints and to how the guardrails were modeled and less sensitive to the inclusion of bracing and thermal gradients in the model. The finite element models using extreme boundary conditions were successful in bracketing the field response. The factors identified from these analyses were considered in the analysis of the Virginia pilot bridge. Different support restraints, and the inclusion of skew and level of composite action in the model

had noticeable impact on both the static and dynamic responses of the bridge. The results from these analyses were used to assist with instrumentation decisions prior to field-testing. The developed model will also be used to help researchers further understand the bridge's behavior and to help explain a variety of phenomena observed in the field.

ACKNOWLEDGEMENT

First, I would like to thank my parents for their love and encouragement through every step of my life. I would also like to thank my committee. I would like to thank Dr.Sotelino for her guidance and patience. I have learned a lot from you in the past two years. I would also like to thank my other committee members, Dr. Wollmann and Dr. Cousins for their continual advice throughout my research. I would also like to thank FHWA for funding this research. I would like to thank other members on the project for their help. Finally, I would like to thank my family and friends for their continuing support without which this would have not been possible.

Table of Contents

Figures

Table

1 Introduction

1.1 Background

In 2007, out of 590,000 bridges, culverts, and tunnels managed by National Bridge Inventory approximately 152,136 bridges were found to deficient or functionally obsolete (FHWA 2009). This number is likely to grow with increased traffic demands, aging and deterioration of bridges, and limited funds. In response to this the Federal Highway Administration initiated the Long Term Bridge Performance Program (LTBP). The objective of this program is to create a comprehensive database of quantitative information by studying the long term performance of selected pilot bridges and to develop a methodology to assess bridge performance (FHWA 2009). Finite element analysis will play an important role to achieve these objectives. It will provide insight into the behavior of the subject bridges and it will help simulate conditions to which the bridges might be exposed to in the future.

1.2 Objective

The present study focuses on the issues related to the development of reliable finite element models with various levels of refinement. As such, the first objective of the present study is to select appropriate modeling techniques that can accurately predict bridge response with reasonable computational cost. The second objective is to study the effect of including specific bridge parameters in the bridge model on the obtained results. The parameters considered include bridge skew, level of composite action between deck and girders as well as guardrail and deck, and level of support restraint. The final objective of this study is to develop finite element (FE) models with various combinations of the above mentioned parameters to provide insight into the behavior of the first pilot bridge selected for field monitoring as part of the LTBP program and to assist with instrumentation decisions associated with live load and dynamic testing.

1.3 Technical Approach

The first and very important step in the development of a finite element model is the selection of an appropriate modeling technique. Over the years various three-dimensional (3-D) modeling techniques have been used by researchers to idealize bridge geometries. They range from using detailed 3-D solid modeling of all bridge components to using the grillage approach. 3-D solid

modeling is usually only feasible for very small and simple bridges because of the limitations in computer memory and the large amount of computing time that is required for the simulation. The grillage approach, on the other hand, is much less time consuming, but it is a simplification of the actual system. Different researchers have explored several alternative approaches with different levels of complexity that fall between the two extremes mentioned above. It is known that some of these methods introduce geometric errors and incompatibilities, which affect the accuracy of the obtained bridge response. Therefore, the first task of the present study was to perform a thorough evaluation of different modeling techniques. In particular, a study was carried out to understand each technique's ability to accurately predict bridge response and the computational cost associated with it.

The second task involved the investigation of the effect of modeling the different bridge parameters on the obtained results. Field data available in the literature was used to validate the selected modeling techniques. From the analyses performed here, it was found that using shell elements to represent the bridge deck, and a combination of beam or shell elements to represent the bridge girders provided excellent accuracy in the results. The analyses also showed that the way specific parameters are modeled can have a significant impact on the bridge's response. In general, it was observed the finite element models using the extreme conditions were successful in bracketing the solutions obtained in the field.

For the pilot bridge, shell elements were used to model both bridge deck and girders flanges and webs so that the bracing could be accurately included in the model. The bracing components were modeled using beam elements. The results from the analysis aided in the development of a rational plan for field monitoring and instrumentation and it is expected that in the future, the results from field tests will be used further to refine the present finite element model. However, these aspects of the research are not within the scope of the present investigation and are not reported here.

1.4 Organization of Thesis

This thesis has been subdivided into six chapters. The second chapter reviews the previously proposed three-dimensional bridge idealizations for the finite element analysis of bridges and the incompatibilities and geometric errors introduced by them. In the third chapter, the ability of several existing modeling techniques to accurately predict bridge response and the computational

cost associated with them was evaluated. In the fourth chapter, the field data available for Wildcat Creek River Bridge and Colquitz River Bridge were used to validate the modeling techniques discussed in the previous chapter. Furthermore, the effect of explicitly including different aspects of bridge parameters in the finite element model, such as bridge skew, level of support restraints, composite action, temperature gradient, and secondary structural elements, on the obtained results was also investigated. In the fifth chapter, the modeling techniques investigated in the previous chapters were used to predict the static and dynamic response of the Virginia Pilot Bridge RT.15. Finally, the sixth chapter summarizes the important findings and provides recommendations for future research.

2 Literature Review

2.1 Introduction

Over the years different methods have been developed by researchers to analyze bridge superstructures. In practice line girder analysis or grillage analysis are implemented because of the simplicity involved in their use. In the line girder analysis, the bridge girder is analyzed as a one-dimensional beam element and distribution factors are used to calculate the actual shear and moment in the girder. This method does not consider the torsional stiffness of the system. In the two-dimensional grillage analysis, the bridge is idealized into a grid of beams lying in one plane and flexural and torsional stiffness of the beam is calculated using the properties of the girders and deck. The accuracy of the results depends on the effort put into the discretization of system into two-dimensional grid. This method does not consider the effect of shear lag, support location, or interaction between girder and deck slab on the bridge response.

With the advances in computer technology in the last two decades, more sophisticated computational methods, such as the finite element method, have been developed and become more accepted by the profession. Today, many engineers prefer to use three-dimensional finite element analysis over the line girder analysis and grillage analysis because it is able to overcome the limitations imposed by the line girder analysis and grillage analysis. This chapter reviews the previously proposed three-dimensional bridge idealizations for the finite element analysis of bridges. It should be noted that some of these idealizations introduce some geometric errors and incompatibilities in the system, which affect their ability to capture the actual response of the bridge. This chapter surveys various three dimensional bridge idealizations along with the different techniques that have been employed by researchers to overcome the geometric errors and incompatibilities.

2.2 Finite Element Modeling of Bridge Superstructures

Different three dimensional finite element modeling techniques have been used for modeling bridge superstructures. These techniques involve a combination of different types of elements for the different parts of the superstructure. Table 2.1 shows the different types of elements that are often used for the different components of a bridge superstructure. It should be noted that this report does not consider the use of three-dimensional solid elements to model all or most of the

components of bridge superstructures. This is because this type of modeling usually produces meshes with a very high number of degrees of freedom, which makes them impractical with current computing capabilities. Furthermore, usually the additional accuracy obtained when using this modeling technique does not justify the additional computational expense.

Table 2.1: Elements used to model each component of bridge superstructures

Bridge Component	Element Type 1	Element Type 2	Element Type 3
Deck	Solid	Shell	-
Girder	Solid	Shell	Beam
Guardrail	Solid	Shell	Beam
Bracing	-	-	Beam

Hays Jr. et al.(1986) and Mabsout et al. (1997) modeled the deck slab using quadrilateral shell elements with five degrees of freedom per node and the steel girders using three dimensional beam elements with six degrees of freedom per node (Figure 2.1). The bridge deck slab and steel girders shared nodes where steel girder is present. This is essentially a two-dimensional finite element analysis and it is not capable of capturing the effect of the offset between the center of gravity of the steel girder and the center of gravity of the deck slab. Furthermore, it cannot capture the system's actual boundary conditions, i.e., the supports in the actual system are located at the bottom of steel girder rather than at the level as the center of gravity of the deck slab.

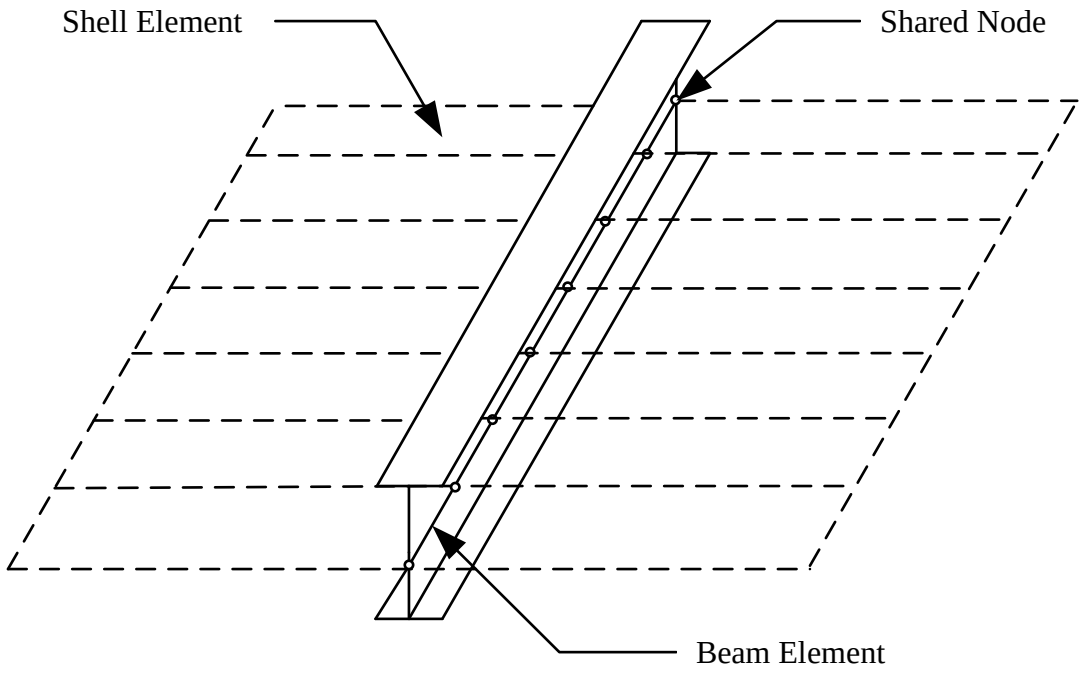

Figure 2.1: Hays Jr. et.al and Mabsout et al. Idealization

Tarhini and Frederick (1992), Mabsout et al. (1997), Eom and Nowak (2001) and Baskar et al. (2002), Queiroz et al(2007) used eight node linear solid brick elements with three displacement degrees of freedom in each node to model the concrete deck. The girders were modeled using quadrilateral shell elements, which contain three displacement and three rotational degrees of freedom per node. (Figure 2.2) The authors did not specify the number of nodes per element. The cross frames were modeled using three-dimensional two-node truss elements with three displacement degrees of freedom per node. In Tarhini and Frederick(1992) full composite action was modeled by imposing no release at the interface nodes at the concrete deck and girders. Queiroz et al.(2007) modeled the longitudinal and transverse reinforcement in the deck slab as a smeared layer of equivalent area in solid brick element.

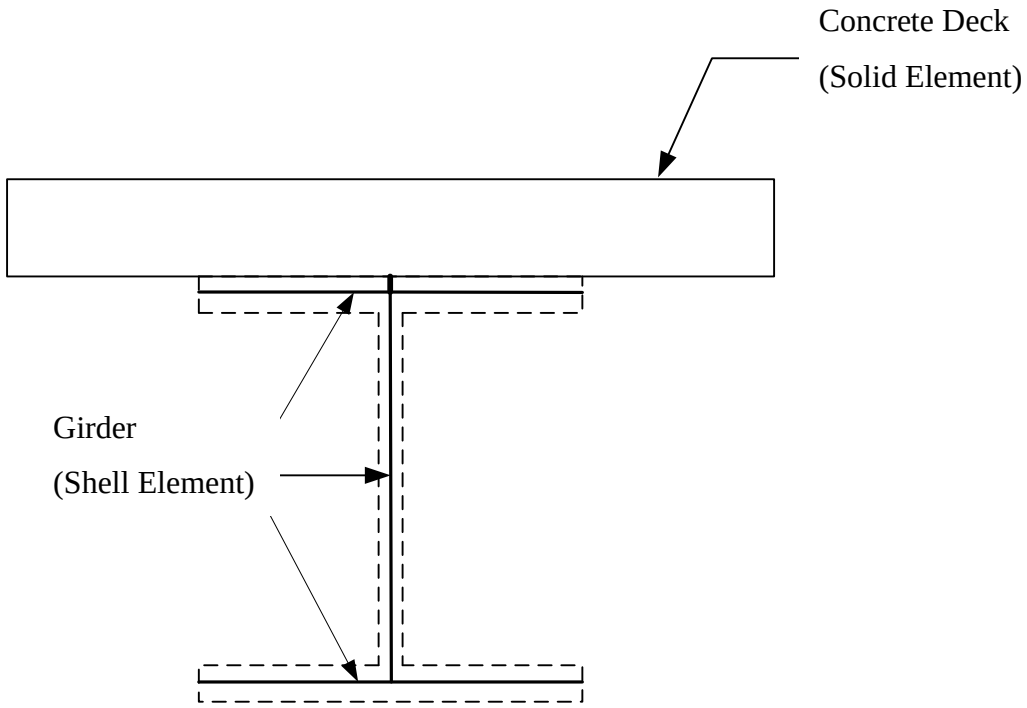

Figure 2.2: Tarhini and Frederick, Tarhini and Mabsout, Wu's Idealization

Wu (2003) also modeled the concrete deck and parapet using twenty node quadratic solid elements with reduced integration to decrease the computational running time. Steel girders were modeled using four node shell elements with reduced integration and transverse shear deformation. Diaphragms were modeled using three-dimensional two-node Timoshenko beam elements with transverse shear deformation. The hinge support was modeled at the bottom flange nodes by constraining all three translational degrees of freedom at one of the support. Roller supports were used to model the remaining supports by constraining only vertical degree of freedom at the bottom flange nodes. In this work, the full composite action between girder and deck was modeled using multi-point constraints. Eamon and Nowak (2004) used a similar modeling technique as Wu (2003) but used hexahedral solid brick elements to model the deck, sidewalk and barriers.

There are number of incompatibilities present in the above models that were not discussed in these references, which can hinder their accuracy. For instance, Tarhini and Frederick (1992) used only one eight node linear solid brick element throughout the thickness of the concrete deck to simulate its flexural behavior. However, it is well known that in order to accurately simulate the flexural behavior of the concrete slab, more linear solid elements are required across the deck

cross section. Furthermore, the adopted eight node three-dimensional solid brick element used to model the bridge deck has linear shape functions and no rotational degrees of freedom, while the quadrilateral shell elements used to model the girder flanges and web are based on quadratic shape functions and contains rotational degrees of freedom. This type of incompatibility can cause gaps or overlap to form between the two types of elements. Another incompatibility also exists between the in-plane rotational degree of freedom of the shell elements used to model the flanges and the drilling degree of freedom of the shell elements used to model the girder web. In their papers, Tarhini and Frederick (1992), Wu (2003) and Eom and Nowak (2001) did not discuss the methods employed to overcome these incompatibilities.

Eom and Nowak (2001) modeled support conditions using three different methods for a simply supported bridge to evaluate the effect of support on live load distribution factors. In the first method a hinge support was used at one end and a roller support was used at the other end. In the second method hinge supports were adopted at both ends. In the third method linear spring elements were used at the top and bottom of the girder flange to model the partial support fixity. Different values can be used for the stiffness of the springs at the top and bottom of the girder flange. For simplicity, Eom and Nowak (2001) used the same values for top and bottom spring stiffness for all supports although the degree of partial support fixity varied from girder to girder. The top and bottom spring stiffness were adjusted to obtain the same strain values as the ones measured during the field test for the girder bottom flange at the mid span.

Tabsh and Tabatabai (2001) and Issa et al. (2000) modeled deck slab using four node rectangular shell elements with six degrees of freedom per node. Each component of the steel girder, i.e., top and bottom flange and web was modeled separately. The top and the bottom flanges were idealized as two-node beam elements with six degrees of freedom per node. The steel web was idealized using four-node rectangular shell elements and the cross frames were idealized using two-node beam elements. Rigid beam elements were used to model the full composite action between the concrete deck and steel girders as shown in Figure 2.3. Bishara et al. (1993) used a similar modeling technique to model the girders but they used three-node linear triangular plate elements to model the deck slab. Machado et al. (2008) also used four-node rectangular shell elements with six degrees of freedom per node, to model the bridge deck. However, the top

flange, bottom flange and the web of the steel girder were modeled using two node three-dimensional Euler beam elements.

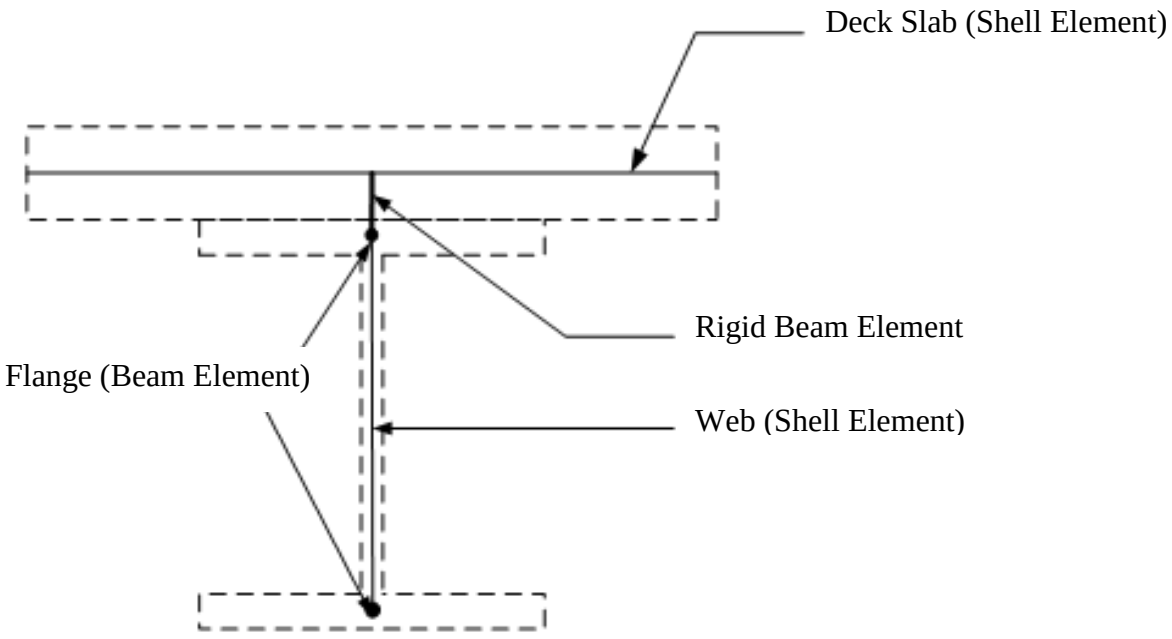

Figure 2.3: Tabsh and Tabatabai Idealization of Deck Slab and Girder

Fu and Lu (2003) idealized bridge deck with isoparametric quadrilateral shell elements and the reinforcement was modeled as a smeared two-dimensional membrane layer with isoparametric plane stress element. The girders were discretized into flanges and web. The flanges were modeled using eight-node plate elements and web by eight-node plane stress elements. This modeling selection clearly generates an incompatibility at the flange and web connection. However, the authors did not discuss this issue or its potential effect on the results. The shear studs were modeled using bar elements (Figure 2.4). Non-linear finite element analysis was carried out to plot the deflected shape of a two span continuous bridge subjected to a point load applied at the midpoint of each span. The finite element analysis results showed good correlation with the experimental results as compared to deflections calculated using transformed area method.

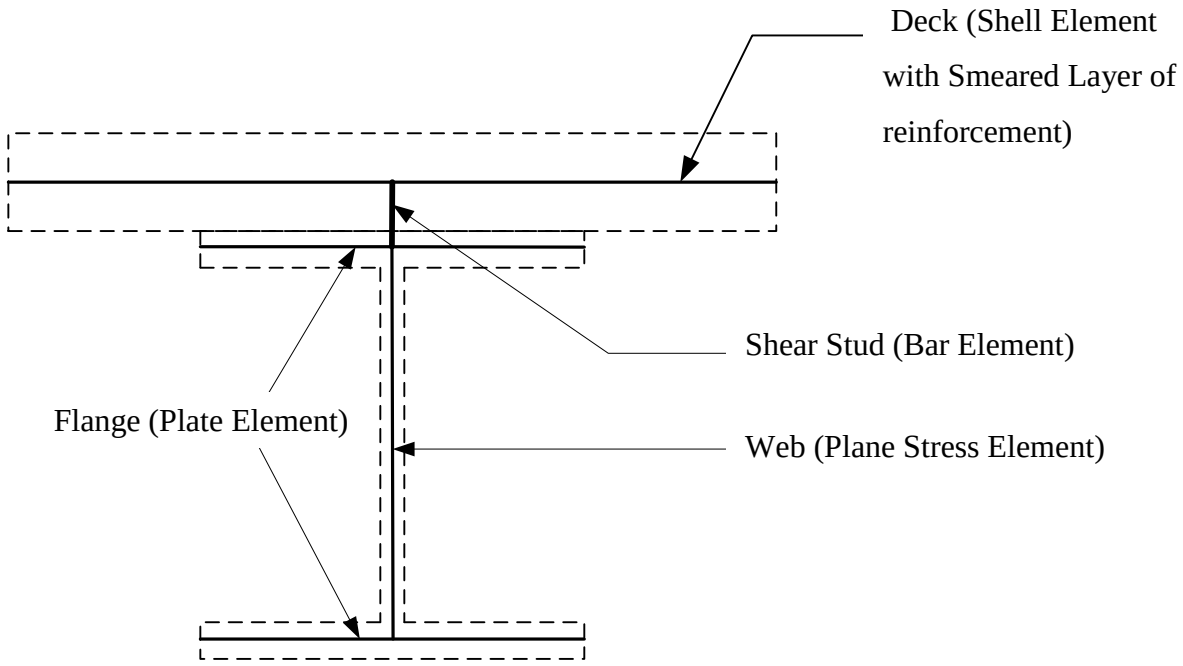

Figure 2.4: Fu and Lu Idealization

Wolek et al.(1996) modeled the slab, girders and diaphragms using three-dimensional eight-node quadratic shell elements. The shell elements representing the part close to the edge of the bridge deck were modeled with increased specific weight to account for the dead load of the guardrail. However, the stiffness provided by the guardrail is not included in the model. The girder web was directly connected to the slab and the upper flange of the girder was not considered in the model to reduce the computational cost. The modulus of elasticity of the concrete was increased to account for the presence of the girder top flange and the slab reinforcement. Two eight-node layered quadratic shell elements were used to model the deck where girders are present as shown in Figure 2.5. The top two layers were non-structural layers and were assigned with a low Young's modulus so that they did not add any stiffness to the structure. The middle layer was assigned the same properties as those of the concrete deck and it was placed in the same plane as that of other shell elements used to model bridge deck. The fourth layer was assigned with the properties of the concrete haunch and its width could be increased or decreased to change the interface stiffness. The bottom most layer was assigned with the same properties as the top flange. The modulus of elasticity of diaphragms was modified from 30,000 ksi to 9200 ksi so that first transverse bending mode of the bridge would match the experimental results.

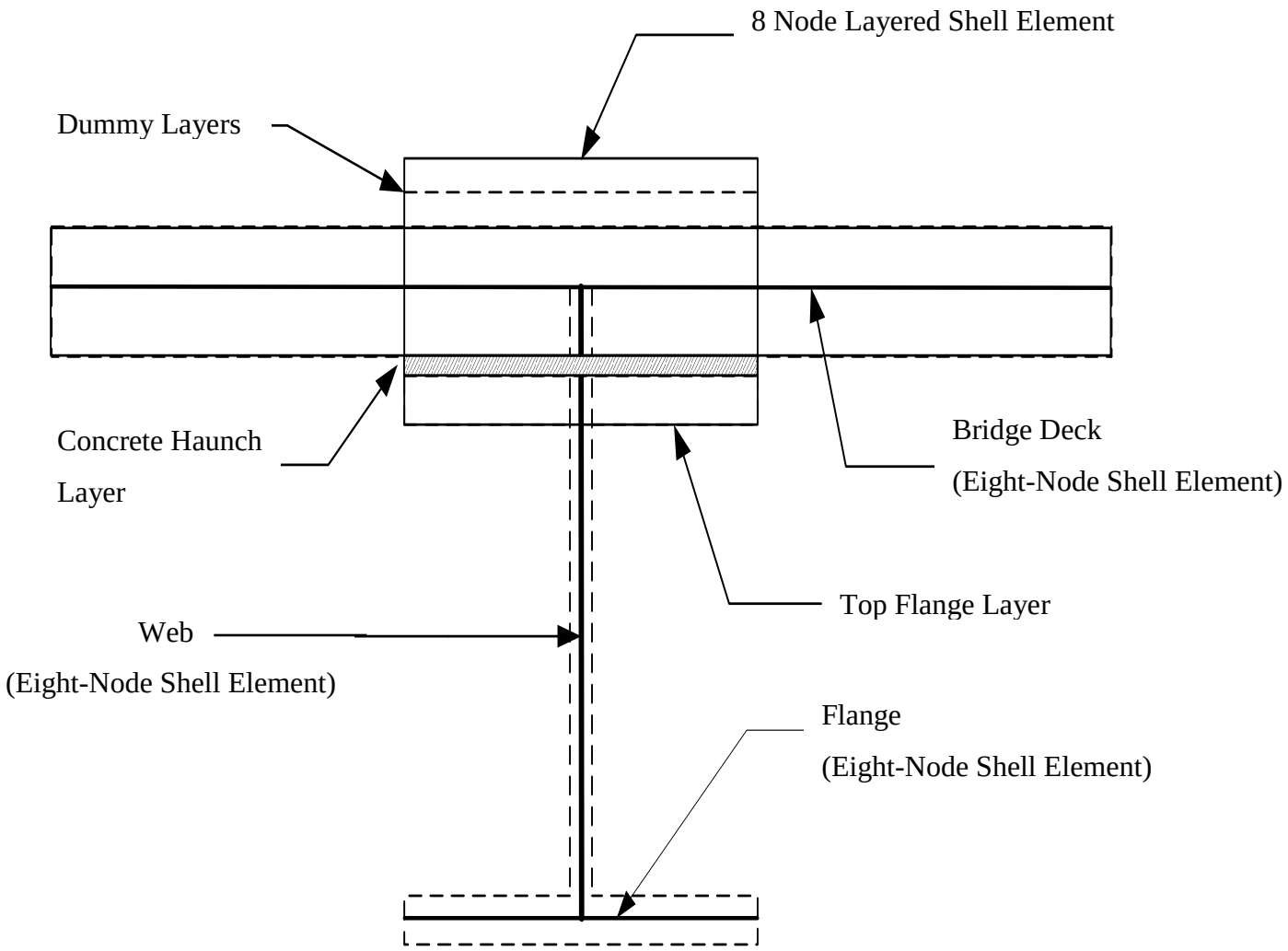

Figure 2.5: Wolek et al. Idealization

Ventura et al.(1996) modeled the concrete deck with shell elements. The number of nodes in these elements was not provided. However, they used an effective thickness for the deck to account for the cracking of concrete and construction variations in the slab thickness. The steel girders were idealized using three-dimensional beam elements with increased moment of inertia to account for the composite action between concrete deck and girder, and were positioned at top flange. The effective moment of inertia (I_{eff}) about x-axis, was calculated using following expression.

$$I_{eff} = I_c - I_{slab}$$ **Equation 2.1**

Where,

I_c Moment of Inertia of Composite Section

I_{slab} Moment of Inertia of Slab

Cross frames were modeled using three dimensional beam elements. Ventura et al. observed that at low levels of vibration the wearing surface contributes mass as well stiffness to the concrete deck thus it was considered in the model. The additional mass of the sidewalk and parapet was included as lumped mass in the model and the increased stiffness of the system was accounted for in the model by increasing the moment of inertia of the exterior girder about the axis of primary bending. The seized restrainer bolts at the bearing were modeled using linear springs with the stiffness obtained from the lateral loading properties of bolts. Ventura et al. did not explain the method used to connect the concrete deck and steel girders.

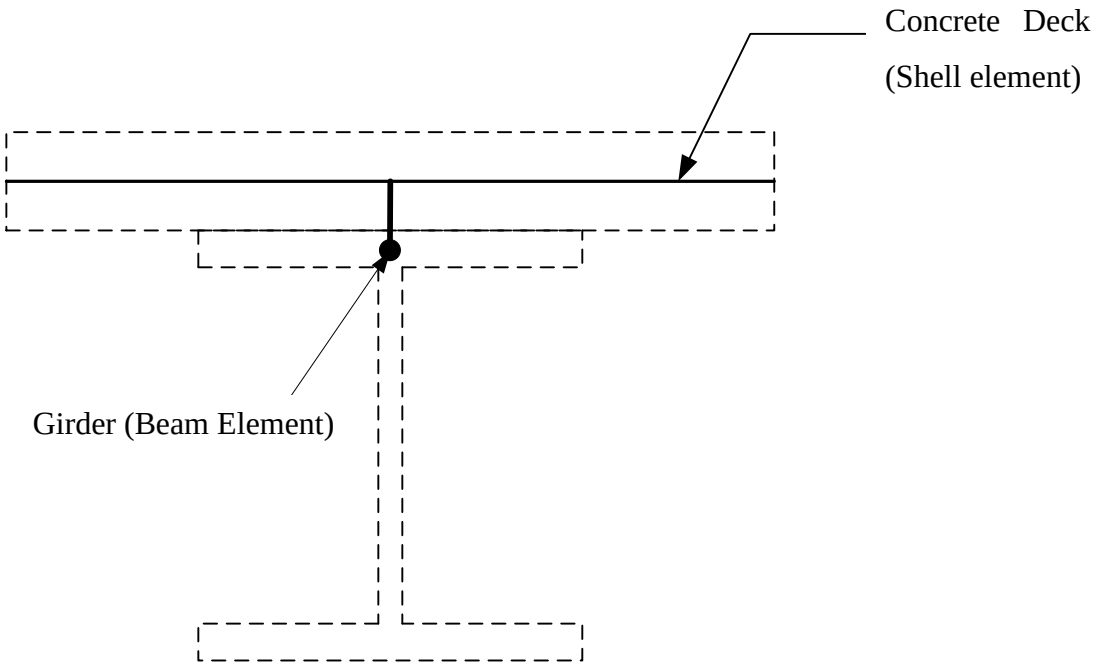

Figure 2.6: Ventura et al. Idealization

Ebeido and Kennedy (1996), Barr et al. (2001), Chen (1999) and Sebastian and McConnel (2000) used eccentric beam model as shown in Figure 2.7 to idealize the bridge superstructure in which the bridge deck was modeled using four node shell elements. The longitudinal steel girders and cross frames were idealized using three-dimensional two node beam elements with

six degrees of freedom each node. Sebastian and McConnel(2000) modeled the longitudinal and transverse reinforcement of the deck using an equivalent smeared layer of reinforcement. Ebeido and Kennedy (1996), Barr et al. (2001), Chen (1999) modeled the full composite action between the bridge deck and the steel girders using multipoint constraint in which the nodes on the shell element act as a master node to constrain the relative motion of girder nodes.

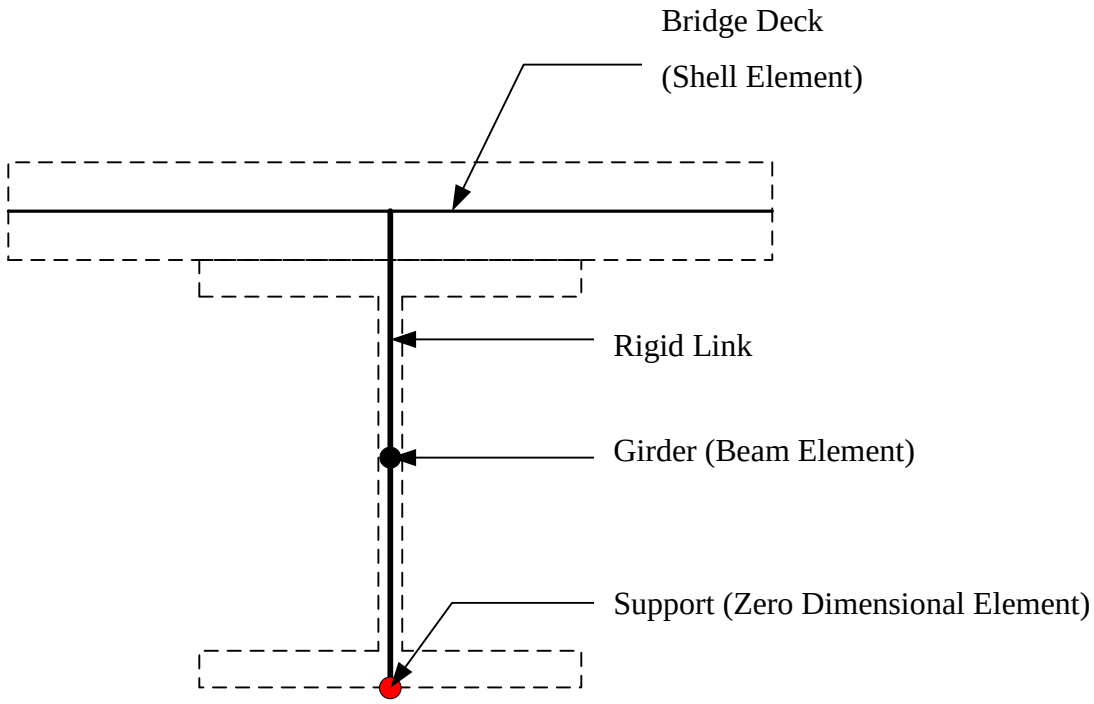

Figure 2.7: Eccentric Beam Model

Gupta and Ma (1977) studied the incompatibility that exists between the beam and shell elements in the eccentric beam model. Commonly used four-node shell elements assume uncoupled axial and flexural mode of deformation. For both these elements, the axial displacement field is interpolated using linear shape functions and the flexural mode is interpolated using cubic polynomial shape functions for the transverse displacement, which gives rise to quadratic expression for the rotation. When the shell and beam elements are at an eccentricity and connected with rigid links the axial displacement of the beam element is equal to the axial displacement of the shell element minus the eccentricity times the shell rotation, which makes it quadratic. This introduces inconsistency in the axial displacement field. This error can be reduced to a negligible value with refinement. In their study they investigated solely a composite beam, more specifically they analyzed a cantilever beam with point load applied at the free end.

They found that the error due to the incompatibility reduced from 69% to 4.3% by increasing number of elements used to model a cantilever beam from 1 to 4.

Miller (1980) eliminated this incompatibility by introducing an additional axial degree of freedom at the mid length of the beam element making the axial displacement field quadratic. Later in the analysis, this additional degree of the freedom was removed from the stiffness matrix by static condensation making the rank of the stiffness matrix equal to that of beam element without additional axial degree of freedom. An additional benefit of this approach is the reduction in computational time.

Chan and Chan (1999), Mabsout et al.(1997) and Mabsout et al. (2000) used the eccentric beam model in which the deck slab is modeled using 8-node isoparametric shell elements with plate and membrane behavior superimposed with five degrees of freedom per node. This element is capable of capturing both in-plane bending and out-of-plane bending. The girders were modeled using three-node quadratic isoparametric beam elements (Figure 2.7). By using quadratic elements, complete compatibility was achieved between the beam and shell elements. Chan and Chan (1999) slaved the transverse nodal displacement of the beam element to that of shell element using a transformation matrix to model the composite action between bridge deck and girders instead of using rigid links.

$$\begin{pmatrix} u_i \\ v_i \\ w_i \\ \theta_{ix} \\ \theta_{iy} \end{pmatrix}_{\text{beam}} = \begin{bmatrix} 1 & 0 & 0 & -e & 0 \\ 0 & 1 & 0 & 0 & -e \\ 0 & 0 & 1 & 0 & 0 \\ 0 & 0 & 0 & 1 & 0 \\ 0 & 0 & 0 & 0 & 1 \end{bmatrix} \begin{pmatrix} u_i \\ v_i \\ w_i \\ \theta_{ix} \\ \theta_{iy} \end{pmatrix}_{\text{shell}} \qquad \textbf{Equation 2.2}$$

As the degrees of freedom of the beam elements are removed from the global stiffness matrix, the computational cost of the model is reduced. Nodal loads on the eccentric beam element can be transformed into equivalent nodal loads on the shell element using the same transformation matrix used in Equation 2.2.

Chung and Sotelino(2006) used four different techniques to model the girders to model the bridge superstructure. In their approach the bridge deck was modeled using shear flexible shell elements (S8R in the commercial software ABAQUS(2007)) and the steel girders were modeled using four different idealizations, named G1, G2, G3, and G4, to assess the suitability of each technique. In the G1 model the girder flanges and web were modeled using shell elements. The shell elements used to model the flanges were placed at the mid-surface of the flanges using the offset option in ABAQUS to obtain the correct moment of inertia of steel girders. The only difference between the G1 and G2 models is that in the latter the flanges were modeled using beam elements placed at the location coinciding with the center of flange. The use of beam elements reduced the computational cost as compared to G1 model. In the G3 model, the girder web was modeled using, a beam element and both flanges were modeled with shell elements. This model was considered further to investigate the incompatibility that possibly exists between model G1 where the in-plane rotational degree of freedom of the flange shell and drilling rotational degree of freedom of the web shell are shared at the flange and web joint. Rigid links were used to connect the shell and beam elements to ensure full composite action. In the G4 model either Euler beam elements or shear flexible Timoshenko beam elements were used to model the steel girder (Figure 2.7). All four models were evaluated numerically by looking at the maximum deflection due to concentrated load applied at the center of a simply supported I-shaped beam considering shear flexibility (Figure 2.8). It should be noticed that the analytical solution to this problem is readily available from the theory of elasticity. The G1 and G2 model required significant mesh refinement to converge to the analytical solution as compared to G3 and G4 model.

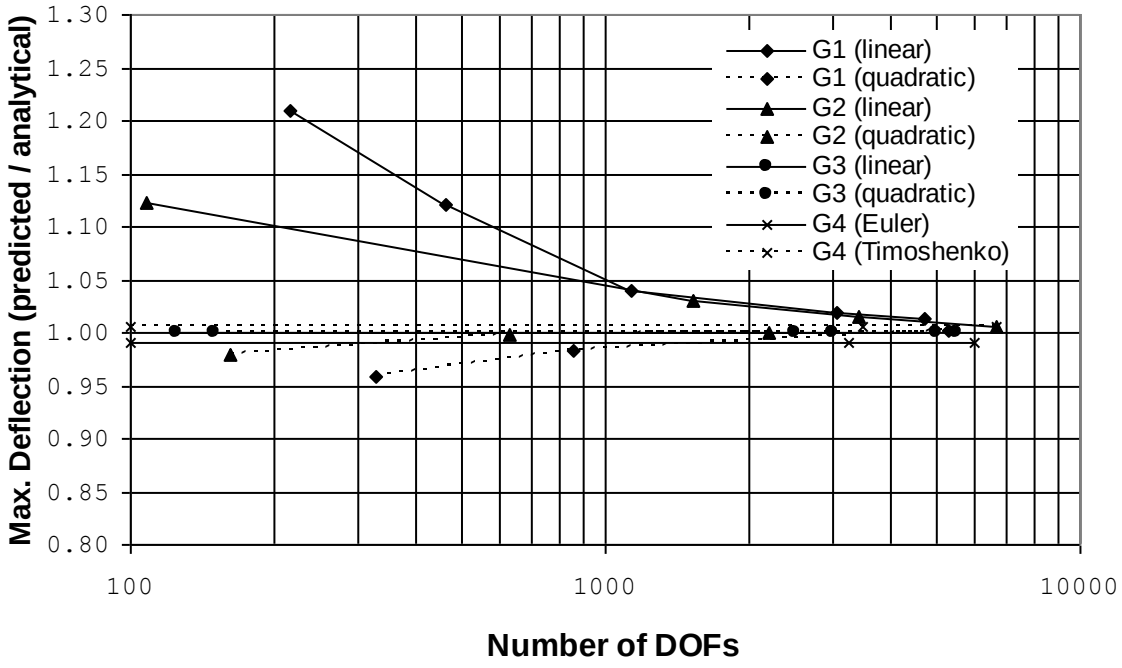

Figure 2.8: Convergence of Finite Element Girder Models. (Chung and Sotelino 2006)

2.3 Modeling of Partial Composite Action

The resistance offered by steel girders to different loads on the bridge depends upon the amount composite action between the bridge deck and steel girders. To model the partial composite action in finite element analysis different methods are proposed by researchers. Some of these methods are discussed next.

Tarhini and Frederick (1992) modeled the partial composite action with three linear spring elements with properties based on the amount of expected slip. Machado (2006) also used the three linear spring to model the partial composite action between the fiber reinforced polymer deck and steel girders. The vertical stiffness of the spring was taken to be equal to the slope of the elastic portion of the plot of bolt tension vs. bolt elongation. The connection was assumed to be a slip critical connection and the horizontal stiffness of the spring was calculated using the slip critical connection provisions in AISC 2001 with horizontal slip of 0.02 inches.

Fu and Lu (2003) modeled shear studs as bar elements (Figure 2.4). This is similar to using two independent linear springs with the longitudinal stiffness given by Equation 2.3 and the tangential stiffness given by Equation 2.4.

$$K_n = \frac{E_s A_s}{h_s} \qquad \textbf{Equation 2.3}$$

Where,

E_s Elastic modulus of shear stud

A_s Cross sectional area of shear stud

h_s Height of shear stud

$$K_t = abe^{-b\gamma} \qquad \textbf{Equation 2.4}$$

Where,

$$a = \frac{P_1^2}{2P_1 - P_2} \qquad \textbf{Equation 2.5}$$

And

$$b = \frac{1}{\gamma_1} \times \log_e \left(\frac{P_1}{P_2 - P_1} \right) \qquad \textbf{Equation 2.6}$$

Where,

P_1 and P_2 Load

γ_1 Interface Slip

Liang et al. (2005) used a three dimensional beam element to model the shear studs. The properties of the beam element were adjusted to have the strength and stiffness of the actual shear connector in a composite beam. A bilinear stress-strain relationship was used to characterize the constitutive behavior of the shear connector material.

Fahmy and Abu-Amar (2008) used three-dimensional eight node continuum element to model the concrete deck and steel girders. Shear studs were modeled using the spot weld option in ABAQUS. This option is a surface interaction model which slaves the nodes on the concrete

surface to the corresponding master nodes on steel beam. They assigned the Shear force vs. Slip relationship of the shear studs to the spot weld option. In particular, they used the idealized hyperbolic curve given by Equation 2.7.

$$Q = \frac{C}{\gamma - A} + B \qquad \textbf{Equation 2.7}$$

Where,

Q	Shear force
γ	Slip
A	Shear force at zero slip (Q_{Origin} , γ_{Origin})
B	Maximum shear corresponding to maximum allowed slip (Q_{max} , γ_{max})
C	Shear corresponding to a point that lies on the actual Shear force vs. Slip curve

Sebastian and McConnel (2000) developed a stub shear connector element to model the individual shear connector or the total shear stiffness at the node. The developed element was comprised of translational and rotational springs. The stiffness of the axial spring was based on the empirical shear force vs. slip relationship of a shear stud. The axial springs allow for the modeling of the partial composite behavior because of the flexibility of the shear stud. The vertical spring with very high stiffness was used to achieve compatibility between the vertical deflections of the concrete deck and steel girder. Similarly, rotational springs with very high stiffness were used to impose rotational compatibility except for the rotation about the axis perpendicular to the concrete deck and steel beam. As the drilling degree of freedom was not considered in the formulation of the deck and steel beam elements, there is no need to allow for this rotation in the shear stub element.

Queiroz et al. (2007) used nonlinear spring elements in the longitudinal direction to model the shear studs using a generalized shear force vs. displacement relationship of the shear studs obtained from the experimental study conducted by Chapman and Balakrishnan (1964). The vertical displacement of the deck slab was coupled with the vertical displacement of the steel

girder. Although the proposed model of the shear connector was unable to capture the interaction between the slab and stud, the authors found that it was effective in predicting the global response of the system.

Baskar et al. (2002) used two different techniques to model the composite action. In the first method surface interaction technique in ABAQUS was used to model the composite action. This technique allows incompatible strains and slip between the nodes in two different sets. More specifically, the bond strength at steel and concrete interface and strength of shear stud were combined and modeled as shear between two surfaces. A bilinear curve similar to shear force vs. slip curve for shear stud was used to model the slip. The surface behavior option in ABAQUS was used to model the vertical tensile strength of the stud. This method was unable to capture local effects such as slab failure and stud connector failure. In the second method, general beam elements were used to model the shear studs and the area of the beam element was modified to account for strength of embedded shear stud in concrete. Both techniques were evaluated by comparing their results with the experimental load vs. deflection plot for a cantilever beam subjected to a point load at the tip. The results obtained using the surface interaction technique was found to be in good agreement with the experimental data. However, even though the second technique was able to match closely the results in the initial stage of the deformation, it had a slower convergence with the post peak load vs. deflection plot and more mesh refinement than in the first method was required for the results to converge to the experimental results

Oehlers et al.(2000) proposed a mathematical model of the interface between the concrete deck and steel girder. It has two components the shear resisted by shear stud and friction between the steel and concrete interface. The shear stud was modeled using two orthogonal springs. A very high stiffness was assigned to the vertical spring to prevent the separation between concrete deck and steel girders. The stiffness of the spring resisting the horizontal shear acting at the interface was calculated using Equation 2.8 and Equation 2.9 (Oehlers and Johnson 1987).

$$K_{dwl} = \frac{P_{st}}{d_{sh}\,(0.16 - 0.0017 f_c)} \quad \textbf{Equation 2.8}$$

$$P_{st} = 4.3 A_{sh} f_u^{0.65} f_c^{0.35} \left(\frac{E_c}{E_s}\right)^{0.40}$$ **Equation 2.9**

Where,

K_{dwl}	Shear stiffness of the shear stud (N/mm)
d_{sh}	Diameter of the shank of the shear stud (mm)
f_c	Compressive strength of the concrete (Mpa)
P_{st}	Static strength of the shear stud (N)
A_{sh}	Area of the shank of the shear stud (mm^2)
f_u	Tensile strength of the shear stud (Mpa)
E_c	Young's Modulus of concrete (Mpa)
E_s	Young's Modulus of steel (Mpa)

The friction at the interface between steel and concrete was calculated using the following equation,

$$F_{friction} = \mu F_{normal}$$ **Equation 2.10**

Where,

$F_{friction}$	Frictional resistance (N)
F_{normal}	Normal force between the concrete deck and steel girder interface (N)
μ	Coefficient of friction between steel and concrete

The force resisted by dowel action of the shear stud was calculated using the following equation,

$$F_{dwl} = K_{dwl}\, \delta$$ **Equation 2.11**

Where,

F_{dwl}	Shear force resisted by the shear stud (N)
K_{dwl}	Shear stiffness of the shear stud (N/mm)
δ	Slip between the steel and concrete interface (mm)

In addition, the total resistance force was calculated as,

$$F_{total} = F_{dwl} + F_{friction} \qquad \textbf{Equation 2.12}$$

Where,

F_{total}	Total shear resistance (N)
$F_{friction}$	Frictional resistance (N)
F_{dwl}	Shear force resisted by the shear stud (N)

Finally, the secant stiffness was calculated using Equation 2.13,

$$K_{sec} = \frac{F_{total}}{\delta} \qquad \textbf{Equation 2.13}$$

2.4 Loading

American Association of State Highway and Transportation Officials(AASHTO 2008) uses tire patch loading with tire pressure uniformly distributed over the contact area for the analysis of bridges subjected to truck loading. Dimensions of the tire patch can be calculated using the following expressions given in AASHTO C3.6.1.2.5(2008).

$$Tire\ width = P/0.8 \qquad \textbf{Equation 2.14}$$

And

$$Tire\ length = 6.4\gamma(1 + \frac{IM}{100}) \qquad \textbf{Equation 2.15}$$

Where,

γ	Load Factor
IM	Dynamic load allowance percent
P	Design wheel load (kips)

In most finite element analysis programs and in ABAQUS, in particular, the application of truck loading using contact area of tire patch is not trivial, since it often requires that a fine mesh be used in the deck such that contact area dimensions of the patch matches the dimensions of the element. This method increases the computational cost of the model and the complexity of deck meshing. Therefore, researchers have developed different approximate and exact techniques to uncouple mesh size and patch loading.

The concept of work equivalent nodal loads can be used to apply a tire patch load on the bridge deck. In this method equivalent nodal loads are calculated such that the work done by the nodal loads in going through nodal displacements is equal to the work done by distributed loads like body forces and surface traction in going through the displacement obtained using the element's shape functions. The equivalent load for a surface traction can be calculated by evaluating the following integral. (Equation 2.16) (Cook et al. 2001)

$$\mathrm{R}_e = \int_S \mathrm{N}^{\mathrm{T}}\mathrm{T}\, dS \qquad \textbf{Equation 2.16}$$

Where,

R_e	Equivalent nodal load matrix
N	Shape function matrix
T	Surface traction
S	Surface area

To use this method the user needs to identify the nodes and the elements that lie on the patch load and the dimensions of the area occupied by the patch load on each of the element, which is not trivial. This method gets further complicated in case of skewed bridges.

Chung and Sotelino (2006) developed a method in which the patch load is discretized into a number of uniformly distributed point loads over the patch area. If the patch is discretized into Q point loads of magnitude P then the equivalent nodal load is calculated using Equation 2.17. Mindlin plate shape functions in the natural coordinate system are used in the calculation of

equivalent nodal loads, which is compatible with the choice of shell elements used to model the bridge deck.

$$\mathrm{R}_e = \sum_{i=1}^{Q} \mathrm{N}^{\mathrm{T}}\, \mathrm{P}_i \qquad \textbf{Equation 2.17}$$

Where,

R_e	Equivalent nodal load matrix
N	Shape function matrix
P	Point load magnitude
Q	Number of point loads

Chung and Sotelino (2006) verified this technique by discretizing the load patch into a number of point loads (i.e. approximate ENF) and calculating the equivalent nodal loads using Equation 2.17 and comparing those results with the results obtained using work equivalent nodal loads (Equation 2.16) for a square plate subjected to distributed loads (i.e. exact ENF). It was observed that this method gives less that 0.5% error for interior and corner nodes when the load patch is discretized into 100-point loads or more.

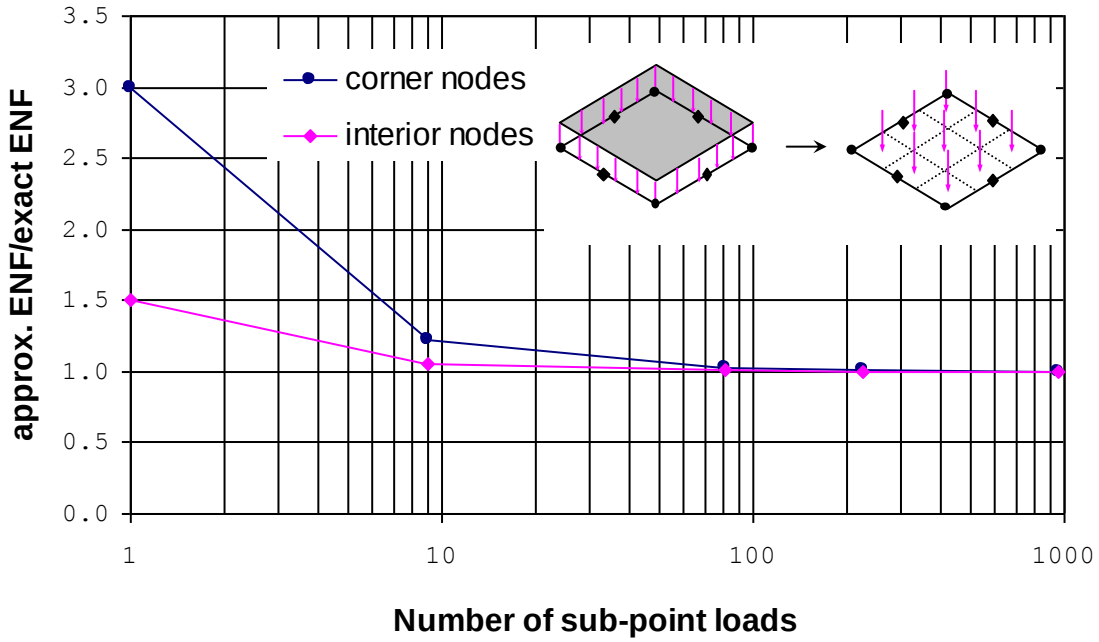

Figure 2.9: Discretization Error of the Patch Load (Chung and Sotelino 2006)

Chen (1995), Eom and Nowak (2001) used the concept of tributary area to calculate the equivalent nodal loads. In this method, the tire patch is applied as a point load at the center of tire patch. The equivalent nodal loads are calculated by multiplying the point load with the ratio of the area confined by lines parallel to element edges between point of application of point load and edge node to total element area as shown in Figure 2.10. Girder strains at mid-span and live load distribution factors were calculated for simply supported case and for the case where all supports are assumed pinned using finite element analysis. These obtained results were able to bracket the experimental results.

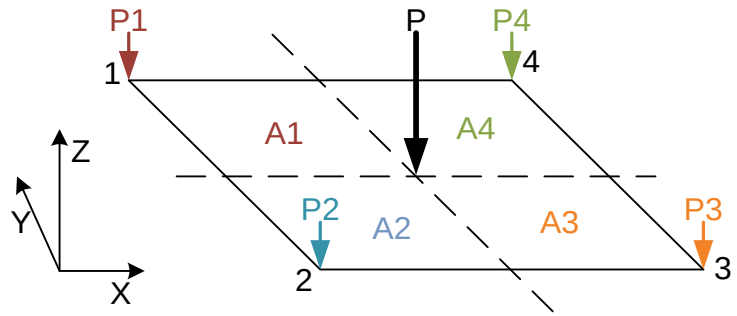

Figure 2.10: Equivalent Nodal Loads Using Tributary Area

Buckler et al. (2000) used contact elements in ABAQUS to model the load patch. In this method, a shell element with area equal to that of the contact area of each tire patch was used to model the truck loading. These shell elements were attached to the bridge deck using contact elements. A low modulus of elasticity was assigned to thin shell elements such that the load patch carried no load. This way the entire load is transferred to the bridge deck. On average the strains were off by 6.3 με for maximum strain of 35 με (off by18%) and deflections were off by 0.0047 in. for maximum deflection of 0.059 in. (off by 8%).

From the discussion above it can be concluded that modeling of the truck patch load using one of the described methods gives acceptable results for girder strains, girder deflections, and live load distribution factors. However, when localized behavior close to the load is desired, explicit modeling of truck patch load is necessary.

2.5 Summary

In this chapter, three dimensional modeling techniques used by researchers to study the bridge superstructure response are reviewed. Some of these modeling techniques have geometric errors and incompatibilities that may affect the bridge response. Therefore, some of the modeling techniques discussed here are further discussed in Chapter 3. The goal of this is to check their ability to accurately predict the bridge response and to compare the computational cost associate with them. Finally, the mathematical model proposed by Oehlers et al.(2000) to simulate partial composite action between girders and bridge deck is adopted in the present research.

3 Finite Element Modeling of Slab on Girder Bridges

3.1 Introduction

Slab on girder bridges are hybrid structures made up of several structural components. Over the years, various three-dimensional modeling techniques have been used by researchers to idealize these structural components as discussed in the Literature Review chapter. The first important step in finite element modeling is the selection of appropriate modeling techniques and elements. The objective of this chapter is to evaluate the ability of several existing modeling techniques to accurately predict bridge response and the computational cost associated with it. Furthermore, the effect of explicitly modeling the different aspects of bridge geometry such as bridge skew, supports, composite action, temperature gradient, and secondary structural elements, on the accuracy of the obtained results is also being investigated.

3.2 Modeling of Bridge Components

This section is organized by first discussing the modeling of primary structural elements, such as bridge deck and girders. This is followed by a presentation of the modeling techniques used to simulate secondary structural elements, such as guardrail and bracing, as well as the techniques used to model composite action, temperature gradient, and boundary conditions.

3.2.1 Modeling of Bridge Deck

Bridge deck behavior is governed predominantly by flexure, which is best modeled using shell elements. ABAQUS (2007) provides a rich library of shell elements. In this research the following elements were considered. Four node linear shell element with full integration with six degrees of freedom per node (S4) and with reduced integration with six degrees of freedom per node (S4R) and with five degrees of freedom per node (S4R5), and eight node quadratic shell element with reduced integration with six degrees of freedom per node (S8R) and five degrees of freedom per node (S8R5). These elements were tested numerically to evaluate their ability to accurately model the bridge deck. ABAQUS shell elements (S4, S4R) are general purpose conventional shell elements which use thick shell theory (Mindlin shell formulation) as the shell thickness increases and use discrete Kirchhoff shell formulation as thickness decreases (ABAQUS 2007). S8R uses a conventional thick shell formulation while S4R5 and S8R5 impose Kirchhoff constraints numerically (ABAQUS 2007). Mindlin shell elements with full integration

are susceptible to locking when elements become thinner. This happens because the shear energy term tends to dominate the total potential energy. This problem can be resolved by using reduced integration to calculate the total potential energy (Cook et al. 2001).

To evaluate accuracy of the displacements that are obtained using these elements , a square steel plate 250 in. by 250 in. in size with varying thickness clamped on all four edges was subjected to a uniform pressure of 0.001 kips/in^2. The maximum central displacement from the finite element analysis was compared against the displacement calculated from the analytical solution using Equation 3.1 (Ugural 1999).

$$w_{max} = \frac{0.00126 p_o a^4}{D} \qquad \textbf{Equation 3.1}$$

Where,

D	Flexural rigidity of plate $D = \frac{E_s h^3}{12(1-\upsilon^2)}$
a	Width (in)
p_o	Uniform pressure (kips/in^2)
E_s	Young's modulus of steel (ksi)
h	Thickness of shell (in)
υ	Poisson's ratio

First, the central displacement for a 1-in. thick shell was obtained using different shell elements from ABAQUS and compared to the exact solution The error level against mesh refinement was plotted and the results are shown in Figure 3.1. From the plot, it is clear that all the elements converge to the exact solution with refinement.

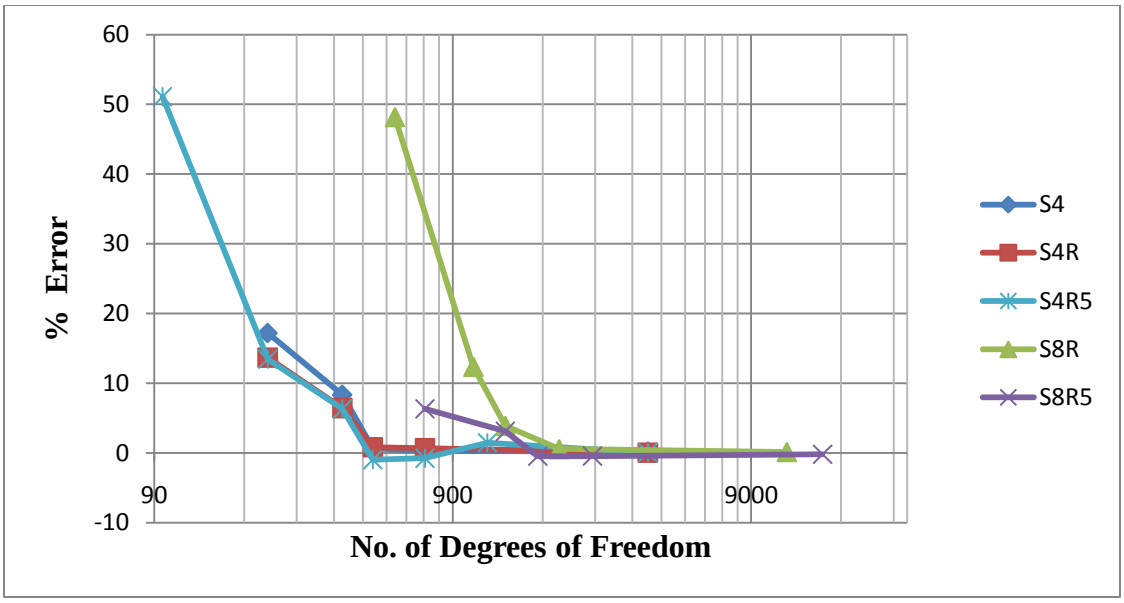

Figure 3.1: Comparison of Maximum Central Deflection of a 1-in Square Plate with Analytical Solution

Next, the central displacements for varying shell thickness that were obtained using the various shell elements in ABAQUS were compared to the respective analytic solutions. The error versus shell thickness was plotted as shown in Figure 3.2. Identical mesh density was used for the various thickness values and different shell elements used in the analysis. From the plot, it can be seen that all the elements, except for S4R5, predict similar response and tend to produce a more flexible structure up to length to thickness (a/h) ratio of approximately 380. The S4R5 element, on the other hand, tends to produce a stiffer response until a ratio a/h of about 140. Finally, in all cases, the errors are less than 4% in magnitude. For thick shell S8R, as the thickness decreases shear term dominates the overall response resulting into increased percent error.

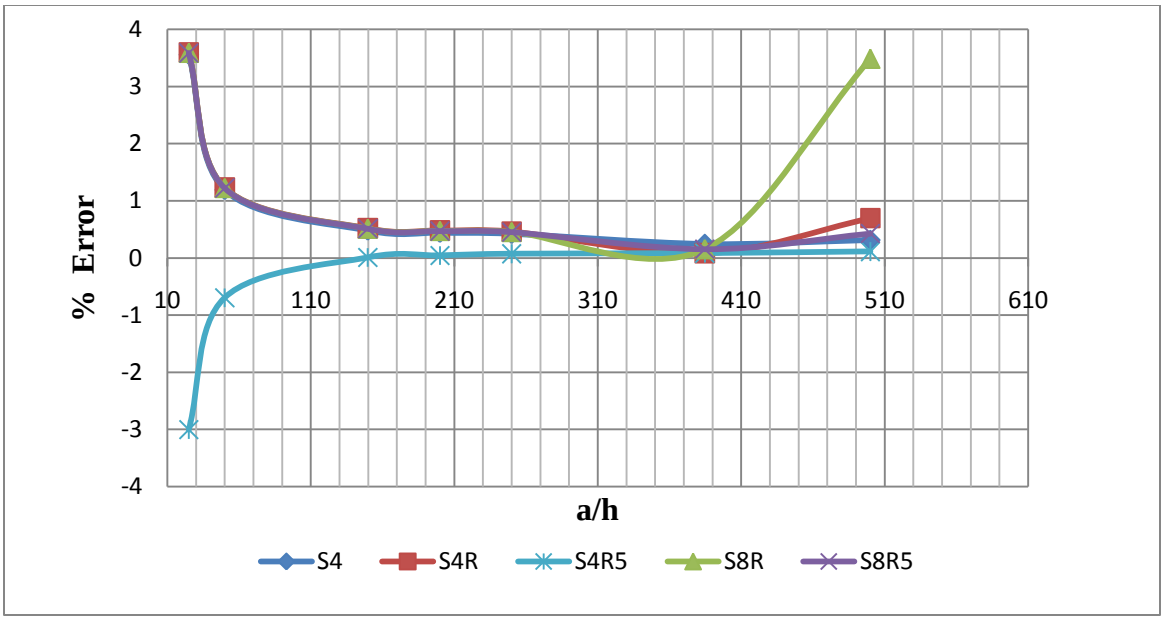

Figure 3.2: Comparison of Maximum Central Deflection of a Square Plate of Varying Thickness with Analytical Solution

To evaluate whether these elements are capable of accurately predicting free vibration response of the bridge deck, the same square steel plate 250 in. by 250 in. in dimension with varying thickness was used. All four edges of the plate were pinned. The analytical solution for the fundamental frequency of vibration was calculated using Equation 3.2 (Fertis 1995).

$$\omega_{11} = \pi^2 \left(\frac{1}{a^2} + \frac{1}{b^2}\right) \sqrt{\frac{D}{\rho h}} \qquad \textbf{Equation 3.2}$$

Where,

ω_{11}	Fundamental frequency of vibration
a	Length of plate
b	Width of plate
D	Flexural rigidity of plate
	$D = \frac{E_s h^3}{12(1-\upsilon^2)}$
h	Thickness of shell
ρ	Weight density

First, the fundamental frequency of vibration of a 1 in. thick square steel plate was calculated using the various shell elements in ABAQUS, as shown in Figure 3.3. As can be seen all the elements tend to predict fundamental frequencies of vibration accurately with refinement. The eight-node quadratic shell elements with reduced integration (both the five degrees of freedom per node (S8R5) and with six degrees of freedom per node (S8R)) tend to converge faster to the exact solution as compared to the other elements.

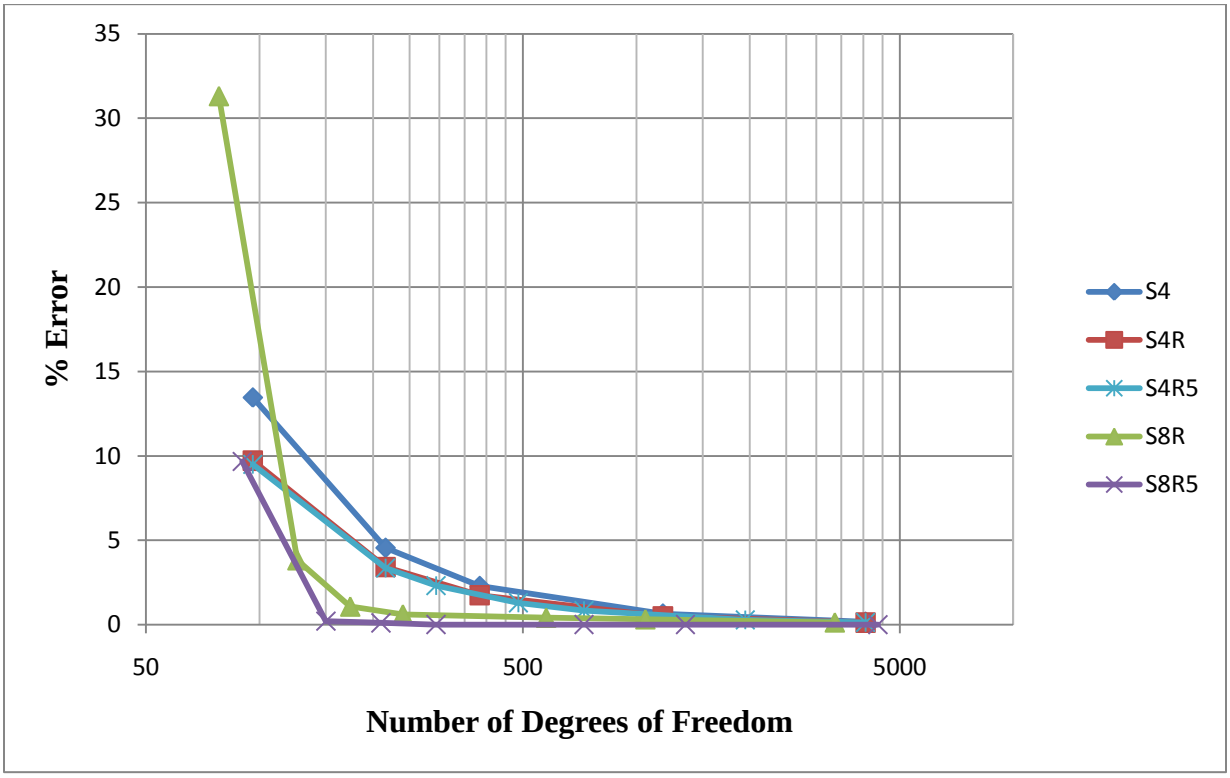

Figure 3.3: Comparison of Fundamental Frequency of Vibration of 1in Thick Square Plate with Exact Solution

Next, the fundamental frequency of vibration of a square steel plate with varying thickness values was obtained using the same ABAQUS elements and compared to the analytical solution. The results are shown in Figure 3.4. Again, identical mesh density was used for all thickness values. As can be seen from this figure, for a length to thickness ratio (a/h) of less than 100, the percentage error between the finite element solution and the exact solution lies between 0.75% and 3.5%. For ratios a/h greater than 100, the errors become very small.

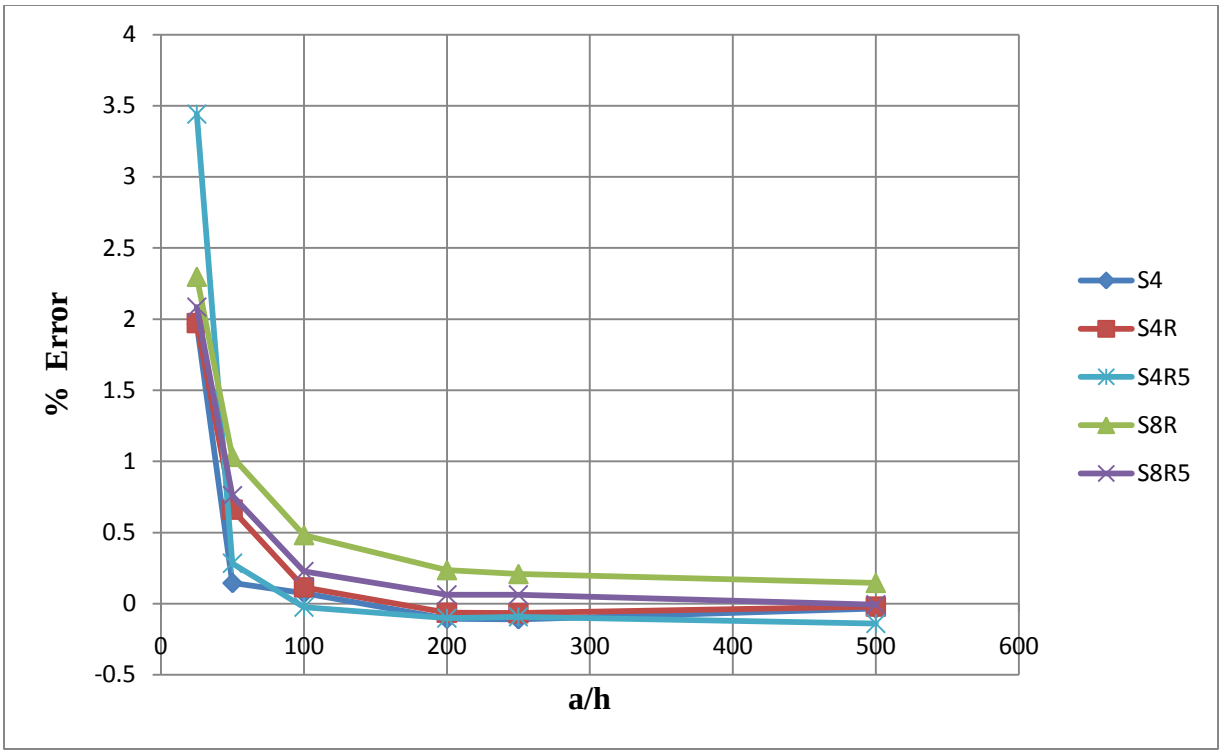

Figure 3.4: Comparison between Fundamental Frequency of Vibration of Square Plate of Varying Thickness against the Analytical Solution

3.2.2 Modeling of Girders

In this subsection, different modeling techniques for girders are investigated. More specifically a parametric study was carried out using four different modeling techniques as shown in Table 3.1. They were evaluated numerically to determine their capability of accurately predicting girder response.

Table 3.1: Girder Models according to adopted Element Types

Model Name	**Element Type**	
	Web	**Flange**
Model-1	Beam element	
Model-2	Beam element	Beam element
Model-3	Shell element	Shell element
Model-4	Beam element	Shell element

The numerical evaluation consisted of comparing the mid-span deflection of a simply supported beam (W16x26) subjected to its self-weight. The analytical solution for this problem considering the effect of shear deformations is given by Equation 3.3. For W16x26 beam shear deformation contributes 1.7% of the total deformation.

$$\delta = \frac{5}{384}\frac{wL^4}{EI} + \kappa\frac{wL^4}{8GA} \qquad \textbf{Equation 3.3}$$

Where,

w	Uniformly distributed load
L	Length
E	Young's modulus of elasticity
G	Shear modulus
I	Moment of inertia of the section
A	Cross sectional area of the section
κ	Form factor

The form factor for an open section was calculated using the empirical expression discussed by Charney et al.(2005) . This expression was selected because despite its simplicity it yielded results very close to the ones predicted by finite element analysis.

$$\kappa = \frac{A}{d_{eff}\, t_w} \qquad \textbf{Equation 3.4}$$

Where,

A	Cross sectional area of the section
d_{eff}	Distance between the center of flanges
t_w	Thickness of web

To evaluate whether the modeling techniques can predict the dynamic response, the fundamental frequency of vibration of a simply supported beam with shear deformations and rotational inertia calculated using Equation 3.5. (Chopra 2001) was compared against the results from finite element analysis.

$$\omega'_n = \omega_n \frac{1}{\sqrt{1 + \left(\frac{n\pi r}{L}\right)\left(1 + \frac{E}{\kappa G}\right)}} \qquad \textbf{Equation 3.5}$$

$$\omega_n = \frac{n^2\pi^2}{L^2}\sqrt{\frac{EI}{m}} \qquad \textbf{Equation 3.6}$$

Where,

ω'_n	Natural frequency of vibration with shear deformations and rotational inertia
ω_n	Natural frequency of vibration
r	Radius of gyration of the section
L	Length of the beam
I	Moment of inertia of the section
E	Young's modulus of elasticity
G	Shear modulus
κ	Form factor calculated using Equation 3.4
m	Mass per unit length

An schematic illustrating Model-1 (often referred to as the eccentric beam model) is provided in Figure 3.5. In this case, beam elements are used to model the entire girder, which are placed at the location of the centroid of the cross-section of the girder. The supports were modeled at the girder bottom. In order to guarantee that plane sections remain plain after deformation, rigid links are used to connect girder and supports as well as deck and girders. The percent error between the analytical solution and the finite element results was calculated using the expression given by Equation 3.7

$$\%\, Error = \frac{(Analytical\ Solution - Finite\ Element\ Solution)}{Analytical\ Solution} \times 100 \qquad \textbf{Equation 3.7}$$

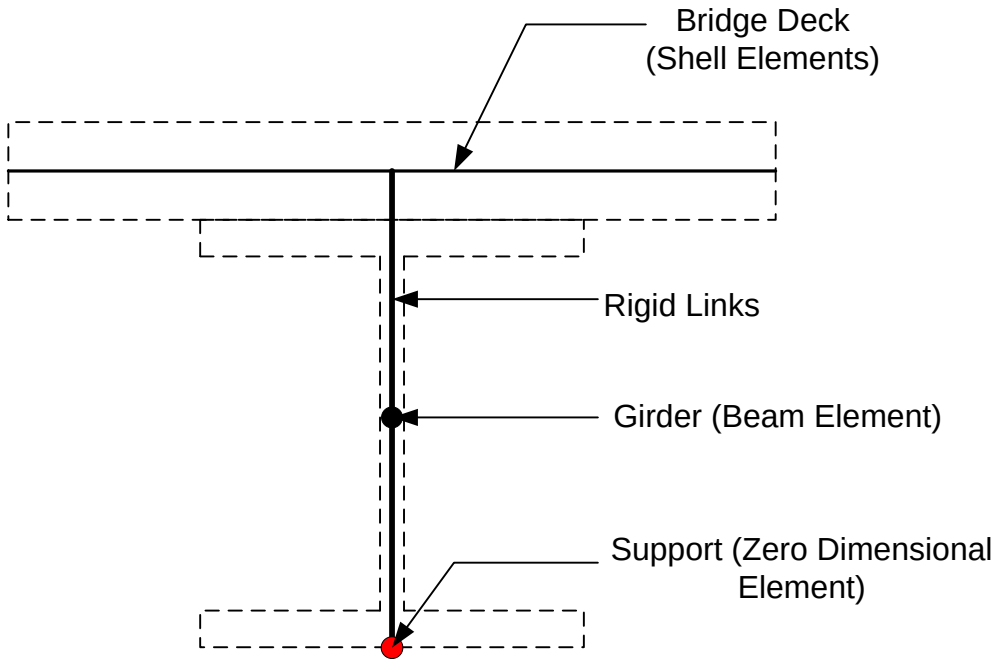

Figure 3.5: Model-1 (Eccentric Beam Model)

ABAQUS provides a number of beam elements. In particular, the linear (B31) and quadratic (B32) beam elements use Timoshenko beam formulation while the cubic beam element (B33) uses Euler-Bernoulli formulation. Timoshenko beam elements (B31, B32) use lumped mass formulation for static and dynamic analysis. The Euler-Bernoulli beam element (B33) uses consistent mass formulation (ABAQUS 2007). Figures 3.6 and Figure 3.7 provide the percent error versus mesh refinement between the finite element analyses results using the various types of beam elements and the analytical solutions for center deflection and natural frequency, respectively. From these results, it can be seen that the quadratic beam element (B32) and the cubic beam element (B33) predict the same response irrespective of mesh refinement, while the linear beam elements (B31) need refinement to converge to the analytical solution. Also, as mentioned in Chapter 2, Gupta and Ma (1977) established that there exists an incompatibility in the axial displacement field of the linear beam element. However, as can be seen from the figures, this error reduces with refinement and the solutions eventually converge to the analytical solution.

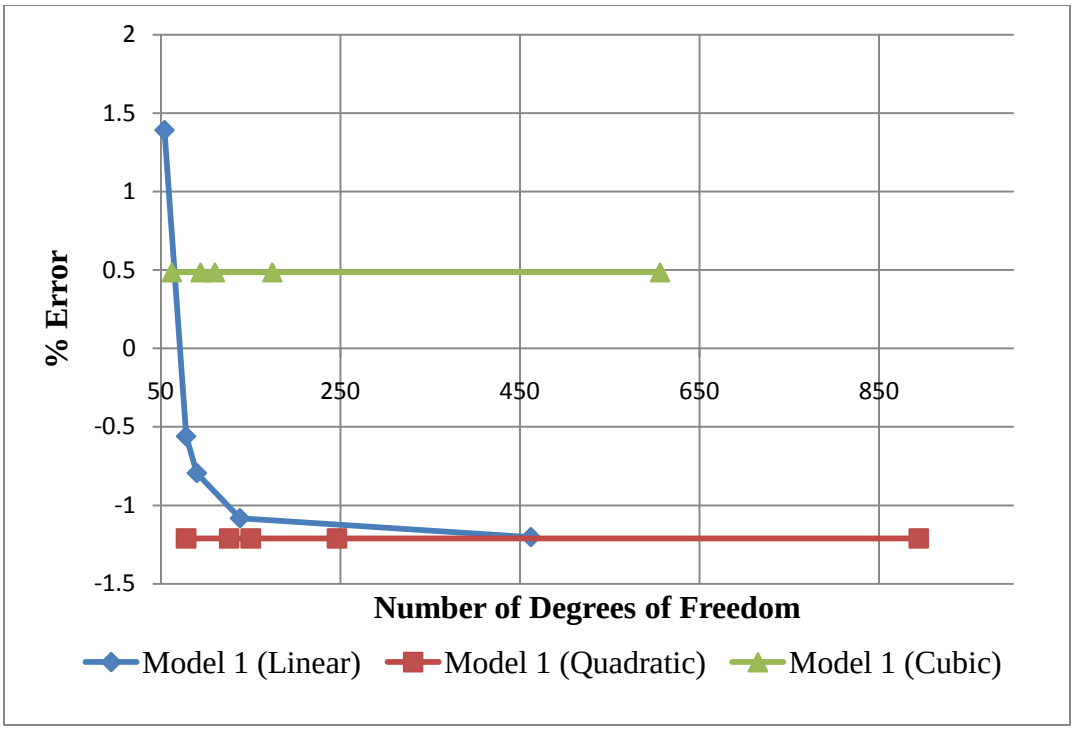

Figure 3.6: Comparison between the obtained Maximum Central Deflection and the Analytical Solution for Model-1

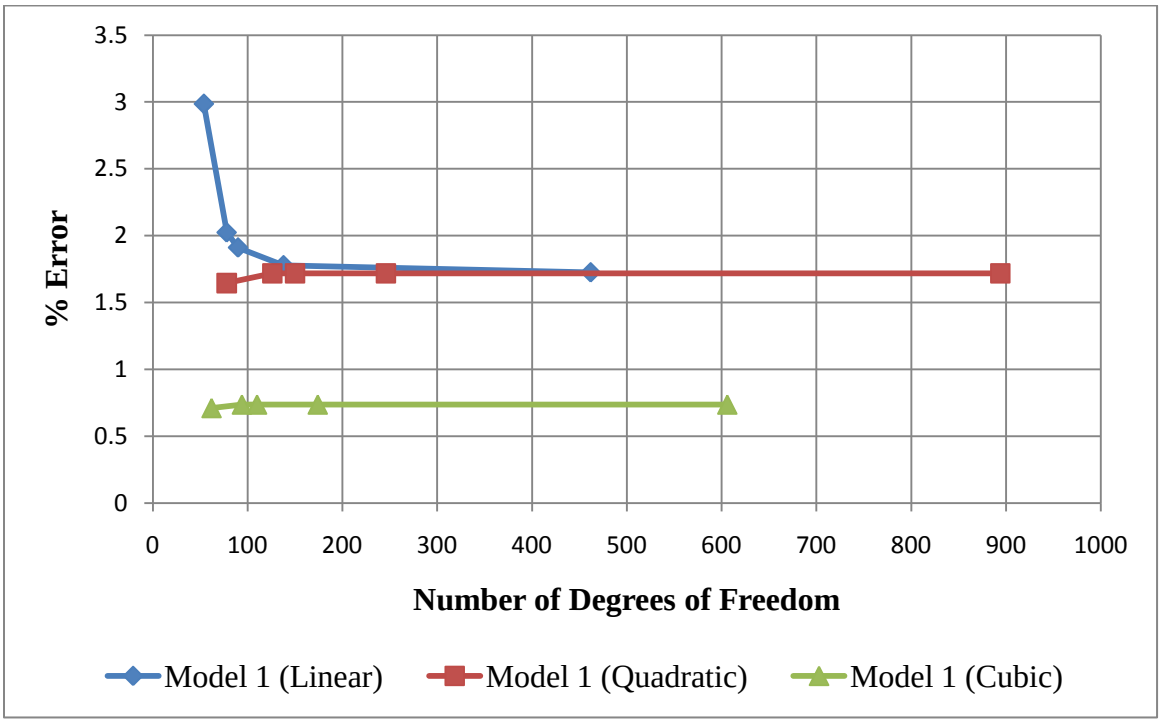

Figure 3.7: Comparison between the obtained Fundamental Frequency of Vibration and the Analytical Solution for Model-1

In Model-2 (referred to as the three beam model), each part of the girder, i.e., top flange, bottom flange and web was modeled separately using beam elements placed at the centroid of each part. The girder flanges and web were connected to each other using rigid links (Beam connector in ABAQUS) as shown in Figure 3.8. The supports were modeled at the girder bottom.

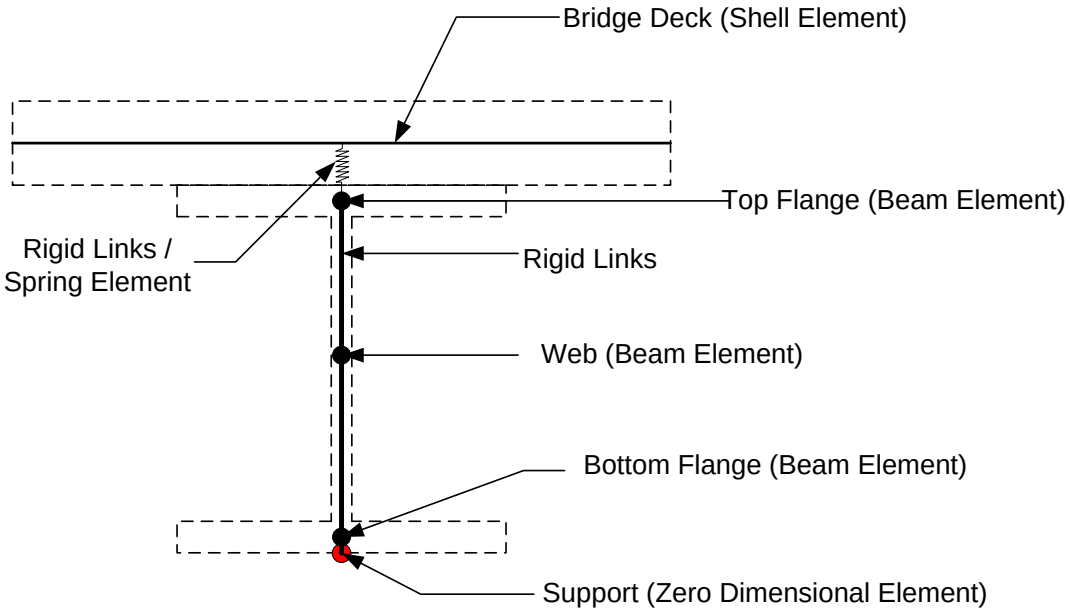

Figure 3.8: Model-2 (Three Beam Model)

Similar to the previous numerical test, Figure 3.9 and Figure 3.10 provide the percent error versus mesh refinement for the various types of elements. As can be seen from these figures, Model-2 gives results within 5% of the analytical solution irrespective of the beam elements used. However, the B33 clearly provides more accurate results when compared to the analytical solution.

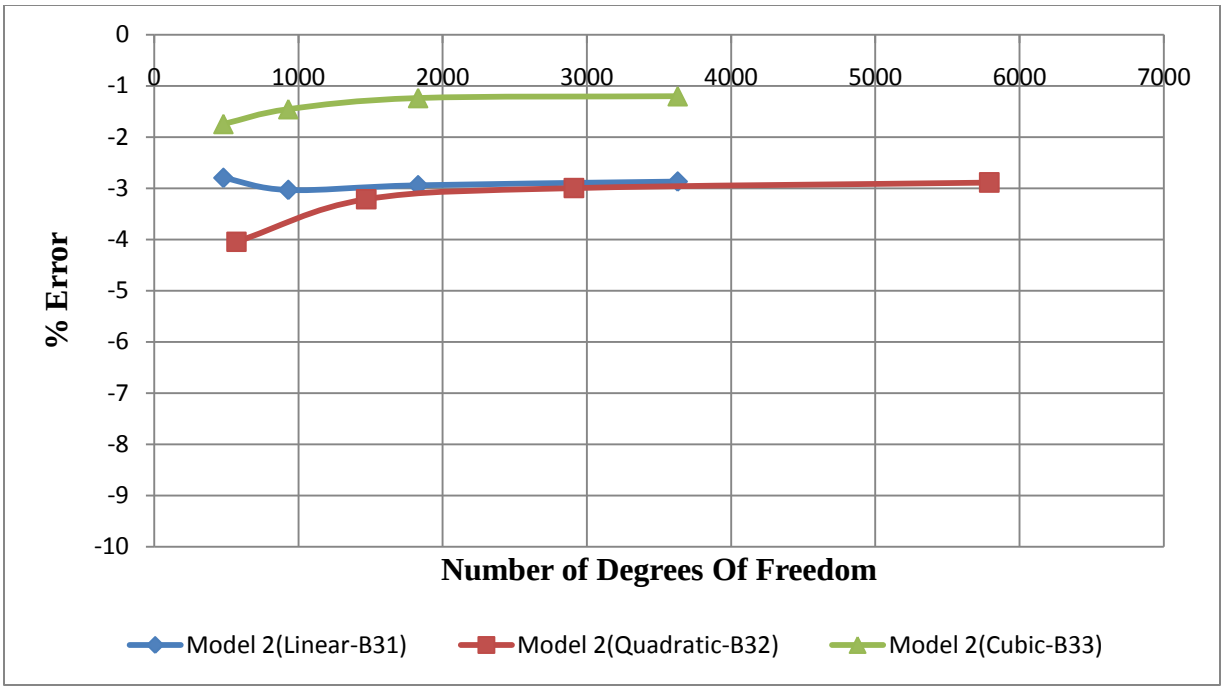

Figure 3.9: Comparison between the Maximum Central Deflection and the Analytical Solution for Model-2

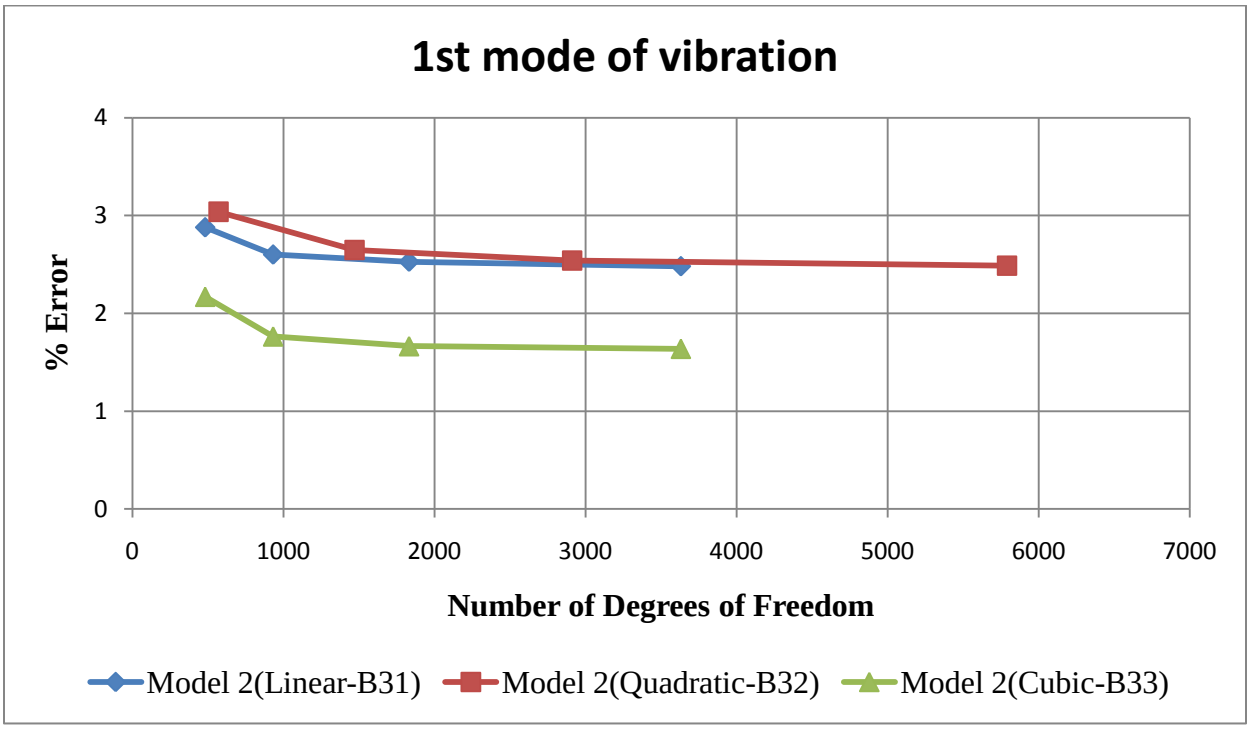

Figure 3.10: Comparison between the Fundamental Frequency of Vibration and the Analytical Solution for Model-2

In Model-3, girder flanges and web were modeled using shell elements as shown in Figure 3.11. Shell elements were modeled at the mid surface of the web and flanges. Modeling flanges at its mid surface results in additional web depth equal to half of the flange thickness as shown schematically in Figure 3.11. Similar numerical testing as described above was conducted for this model. As it can be seen from Figure 3.12 and Figure 3.13 the additional web, depth does not appear to have any significant effect on the solution. It should be noted that there exists an incompatibility between the in-plane rotational degree of freedom of the flange shell elements and the drilling degree of freedom of the web shell elements. However, from Figure 3.12 and Figure 3.13 the error incurred because of this incompatibility tends to reduce with mesh refinement.

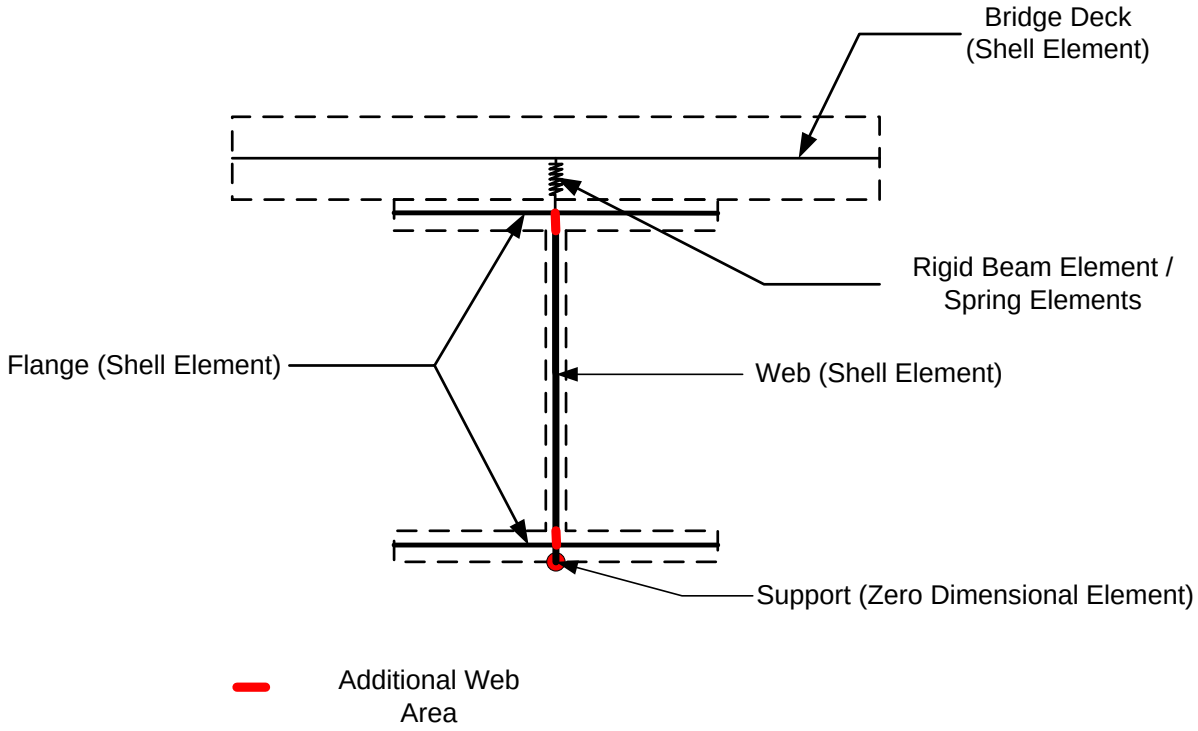

Figure 3.11: Model-3

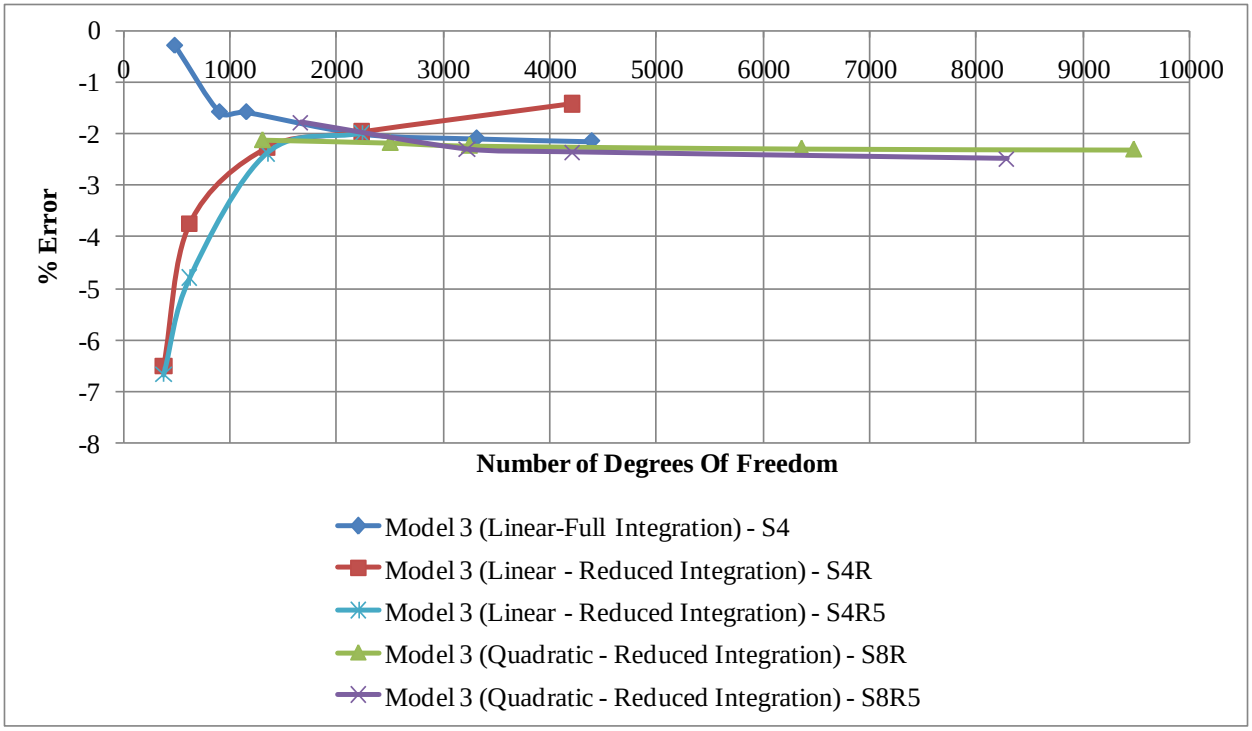

Figure 3.12: Comparison between the Maximum Central Deflection and the Analytical Solution for Model-3

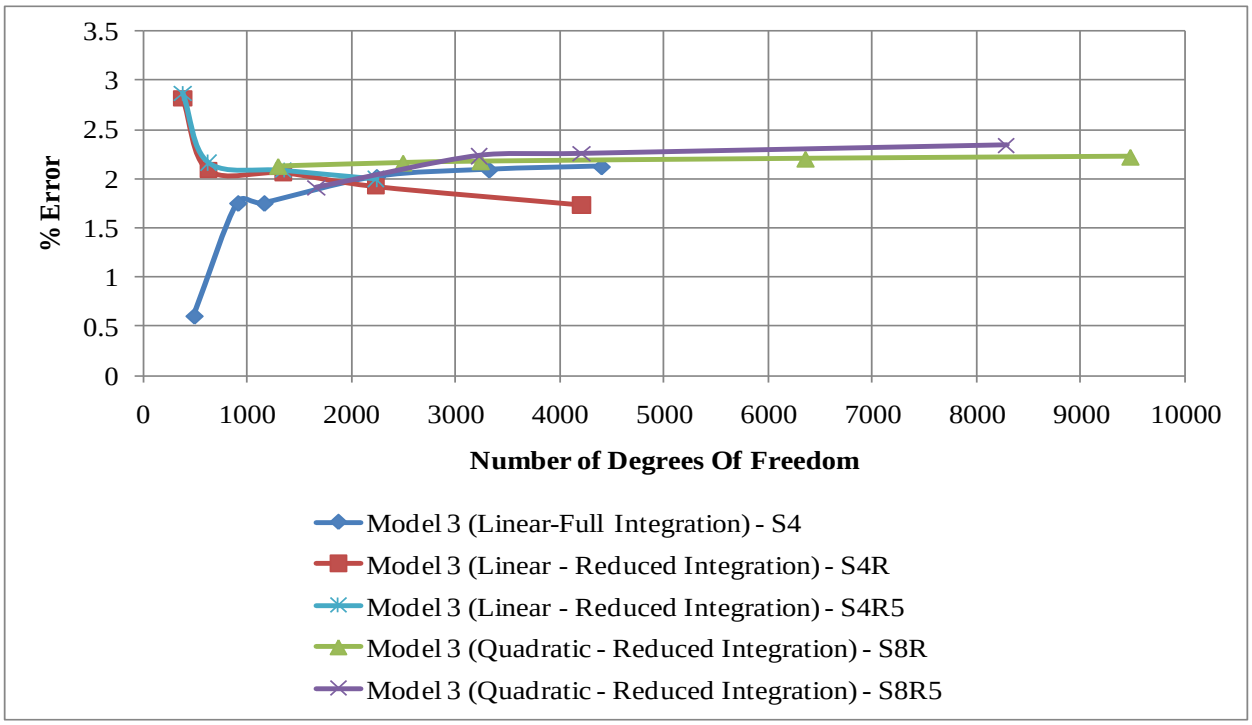

Figure 3.13: Comparison between the Fundamental Frequency of Vibration and the Analytical Solution for Model-3

In Model-4, the girder web was modeled using beam elements placed at the centroid of the web and girder flanges were modeled using shell elements at the mid-surface of flanges. The girder flanges and web were connected to each other using rigid links. This model was used to investigate the incompatibility at the element connection between web and flange in Model 3.

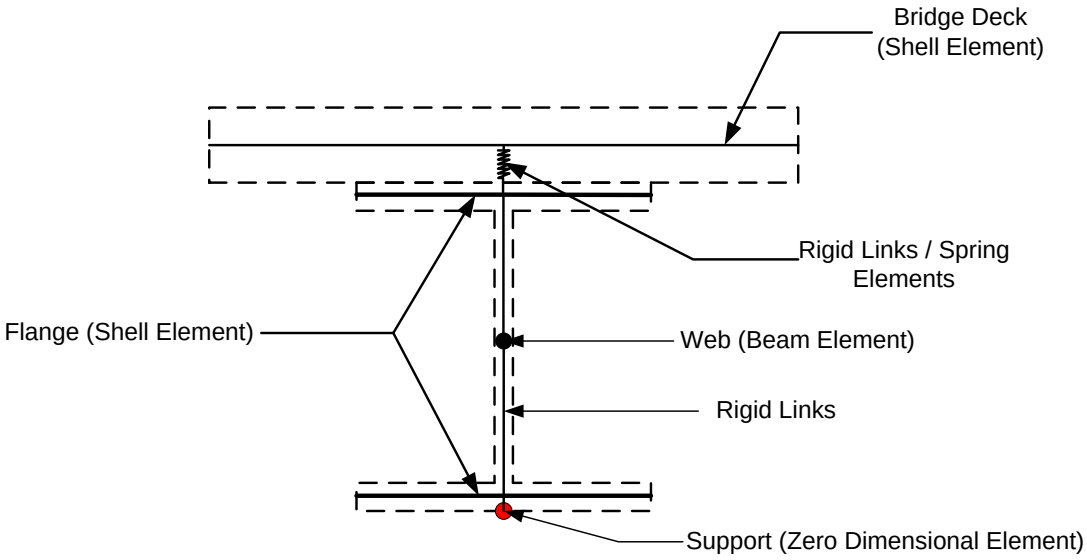

Figure 3.14: Model-4

As it can be seen from Figure 3.15 and Figure 3.16, linear and quadratic models converge within 2.5% of the analytical solution with refinement. Significant mesh refinement was required to converge when compared to model-1.

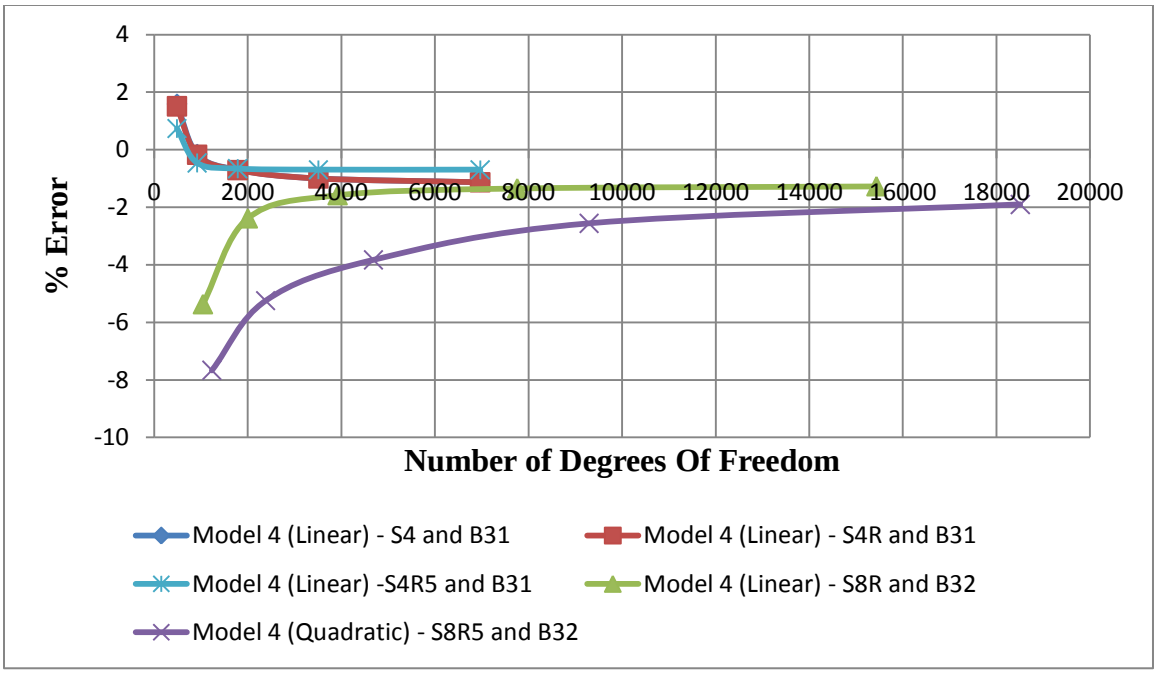

Figure 3.15: Comparison between the Maximum Central Deflection and the Analytical Solution for Model-4

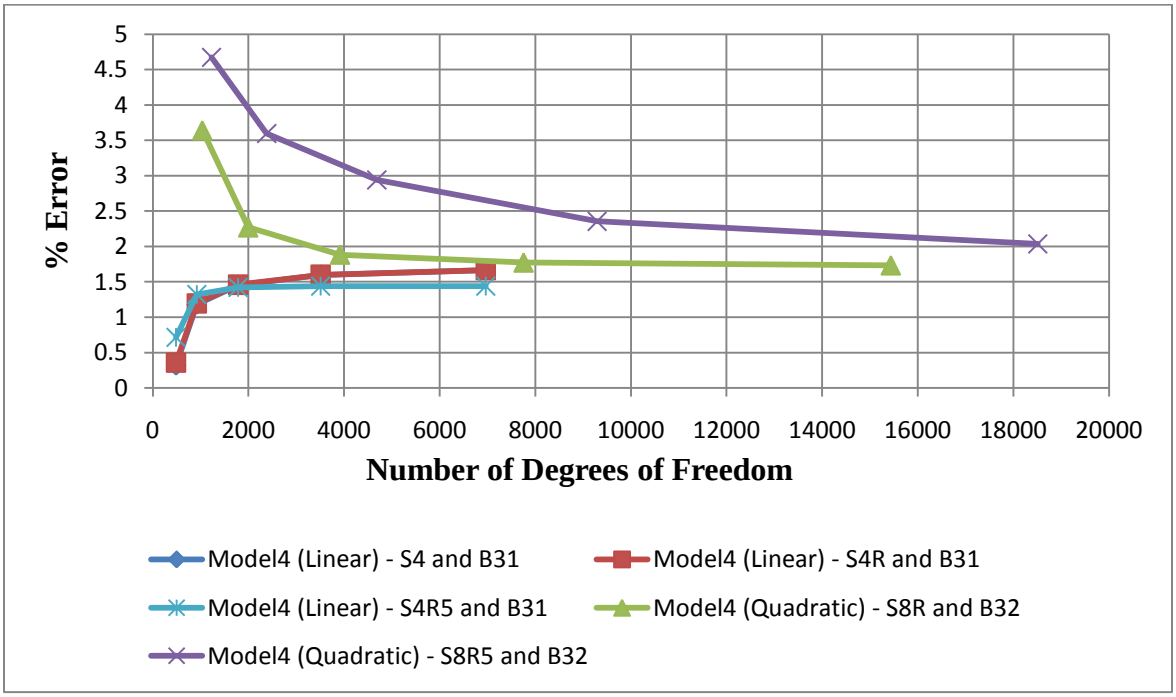

Figure 3.16: Comparison between the Fundamental Frequency of Vibration and the Analytical Solution for Model-4

The numerical evaluation carried out shows that Model-2, Model-3 and Model-4 require significant mesh refinement to converge, while Model-1 was able to produce results with less than 1.5% error irrespective of the level of mesh refinement. Therefore, Model-1 was selected to predict the global response of the bridge. While other models would be used when the local behavior of the bridge or detailed modeling of cross bracing or partial composite action is considered.

3.2.3 Modeling of Secondary Elements

Secondary elements, such as bracing, diaphragms, and guardrails, are intrinsic parts of bridge superstructures and may have a significant effect on their response to loads. This is because they not only add mass but also stiffness to the structure which affects the structural response. In this subsection, a thorough investigation is carried out to study the effect of explicitly modeling these secondary elements on the response of bridges.

3.2.3.1 Bracing

Two different methods were considered to model the bracing. In the first method, each part of the bracing assembly was modeled using single linear beam element (ABAQUS B31). Since, no member loads were applied to the bracing the maximum order of the deflected shape would be cubic and the shape functions assumed in case of linear beam element are cubic. Therefore, it should able to represent the deflected shape correctly.

In the second method, entire bracing assembly was represented by a single beam element modeled at the girder centroid. The effective cross sectional area was calculated by imposing unit displacement in the horizontal direction to the bracing assemblage. This effective cross sectional area as calculated using Equation 3.8 was assigned to the beam element with very low moment of inertia so that the beam element behaves as an axial member. Rigid links were used to connect the bracing with the girder. If the connection details were available between the bracing and girder, spring elements can be used to model the connection.

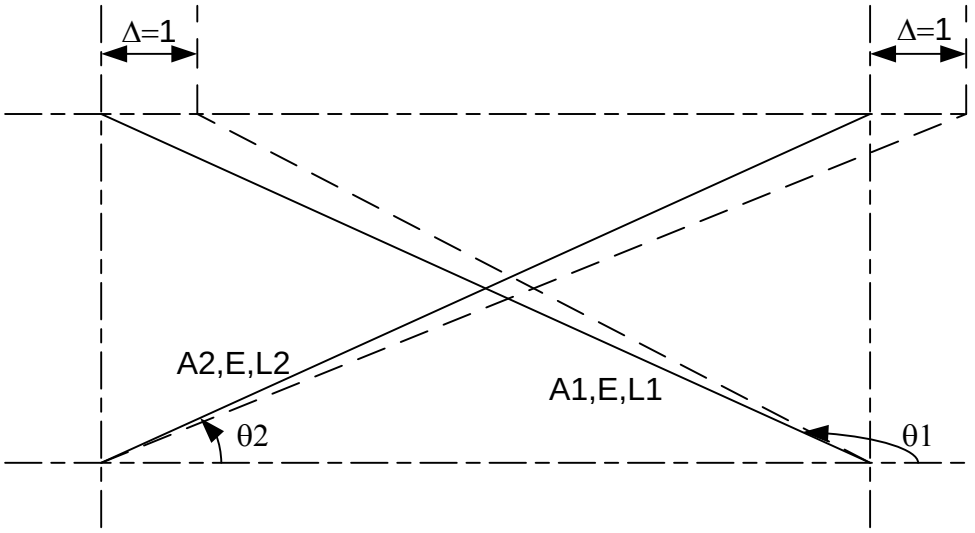

Figure 3.17: Bracing Effective Cross Sectional Area

$$\frac{A_{effective}}{L} = \sum_{i=1}^{n} \frac{A_i}{L_i} (\cos\theta)^2 \qquad \textbf{Equation 3.8}$$

Where,

$A_{effective}$	Effective cross sectional area
L	Girder spacing
A_i	Cross sectional area of bracing element
L_i	Length of bracing element
θ	Angle between the bracing element and the positive direction of the x-axis measured in the clockwise direction.

3.2.3.2 Guardrail

Depending on the type of guardrail and the details of its connection to the bridge deck, the level of stiffness contribution of the guardrail to the bridge superstructure will vary. In this study, the two extreme cases were considered: full composite action and no composite action. To model composite action two different methods were used to model the guardrails. In the first method, guardrails were modeled explicitly using beam elements placed at its centroid. Rigid links (Beam connector in ABAQUS) were used to model the full composite action between the

guardrail and bridge deck. In this modeling style, when the connection details are available then the rigid links can be replaced by spring elements with appropriate stiffness to model the connection.

In the second method continuous guardrails were modeled implicitly as an additional slab width ($\Delta\omega$) along the entire length of the bridge calculated using Equation 3.9 (AASHTO 2008).

$$\Delta\omega = \frac{A_b}{2t_s} \qquad \textbf{Equation 3.9}$$

Where,

A_b Cross sectional area of guardrail

t_s Thickness of deck slab

For the case where no composite action is expected, only the guardrail's mass not its stiffness was modeled. To achieve this, the nonstructural mass option in ABAQUS was used and the guardrails' mass was a uniformly distributed over the area occupied by the guardrails.

3.2.4 Modeling of Composite Action

The modeling of both full and zero composite action between concrete deck and girders as well as between concrete deck and guardrails were considered in this investigation. To model full composite action, rigid links were used. Rigid links kinematically constrain all six degrees of the freedom between the two connected nodes. Alternatively to using rigid links, multi-point constraints in ABAQUS(2007) could have been used. Multi-point constraint eliminates degrees of freedom at the slaved node using Lagrange multipliers, thus, reducing the size of stiffness matrix. Therefore, no external load can be applied directly to degrees of freedom of slaved nodes. Rigid links, on the other hand, do not eliminate degrees of freedom at the slaved nodes, which allows for the application of external loads and constraints at the slaved nodes.

When the eccentric beam model was used to model the bridge superstructure, an additional node was inserted at the top of top flange. Spring elements and rigid links were connected in series to model the partial composite action as shown in Figure 3.18. When Model-2, Model-3, and Model-4 were used to model the girders, then spring elements were used to connect the top flange to the bridge deck as shown in Figure 3.8, Figure 3.11 , and Figure 3.14, respectively.

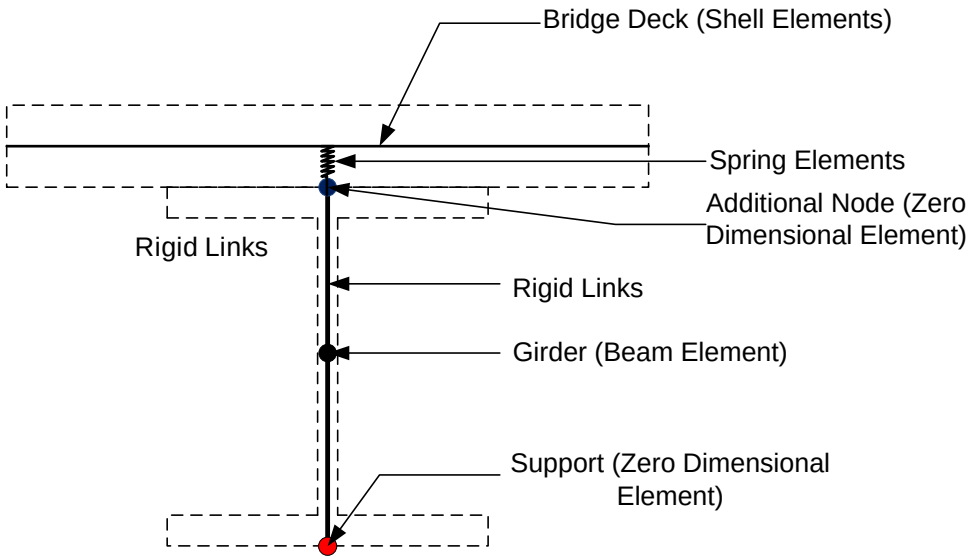

Figure 3.18: Eccentric Beam Model with Spring Elements and Rigid Links in Series to Model Partial Composite Action

3.2.5 Modeling of Boundary Conditions

In this study, the bridge substructure such as piers and abutments were assumed to be perfectly rigid. Therefore, the supports were modeled by restraining the appropriate degrees of freedom at the underside of the bottom flange using zero dimensional elements. Rigid links were used to connect the girders to the zero dimensional elements. To simulate a pin support, displacements in all three directions were constrained. To model a roller support, vertical and transverse displacements as well as the rotations along longitudinal and vertical axes were constrained. To model a frozen support, displacements and rotations in all three directions were constrained. However, the actual support condition lies in between the ideal support conditions discussed. If the actual support details or field test results are available then spring elements can be used to simulate the actual level of restraining provided by the supports.

3.3 Summary

This chapter assessed the suitability of different modeling techniques and elements used to model primary bridge elements. All the shell elements in ABAQUS library were found to be adequate to model the behavior of bridge deck. Model-1 (Eccentric beam model) was selected to model the global behavior of the girders while Model-3 was selected to model the localized

response of the bridge or detailed modeling of bridge components. Different methods that will be used in future to model the secondary bridge elements, composite action and boundary conditions were discussed in detail in later half of the chapter.

4 Effect of Bridge Parameters on the Response of Bridges

The main objective of this chapter is to validate the adopted modeling techniques described in chapter 3 using the field data available in the literature. More specifically, two bridges were considered: Colquitz River Bridge in Canada (Ventura et al. 1996) and the Wildcat Creek River Bridge in Indiana (Machado 2006). This chapter begins with description of each bridge and then the comparison between results obtained in the field, and the ones obtained using finite element analysis.

4.1 Case Study Bridges

This section provides the detailed description of each bridge and the assumptions made in their respective finite element models.

4.1.1 Wildcat Creek River Bridge

Experimental testing for the determination of natural frequencies of the Wildcat Creek bridge was carried out by Machado(2006). The 216-ft bridge has five spans (28ft + 50ft + 60ft + 50ft + 28ft) and is 27ft-10in wide. The first and last spans are separated from the three spans in the middle by expansion joints. In this investigation, it was assumed that the expansion joint completely separates the three internal spans from the end spans making them behave independently. Therefore, only the three intermediate spans were considered for the present finite element analyses. The bridge has a 15 degrees skew and a 7in. reinforced concrete deck that is supported by five continuous steel girders (W30x124) spaced at 5ft-7in. as shown in Figure 4.1. It was assumed that the diaphragms (C15x33.9) were connected to the girders at every 12 ft, starting at 2ft from the abutment. The reinforced concrete guardrail was assumed to act fully composite with the bridge deck. The details of the geometry of its cross section are shown in Figure 4.2. Finally, the material properties of the bridge components used in the analyses are provided in Table 4.1. To study the effect of assumptions made for the analyses and the effect different modeling parameters a detailed parametric study was carried out and the results are discusses later in the chapter.

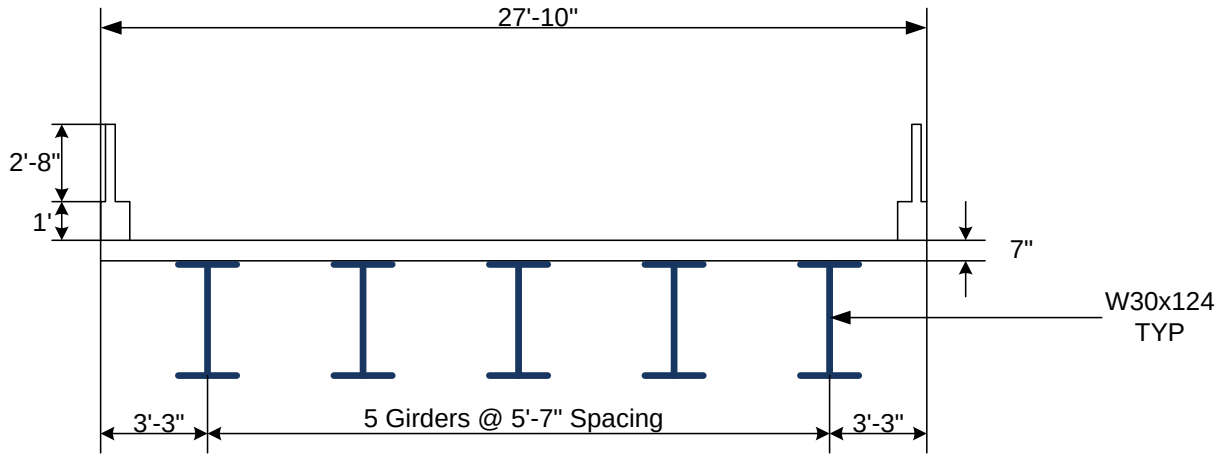

Figure 4.1: Cross Section of Wildcat Creek River Bridge

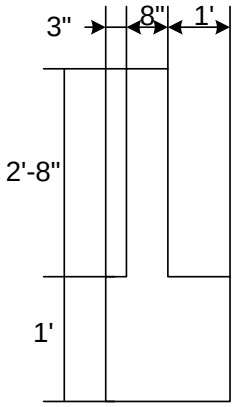

Figure 4.2: Guardrail Cross Section

Table 4.1: Material Properties (Wildcat Creek River Bridge)

Bridge Component	Young's Modulus of Elasticity	Unit Weight	Poisson's Ratio
Deck Concrete and Guardrail (f_c'= 3ksi)	3625 ksi	150 lb/ft^3	0.2
Girder and Diaphragms	29000 ksi	490 lb/ft^3	0.3

Figure 4.3 shows the comparison between the analytical and experimental frequency of vibration for this bridge modeled with skew. For this analysis, the left most support was pinned and all other supports were rollers. Bridge deck was modeled using thin shell (S8R5) and thick shell (S8R) elements, and girders, bracing and guardrail were modeled using B32 beam elements.

Thick shells yielded a 1% stiffer response than that obtained using thin shell. This is not surprising, since the displacement based finite element analysis is known to provide stiffer response (Cook et al. 2001).

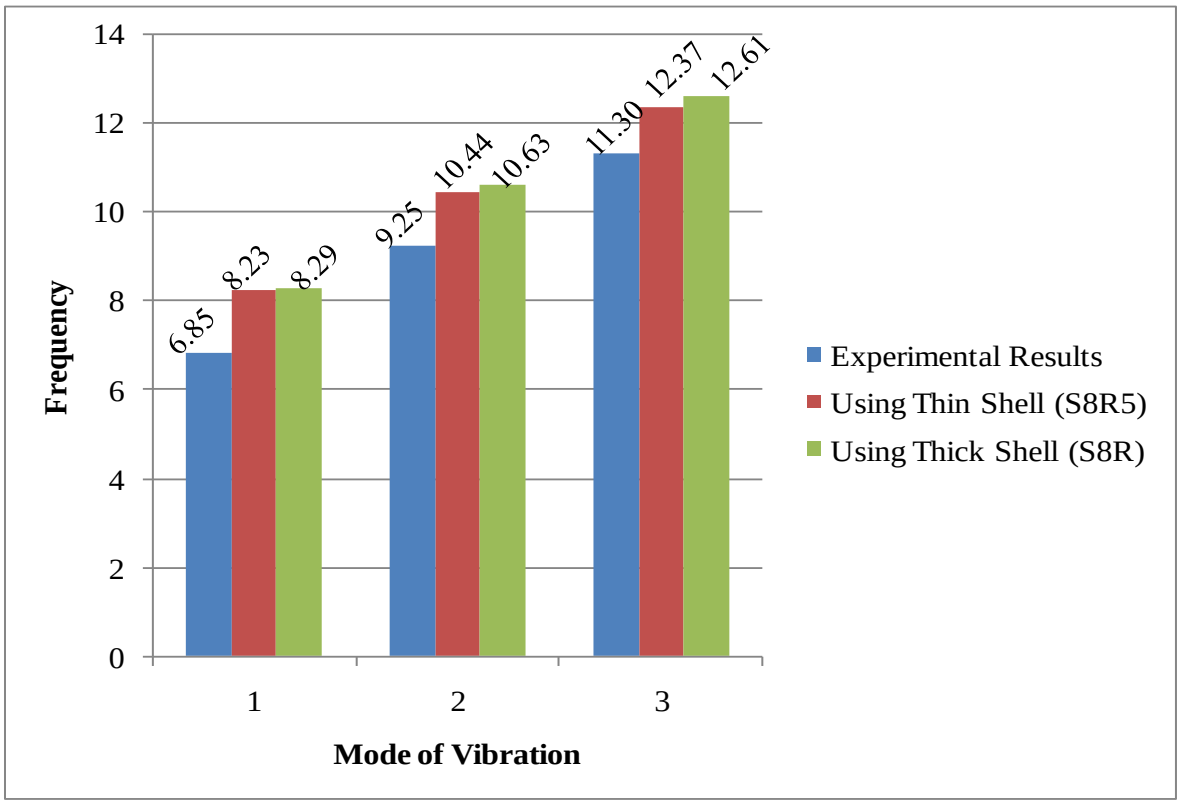

Figure 4.3: Element Formulations and Natural Frequency

4.1.2 Colquitz River Bridge

Ventura et al. (1996) determined the dynamic characteristic of a five span continuous bridge using the pullback test. The bridge has a total length of 270ft and five spans of various lengths (46ft + 59ft + 60ft + 59ft + 46ft) and is 39ft wide. Six continuous steel girders (W33x141) support the 7.08 in. concrete deck spaced at 6ft-6in. center to center spacing as shown in Figure 4.4. The girders rest on the abutments and four concrete bents. Each span has three intermediate diaphragms (MC18x42.7) as well as end diaphragms (MC18x42.7) over the end abutments and interior piers. The bridge deck has a wearing surface with a varying thickness of 2in. to 3.5in. For which no further details were available, therefore its mass and stiffness both were neglected in the model. As was done in the previous case study, the supports were modeled at the bottom of the girder and effect of substructure on the dynamic response was neglected. The concrete

guardrail (7.5in.x2ft) was assumed to be fully composite with the bridge deck. Finally, the material properties adopted in the model are given in Table 4.2.

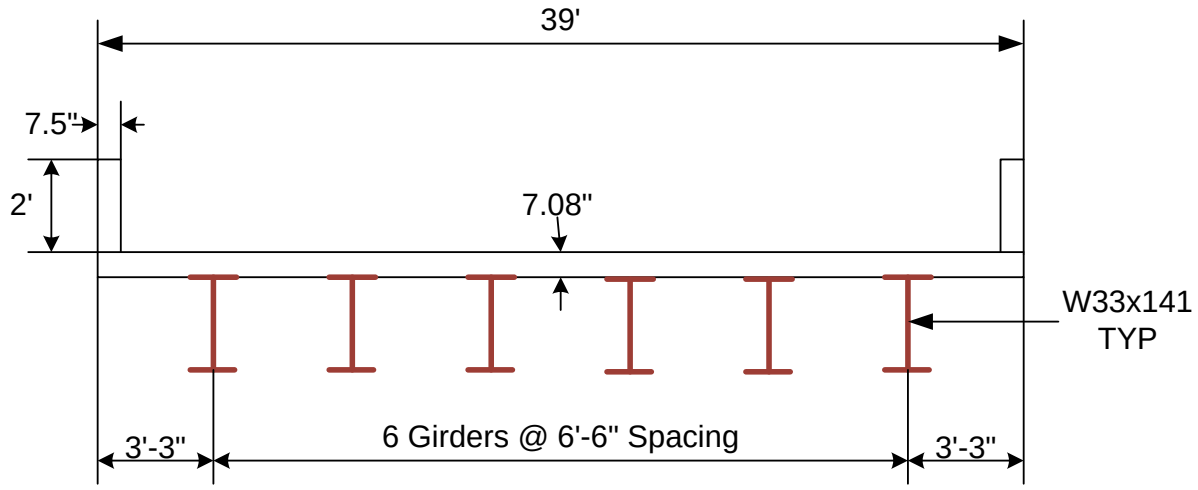

Figure 4.4: Cross Section of Colquitz River Bridge

Table 4.2: Material Properties (Colquitz River Bridge)

Bridge Component	Young's Modulus of Elasticity	Unit Weight	Poisson's Ratio
Deck Concrete and Guardrail (f_c'= 4ksi)	3834 ksi	150 lb/ft^3	0.2
Girder and Diaphragms	29000 ksi	490 lb/ft^3	0.3

Figure 4.5 shows the comparison between the analytical and experimental frequency of vibration. For this analysis, the left most support was assumed pinned and all other supports were assumed roller. The bridge deck was modeled using thin shell (S8R5) and thick shell (S8R) elements, and girders, bracing and guardrail were modeled using B32 beam element. Use of thick or thin shells to model the bridge deck had a very small impact on the natural frequency of the bridge predicted by finite element analysis and both element formulations yielded frequencies stiffer that that obtained experimentally.

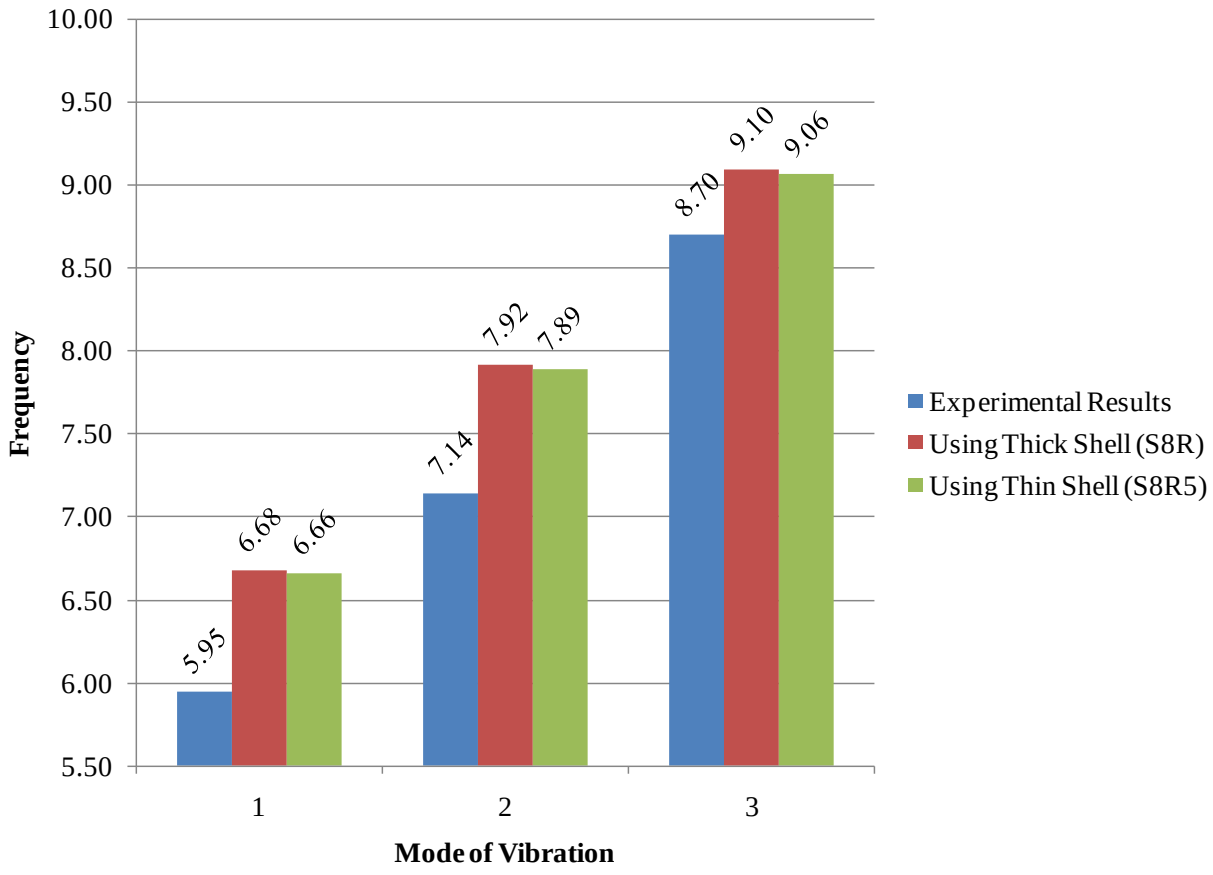

Figure 4.5: Element Formulations and Natural Frequency

4.2 Effect of Skew

To study the effect of skew on the modal response of the bridge, two separate models of Wildcat Creek River Bridge were analyzed. For both models with 15 degree skew and without skew, the left most support was assumed pinned and all other supports were assumed rollers. For this analysis, both thin and thick shell elements were considered, and full composite action was assumed between the bridge deck and girder, and guardrail and bridge deck.

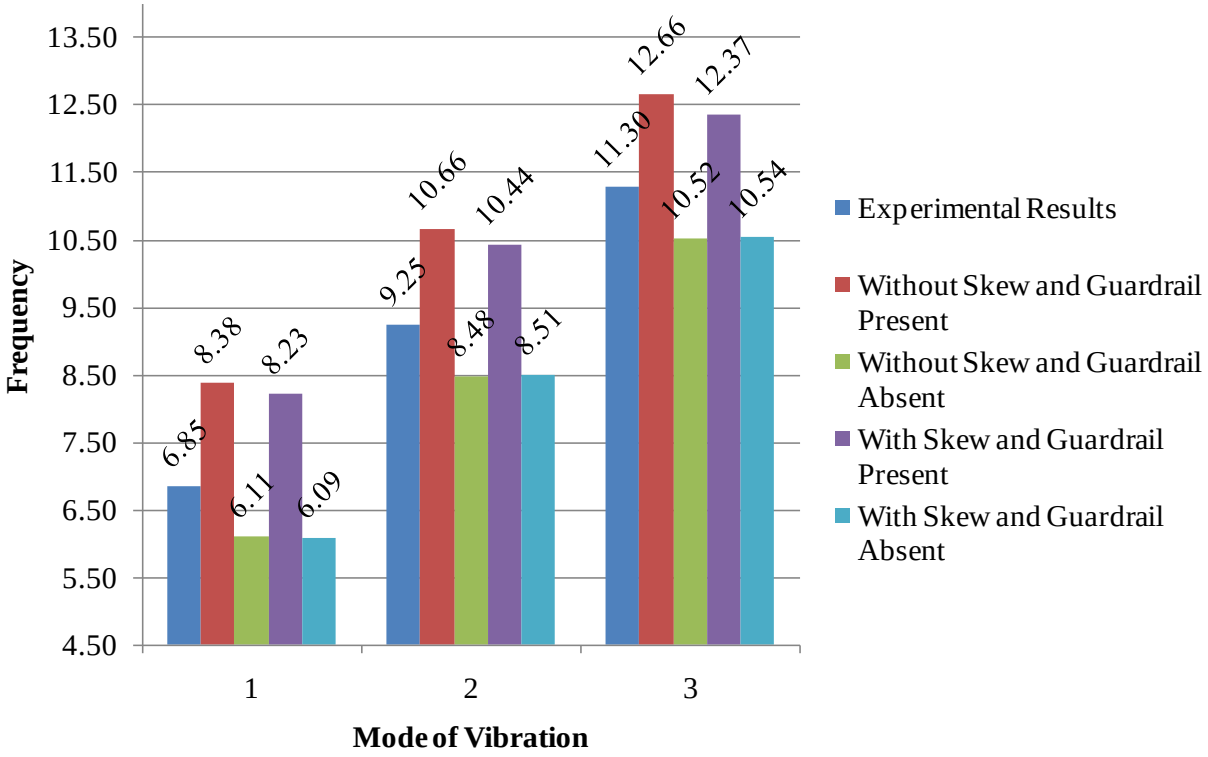

Figure 4.6: Effect of 15 degree Skew and Guardrail on Natural Frequency (Bridge Deck – S8R5 and Girders, Bracing and Guardrail – B32)

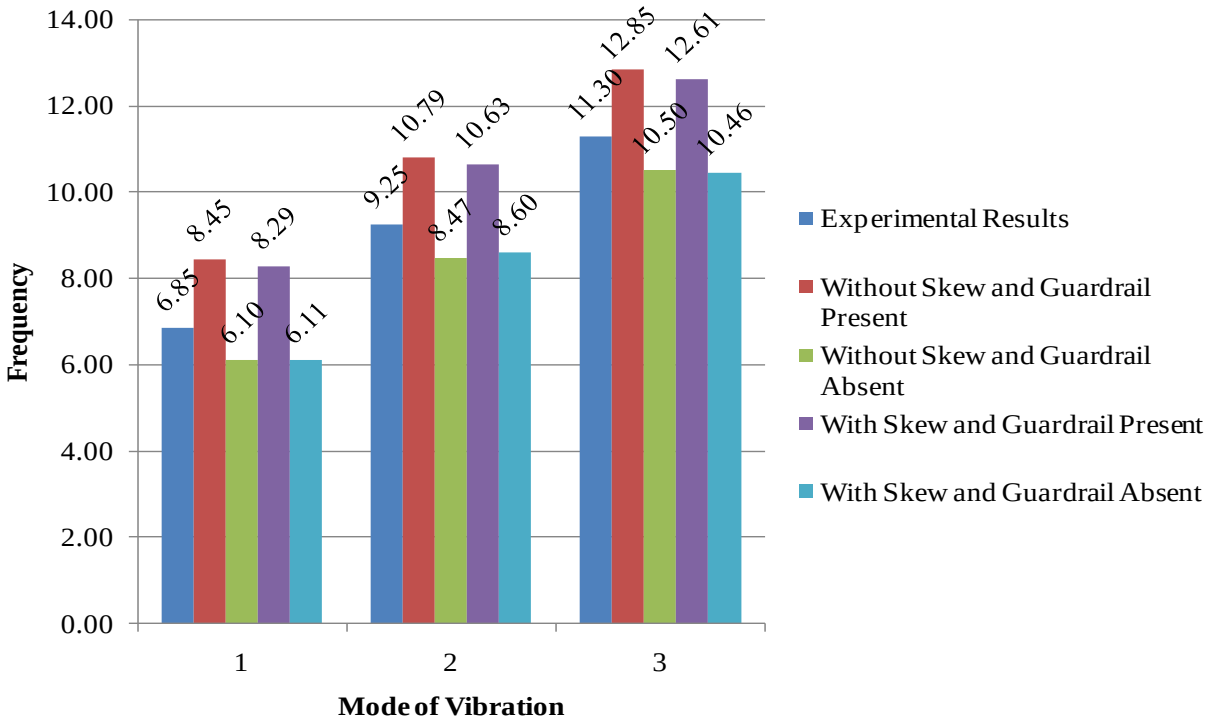

Figure 4.7: Effect of 15 degree Skew and Guardrail on Natural Frequency (Bridge Deck – S8R and Girders, Bracing and Guardrail – B32)

Figure 4.6 and Figure 4.7 show the comparison between the analytical and experimental frequency of vibration for the bridge when the bridge was modeled without and with skew respectively. The first three frequencies of vibration were lower in case of a skewed bridge. This effect will be more predominant in case of a bridge with higher skew. Similar to previous case, use of thick shell to model bridge deck yielded stiffer response than when thin shell was used.

4.3 Effect of Guardrail Idealizations

To investigate the effect of guardrail on bridge response, three different approaches discussed previously in Section 3.2.3.2 were used. For both the bridges, the left most support was assumed pinned and all other supports were assumed roller. Eccentric beam model was used for this study in which the bridge deck was modeled using thin shell (S8R5), and girders, bracing and guardrail were modeled using beam element B32.

4.3.1 Wildcat Creek River Bridge

From the results shown in Figure 4.6 and Figure 4.7, it can be seen that guardrail modeling has a significant effect on the response of the bridge. Therefore, further investigation was carried out. The results are as presented in Table 4.3. It should be noticed that when the guardrail was modeled as a non-structural mass for a skewed bridge with staggered bracing the third flexural mode could not be obtained. From the results, it can be seen that none of these methods were able to give a close representation of the effect that the guardrails' mass and stiffness impart on the bridge. However, these methods were able to bracket the measured response. There are many other factors that could have affected bridge response, such as actual support conditions and the materials' properties.

Table 4.3: Effect of Different Guardrail Modeling Techniques on the Modal Response Using Eccentric Beam Model

Guardrail Modeling	Flexural Mode					
	1st Mode	% Error	2nd Mode	% Error	3rd Mode	% Error
Experimental Results	6.85		9.25		11.3	
Bridge Modeled without Skew						
Using Beam Element	8.38	-22.35	10.66	-15.27	12.66	-12.0
Using Additional Width as per AASHTO (2008)	5.63	17.83	7.72	16.52	9.39	16.95
Using Non-Structural Mass	5.04	26.48	6.94	25.02	8.46	25.17
Guardrail Absent	6.11	10.87	8.48	8.29	10.52	6.88
Bridge Modeled with Skew and Staggered Bracing						
Using Beam Element	8.23	-20.09	10.44	-12.88	12.37	-9.46
Using Additional Width as per AASHTO (2008)	5.60	18.26	7.68	16.95	9.22	18.42
Using Non-Structural Mass	5.10	25.49	7.07	23.63	-	-
Guardrail Absent	6.10	11.02	8.51	7.99	10.54	6.74

4.3.2 Colquitz River Bridge

Using beam elements yielded stiffer response as compared to experimental results because this simulates full composite action which may not be the case in the field. Furthermore, the adopted boundary condition for these models were assumed to be Pin-Roller-Roller, which as seen before produced stiffer response. Guardrail modeled implicitly using additional deck width and using nonstructural mass yield the response closests response to the experimental results. Higher modes of vibration were found less sensitive to the methods used to model guardrails.

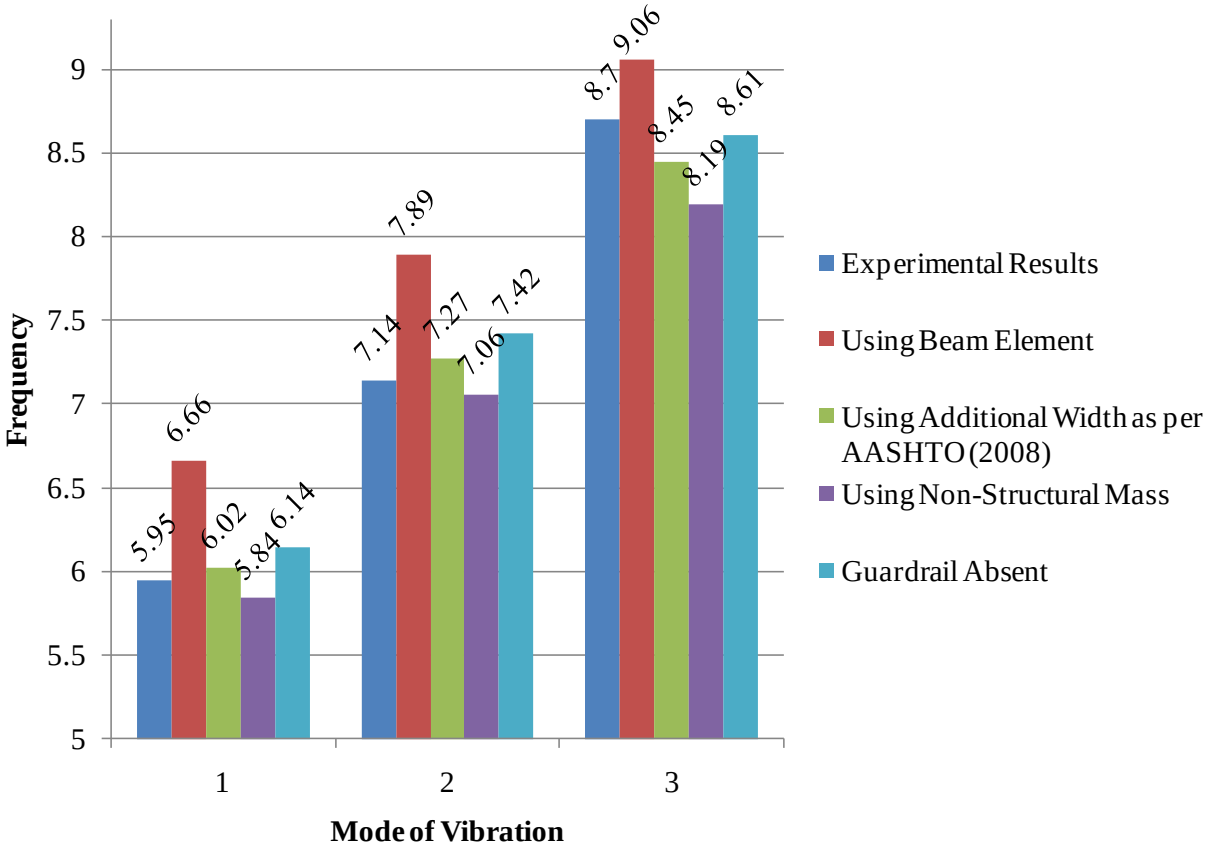

Figure 4.8: Effect of Different Guardrail Modeling Techniques on the Modal Response

4.4 Effect of Support Restraints

To investigate the effect of support restraints on the bridge response several combinations of support restraints were considered. For both the bridges, eccentric beam model was used for the study in which bridge deck was modeled using thin shell (S8R5), and girders, bracing and guardrail were modeled using beam elements (B32). Full composite action was assumed between the bridge deck and girders, and guardrail and bridge deck. Table 4.4 and Figure 4.9 shows the

effect of support restraint on both bridges. As can be seen, support conditions have a considerable effect on the modal response of the bridge. Also for the higher modes, the frequencies become less sensitive to the support variations.

4.4.1 Wildcat Creek River Bridge

Table 4.4: Effect of Support Restraint on Modal Response Using Eccentric Beam Model

Support Condition	Flexural Mode					
	1st Mode	% Error	2nd Mode	% Error	3rd Mode	% Error
Experimental Results	6.85		9.25		11.3	
Bridge Modeled without Skew						
Left Support Pinned and All Other Supports as Roller Support	8.38	-22.35	10.66	-15.27	12.66	-12.07
All Supports Pinned	11.72	-71.11	14.91	-61.16	15.11	-33.68
All Supports Frozen	12.47	-82.07	16.26	-75.83	16.30	-44.27
Bridge Modeled with Skew and Staggered Bracing						
Left Support Pinned and All Other Supports as Roller Support	8.23	-20.09	10.44	-12.88	12.37	-9.46
All Supports Pinned	11.45	-67.20	14.57	-57.51	14.76	-30.67
All Supports Frozen	12.21	-78.18	15.94	-72.35	15.97	-41.33

4.4.2 Colquitz River Bridge

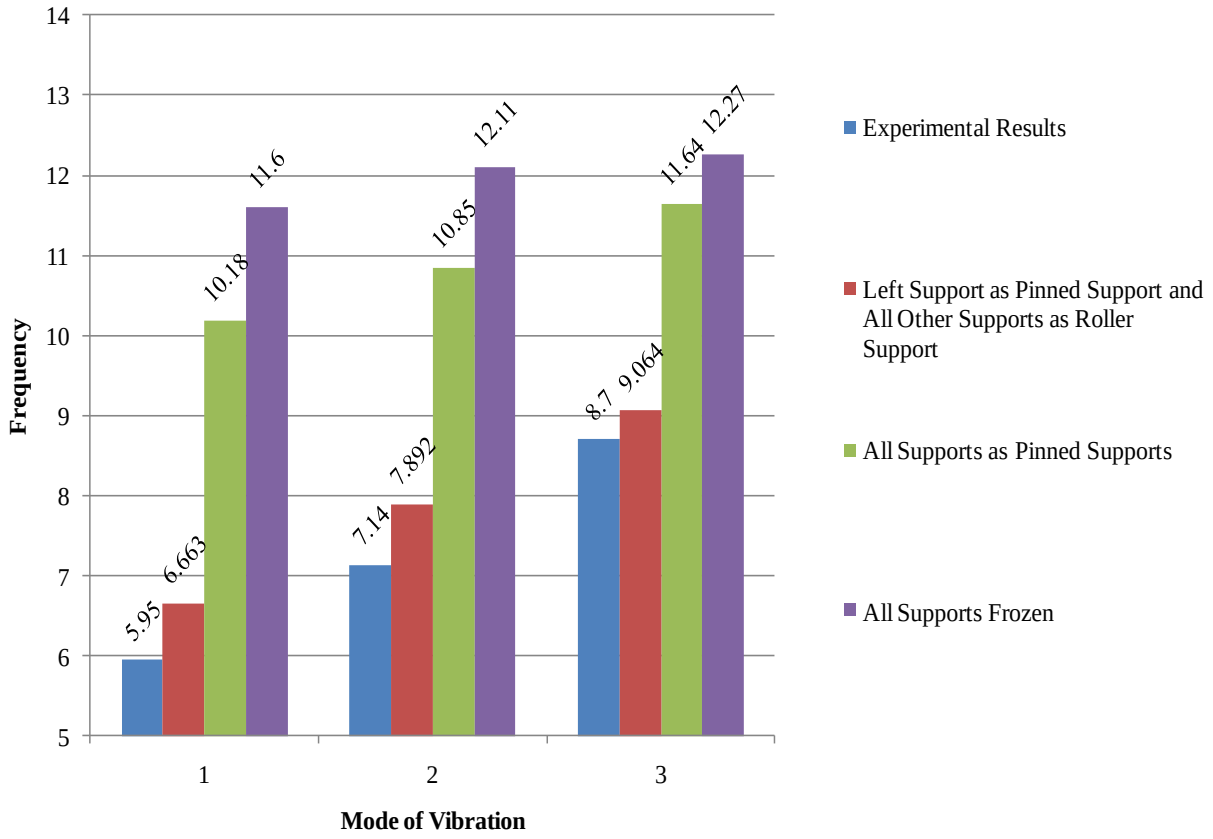

Figure 4.9: Effect of Support Restraint on Modal Response Using Eccentric Beam Model

4.5 Effect of Bracing

To investigate the effect of bracing on the modal response of the bridge, the bracing elements were idealized as either truss or beam elements. Once again, eccentric beam model was used for the study and the left most support was pinned and all other supports were rollers. As can be seen from the results, modeling the bracing using truss elements or beam elements does not appear to have any significant effect on the modal response. As expected, when bracing was not considered in the model, the structure's response was more flexible. It is expected that the inclusion or not of bracing in a model would have a considerable impact on the obtained torsional modes of vibration.

4.5.1 Wildcat Creek River Bridge

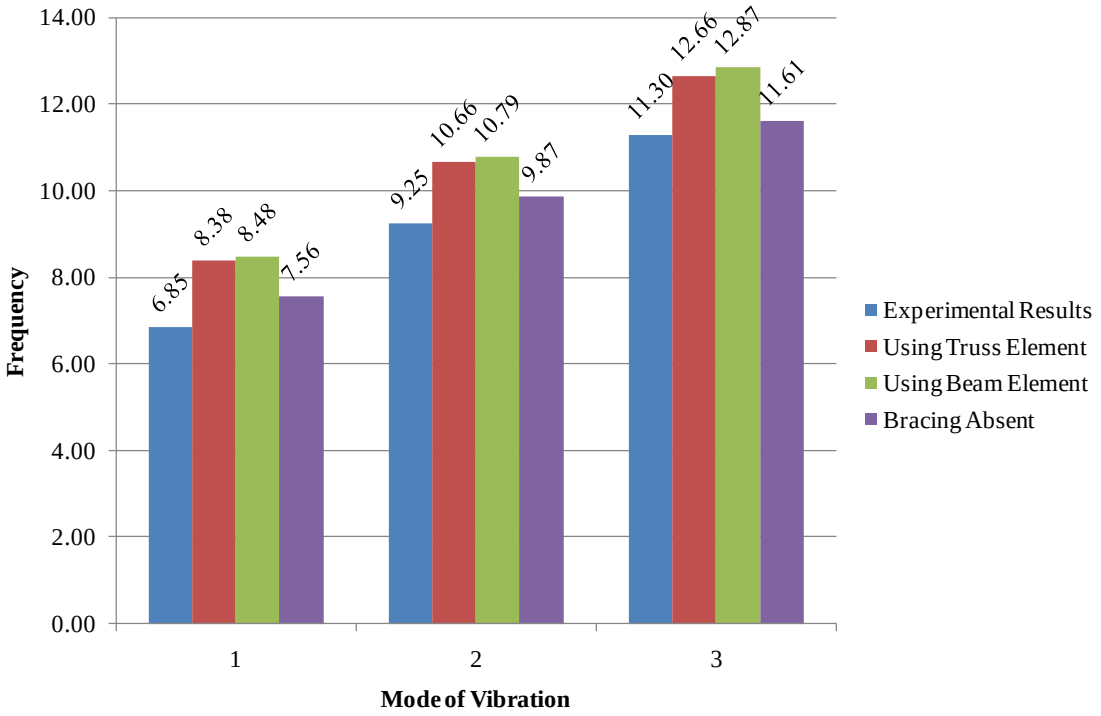

Figure 4.10: Effect of Different Bracing Modeling Techniques on Modal Response of Bridge Modeled without Skew

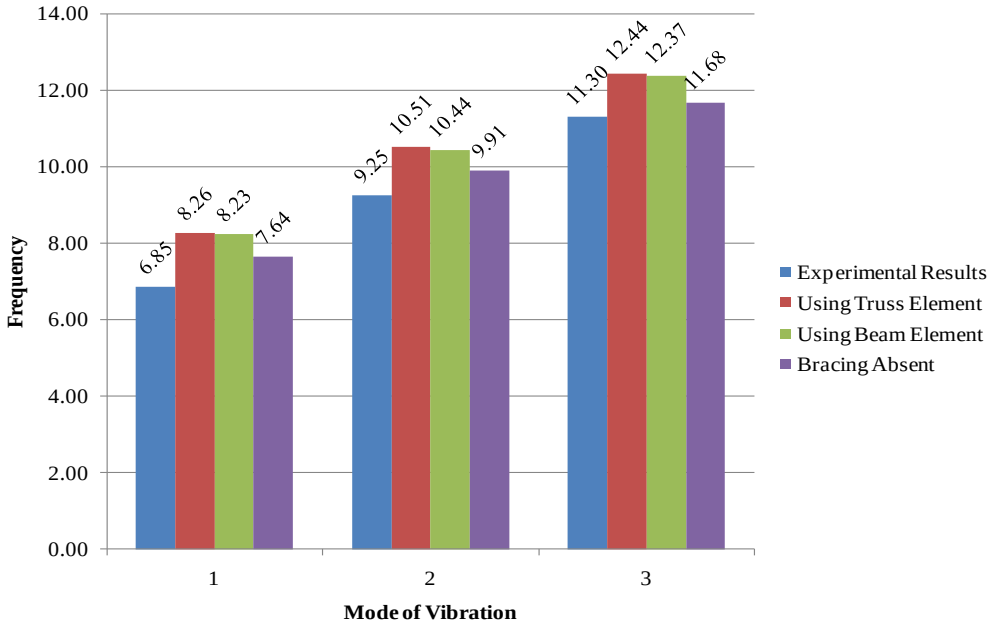

Figure 4.11: Effect of Different Bracing Modeling Techniques on Modal Response of Bridge Modeled with Skew and Staggered Bracing

4.5.2 Colquitz River Bridge

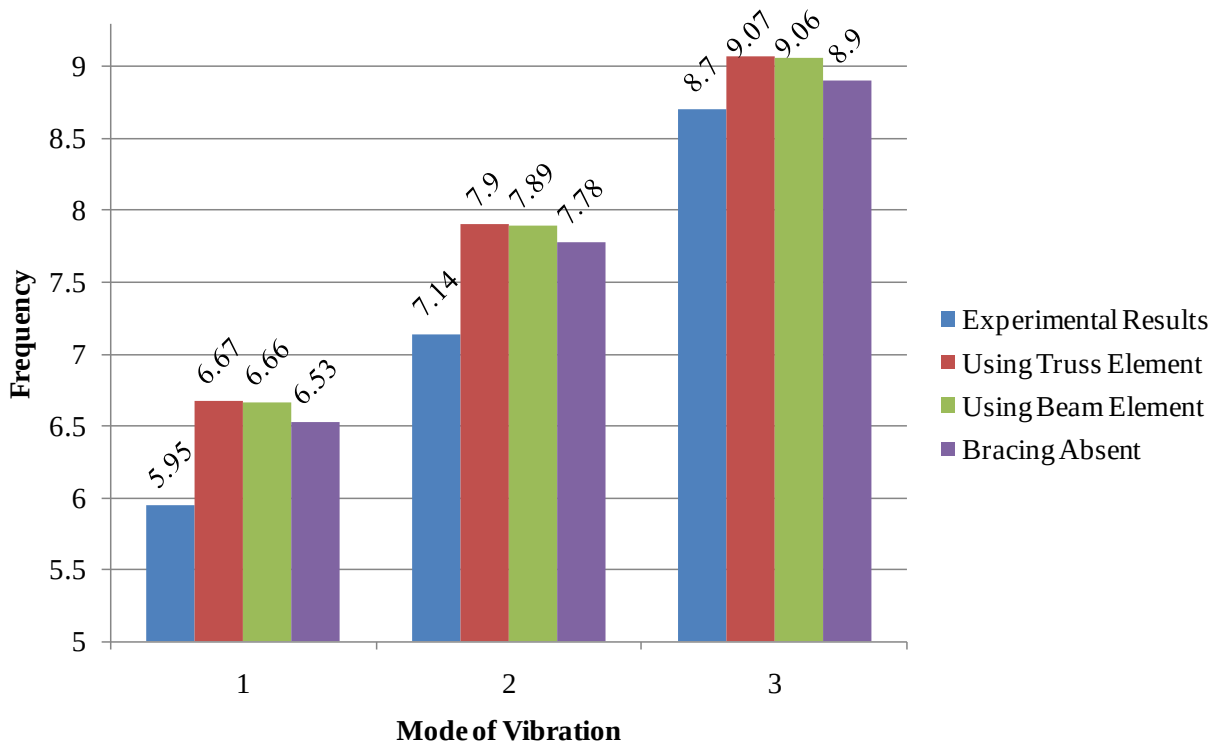

Figure 4.12: Effect of Different Bracing Modeling Techniques on Modal Response of Bridge

4.6 Effect of Thermal Gradient

Thermal gradient alters the modal response of the bridge because it introduces initial stresses and displacements in the structure. Linearly varying thermal gradient was assumed throughout the concrete deck and a constant temperature is assumed throughout the steel girder for both the bridges as shown in Figure 4.13. The assumed thermal gradient is similar to that of AASHTO thermal gradient for flexure with an additional constant temperature to account for axial deformation. The eccentric beam model as discussed before was used with different support conditions. Different combinations of support restraints were considered for this study to assess the impact of thermal gradient on them.

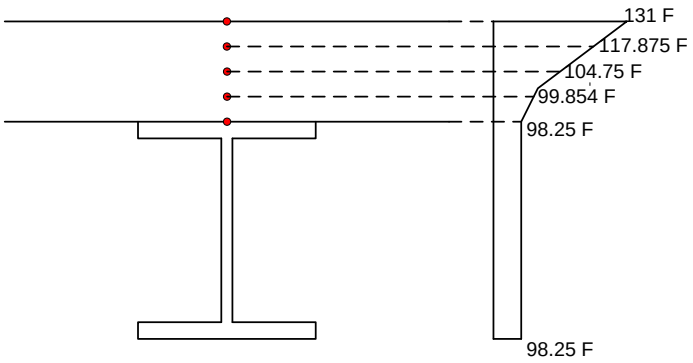

Figure 4.13: Thermal Gradient

4.6.1 Wildcat Creek River Bridge

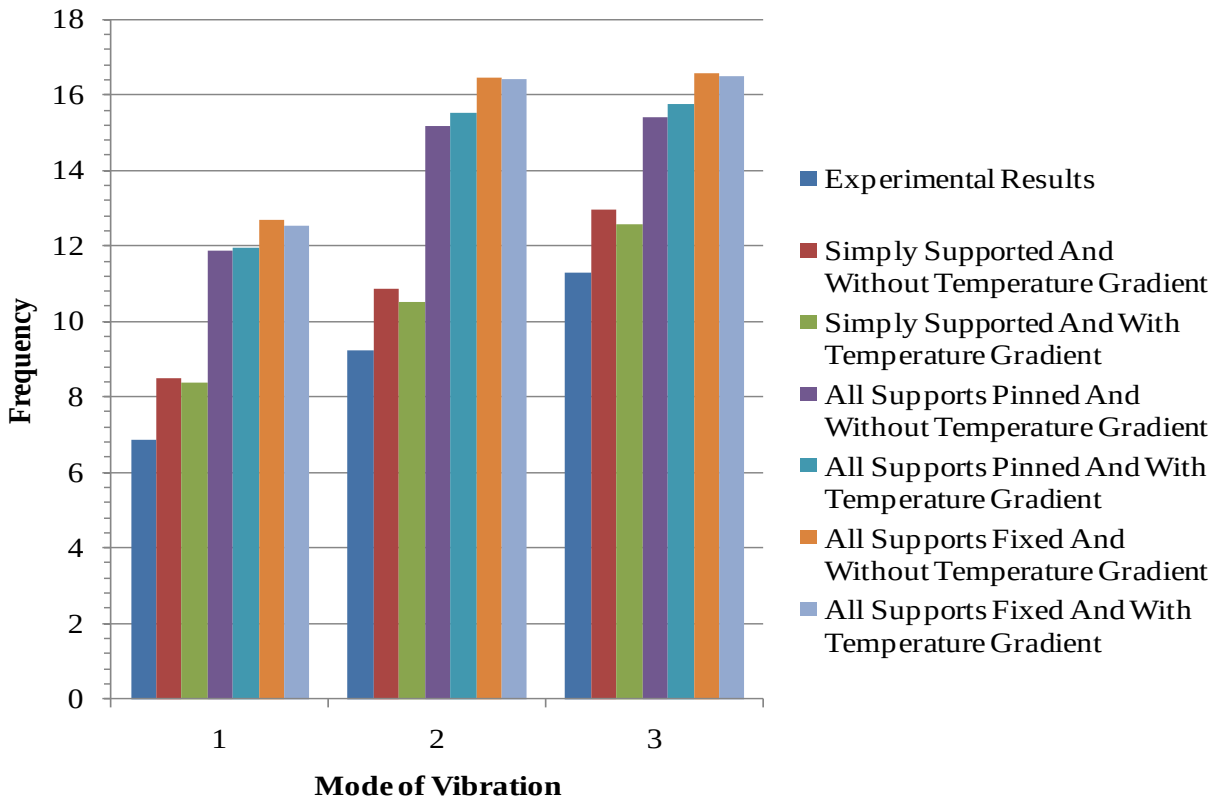

Figure 4.14: Effect of Thermal Gradient on Modal Response for a Bridge Modeled without Skew Using Eccentric Beam Model

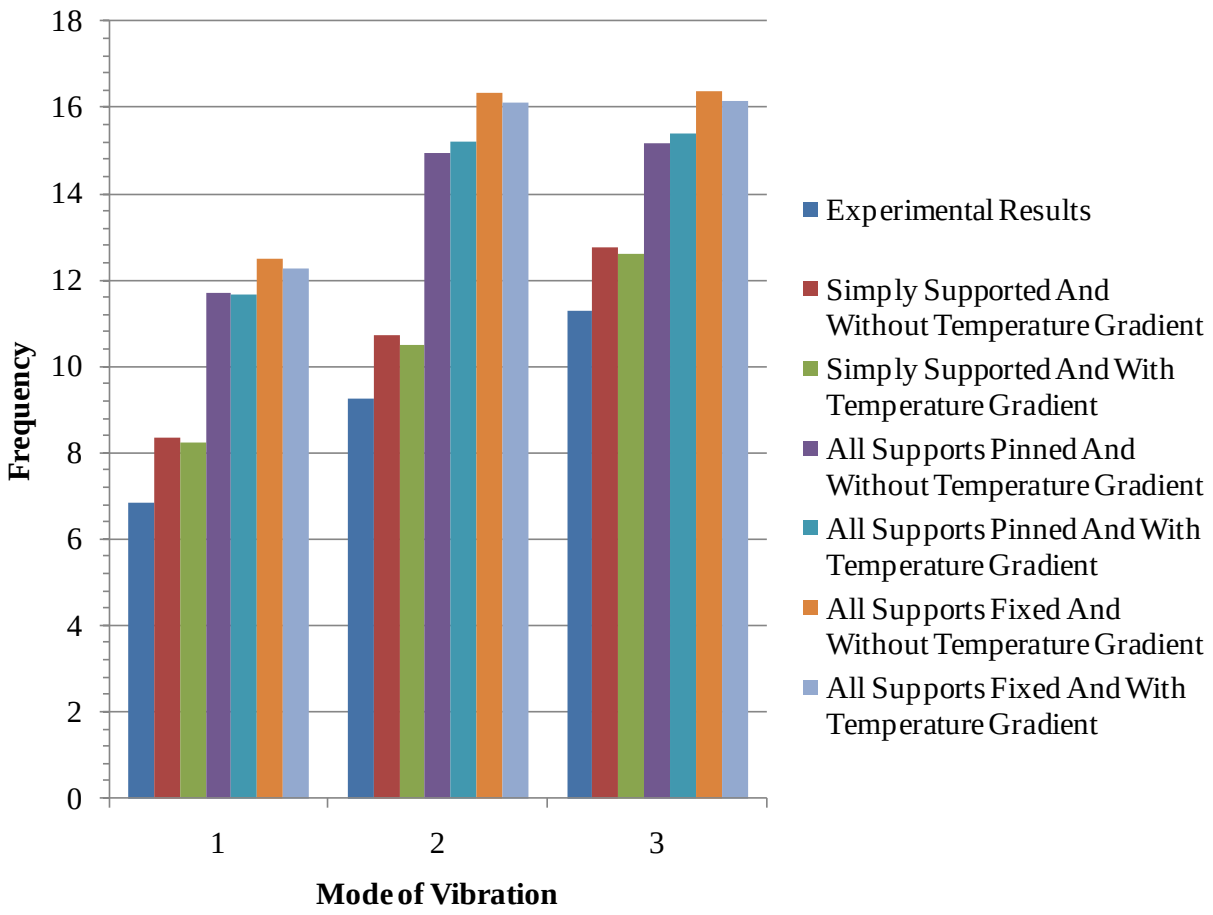

Figure 4.15: Effect of Thermal Gradient on Modal Response for a Bridge Modeled with Skew Using Eccentric Beam Model

The thermal gradient softens modal response of the bridge very slightly except for the case when all supports were pinned.

4.6.2 Colquitz River Bridge

The thermal gradient softens modal response for all the cases of support restraints.

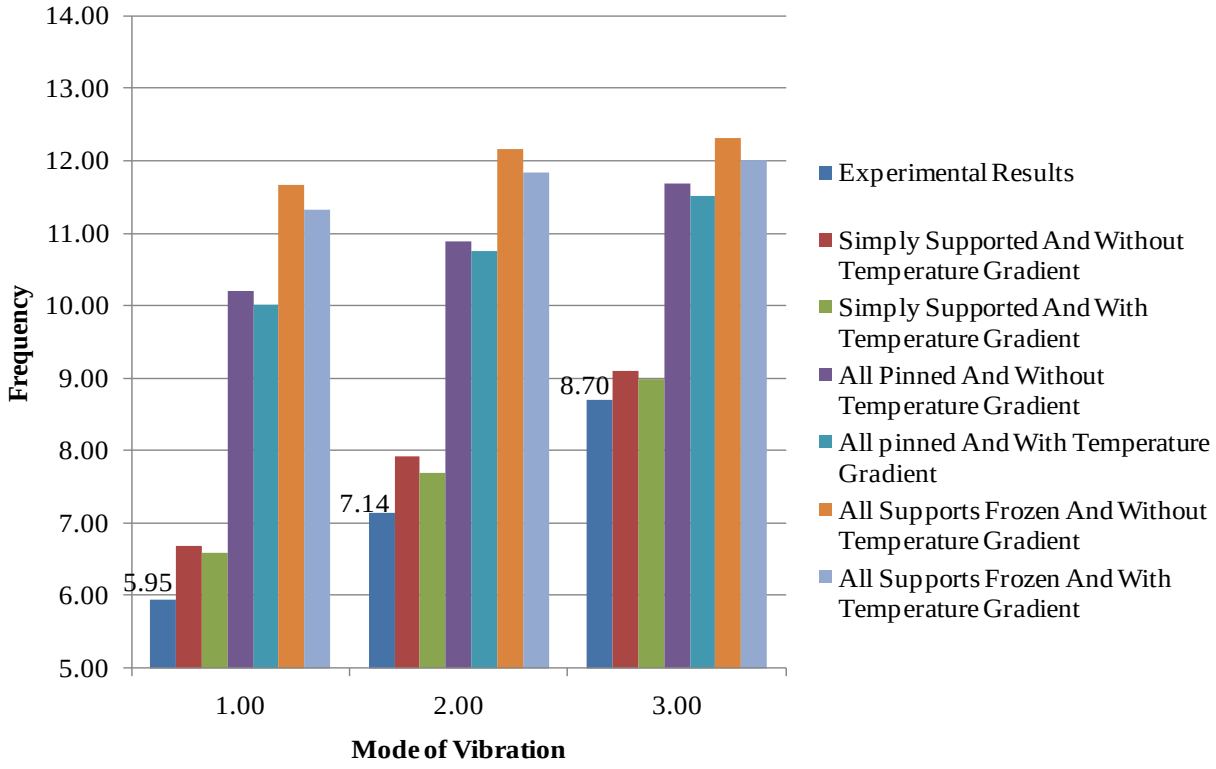

Figure 4.16: Effect of Thermal Gradient on Modal Response of a Bridge Modeled Using Eccentric Beam Model

4.7 Results Using Different Modeling Techniques

To evaluate capabilities of different modeling techniques to predict bridge response, both bridges were modeled using three different girder idealizations discussed in 3.2.2. For this analysis, the left most support was pinned and all other supports were rollers. Guardrail was modeled using beam elements and was assumed fully composite with the bridge deck. Also, girders were assumed to be fully composite with the bridge deck for this study. For all the three models considered, bracing was modeled using beam elements.

4.7.1 Wildcat Creek River Bridge

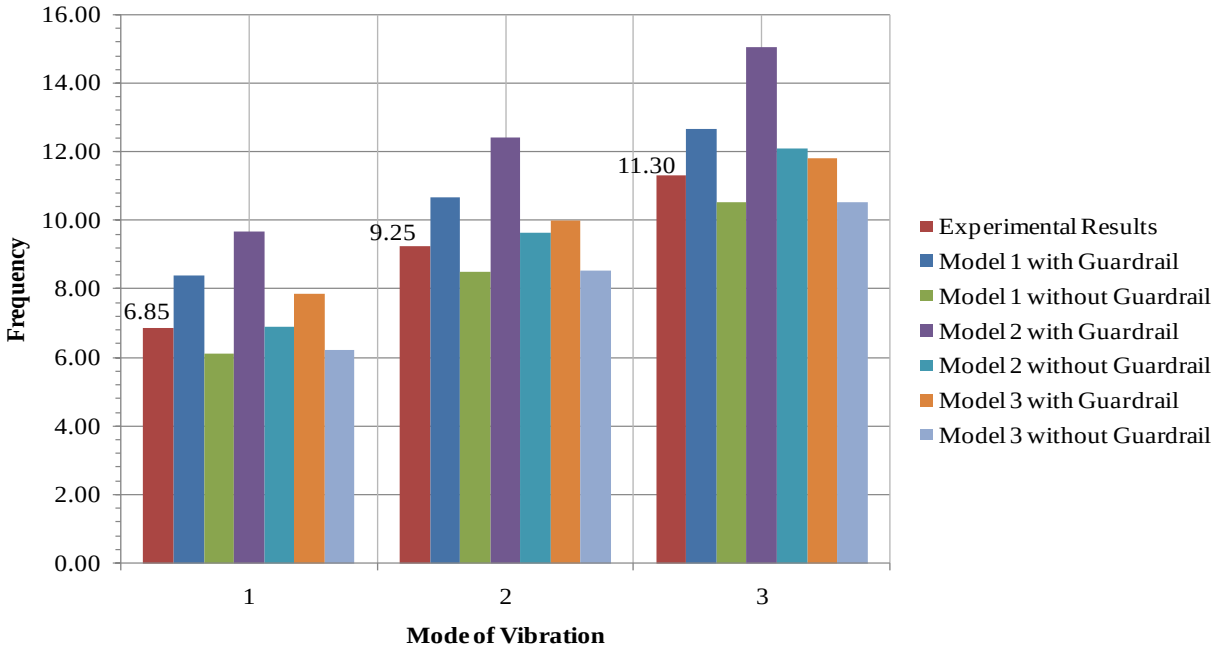

Figure 4.17: Modeling Techniques and Modal Response for a Bridge Modeled without Skew

4.7.2 Colquitz River Bridge

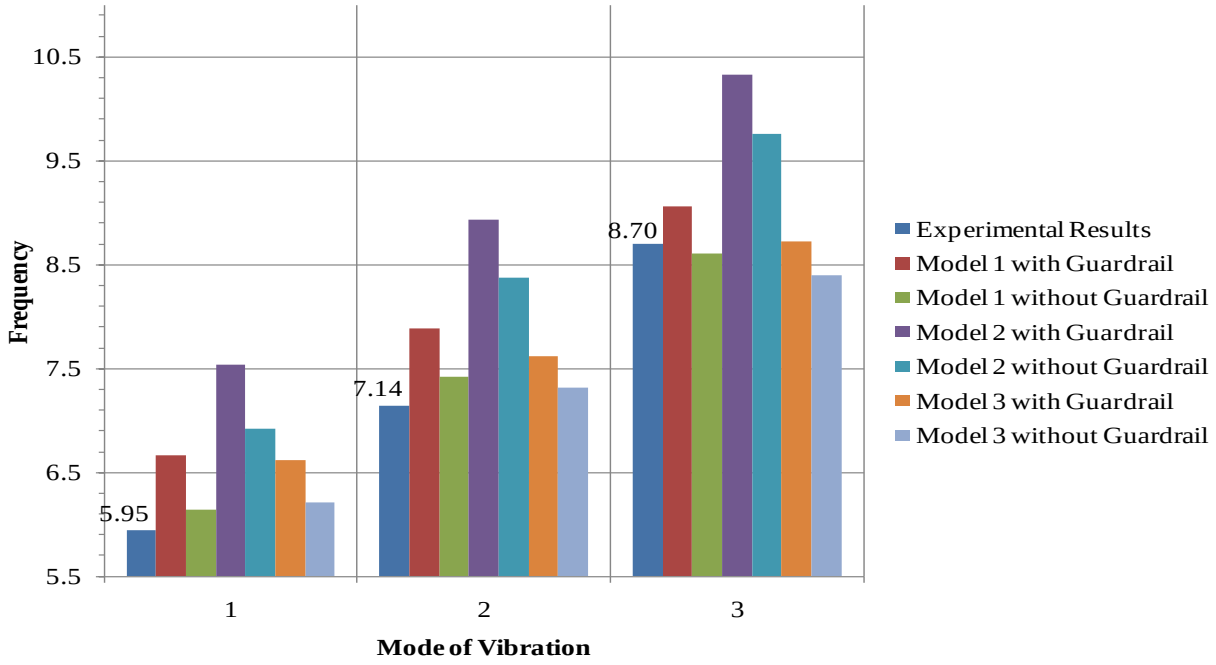

Figure 4.18: Modeling Techniques and Modal Response

For both the bridges, Model-2 showed much stiffer response. While Model-3 predicted more flexible response than Model-1 for all the modes. Therefore, Model-2 was not considered further in the analysis.

4.8 Summary

In this chapter, the different modeling techniques discussed in Chapter 2 were tested using the experimental data available for Wildcat Creek River Bridge and Colquitz River Bridge. Use of thin shell or thick shell to model the bridge deck had a slight impact on the natural frequencies predicted by the finite element analysis. In case of Wildcat Creek River Bridge, modeling skew and staggered bracing yielded more flexible response than that obtained using model without skew. Guardrail models and support restraint had a significant effect on the modal response. Bracing models and thermal gradient had slight impact on it.

5 Long Term Bridge Performance Program Virginia Pilot Bridge RT.15

5.1 Introduction

The first pilot bridge selected for the Long Term Bridge Performance project is located in Northern Virginia on Route 15. In the present study, a finite element model of the bridge was developed and analyzed for various loading conditions. Both the static and the dynamic behaviors of the bridge were investigated. In addition to understanding the bridge behavior, another goal of these analyses was to provide guidance for the field-testing instrumentation of the bridge as well as to help with decisions associated with the instrumentation for long-term monitoring of the bridge. In this chapter, the developed finite element model and the obtained static and dynamic responses of the pilot bridge are presented.

5.2 Description of the Virginia Pilot Bridge RT.15

The Virginia Pilot Bridge (Figure 5.1) is US Route 15 bridge over I-66 in Prince William County, Virginia. The southbound bridge of the two twin structures was selected for this study. It is a two span continuous bridge with total length of 272 ft. (136ft +136ft) with total width of 42 ft.; six continuous steel girders with varying cross section along the length support its 8.625 in. concrete deck. The varying cross section of the girder (Figure 5.2) was modeled using two different girder cross sections calculated using the weighted average as shown in Figure 5.8. The longitudinal and transverse stiffeners used to stiffen the girder web were not considered in the model because the stiffeners contribution to the girder stiffness is very small. The girders are spaced at 7ft-6in. center to center transversely as shown in Figure 5.3. The bridge has a skew of 17.45 degrees. The girders rest on the abutments at the ends and on piers at the interior support. Finally, the material properties of the bridge components used in the analyses are provided in Table 5.1.

Figure 5.1: Virginia Pilot Bridge RT.15 (Bapat 2009)

Figure 5.2: Haunched Girder Cross Section (Bapat 2009)

Table 5.1: Material Properties

Bridge Component	Young's Modulus of Elasticity	Unit Weight	Poisson's Ratio
Deck Concrete and Guardrail	4000 ksi	150 lb/ft^3	0.2
Girder and Diaphragms	29000 ksi	490 lb/ft^3	0.3

Figure 5.4 shows the dimensions of the precast guardrail cross-section. Guardrail segments were made composite with the bridge deck using anchor rods. For analysis purposes, the two extreme conditions were considered: a) the guardrail was modeled as fully composite, b) the guardrail was modeled as non-composite with the bridge deck. In the latter case, the guardrail imparted only mass to the structure. These two cases were selected to bracket the response. Figure 5.5, Figure 5.6 and Figure 5.7 show the schematic of the bracing and the structural members used in the bracing.

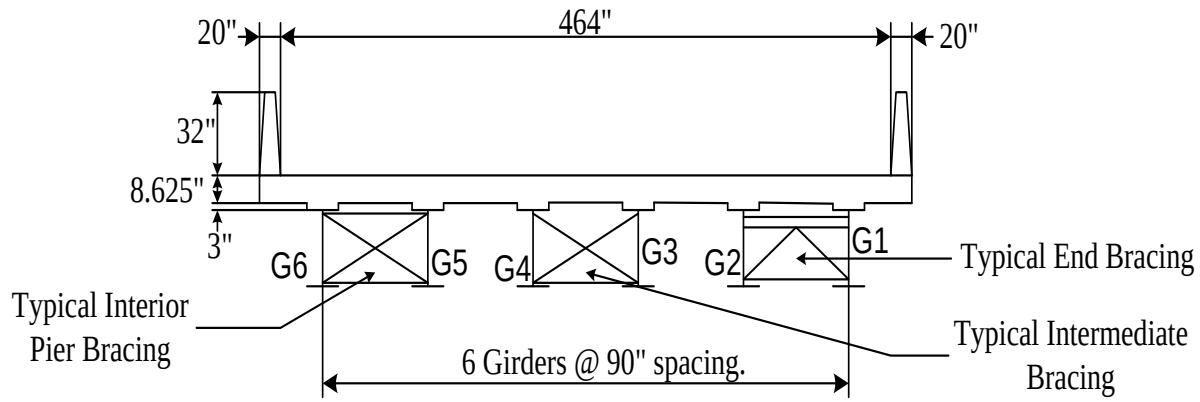

Figure 5.3: Virginia Pilot Bridge RT.15 Cross Section

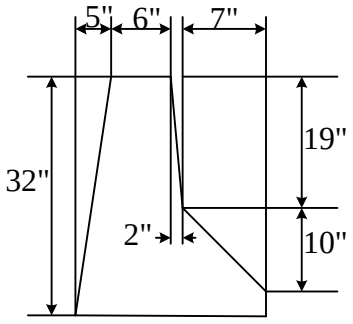

Figure 5.4: Guardrail Cross-Section

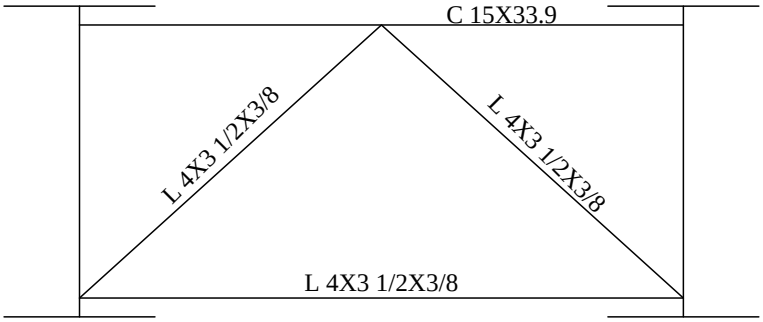

Figure 5.5: Typical End Bracing

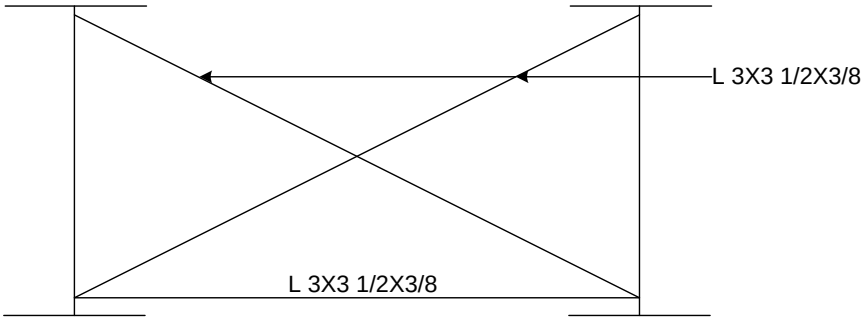

Figure 5.6: Typical Intermediate Bracing

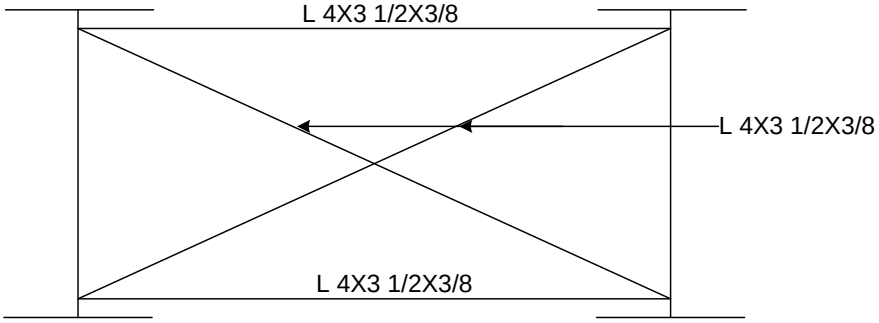

Figure 5.7: Typical Interior Pier Bracing

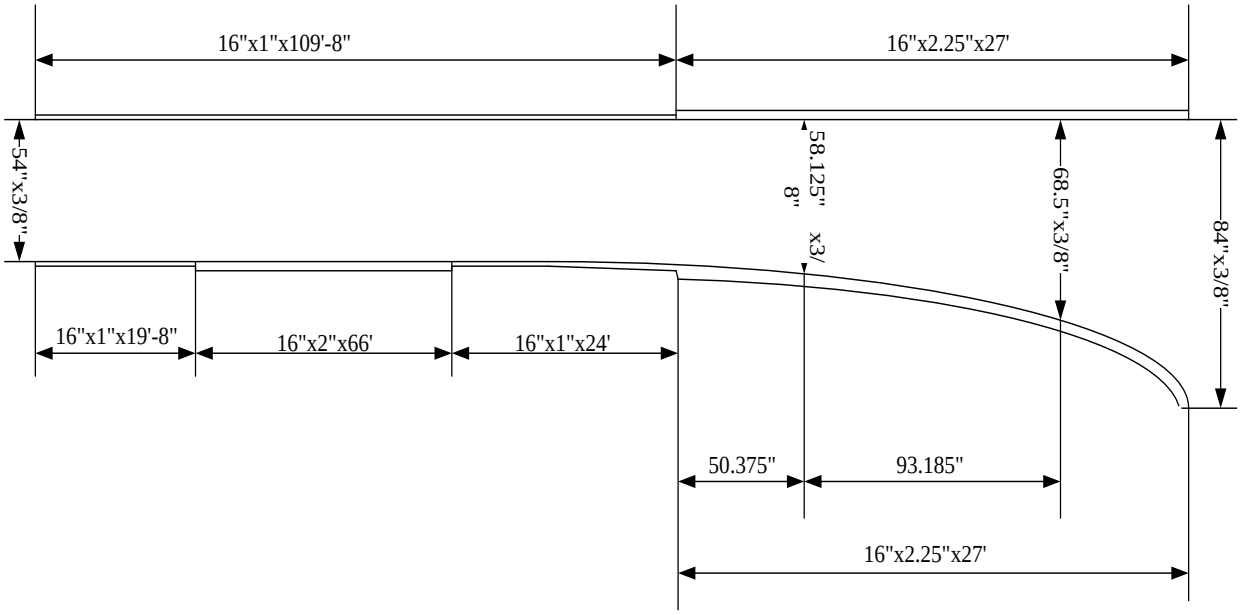

Girder Cross Section

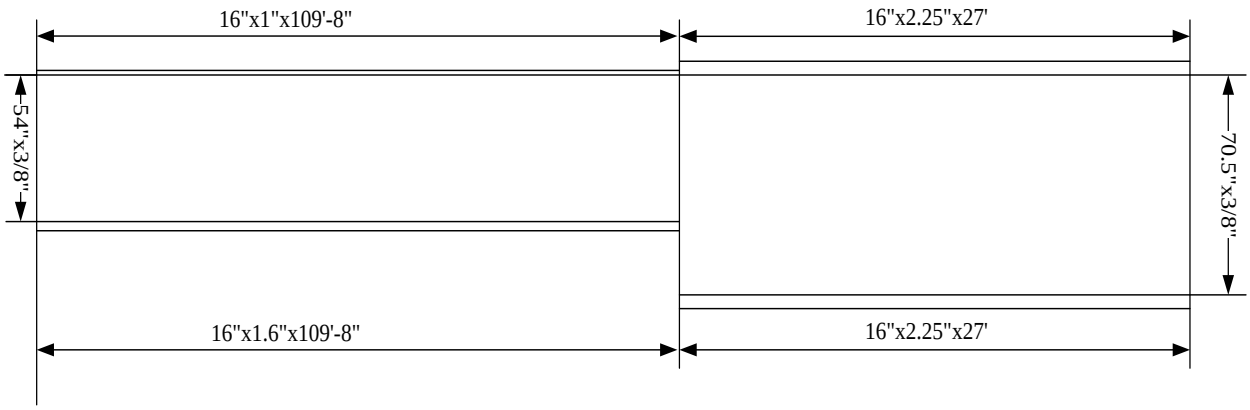

Averaged Girder Cross Section

Figure 5.8: Actual and Averaged Girder Cross Section

5.3 Finite Element Model of Virginia Pilot Bridge RT 15

In this bridge, cross frames made up of angles and channels were used as bracing. To capture the effect of the bracing on the response, individual bracing components were modeled using linear beam elements (B31 in ABAQUS). The linear general-purpose shell in ABAQUS has the ability to switch from discrete Kirchhoff thin shell to moderately thick shell formulation (Mindlin shell) as the thickness increases. The bridge deck generally has a characteristic length to thickness ratio of greater than 15 therefore behaving as a thin shell, while girder flanges and web characteristic length to thickness ratio changes depending upon their thickness. Therefore, the linear general-

purpose shell element with six degrees of freedom per node with reduced integration (S4R in ABAQUS) was used to model the bridge deck and girders. The bridge girders have a varying cross section along the length. However, for the analysis purpose it was modeled using two different cross sections, which were calculated using the weighted average as shown in Figure 5.9 . From Figure 5.5, Figure 5.6 and Figure 5.7, it is clear that bracing is connected at an offset from the bottom flange of the girder. This offset was ignored in the model and bracing was directly connected at the junction of flange and web. This simplification was done because the objective of the analysis was to study the global behavior of the bridge and this local effect would not have a measurable impact on the global behavior. The supports were modeled at the bottom of the girder. The developed finite element model is illustrated in Figure 5.10.

From the parametric studies performed for the Wildcat Creek River Bridge and the Colquitz River Bridge, it was found that support variation and modeling of the guardrail had a significant impact on the responses of these bridges. Therefore, different supports conditions from simply supported to completely frozen supports were considered. To study the impact of guardrail model on the bridge's response, three different methods were used to model it as discussed in chapter 3.

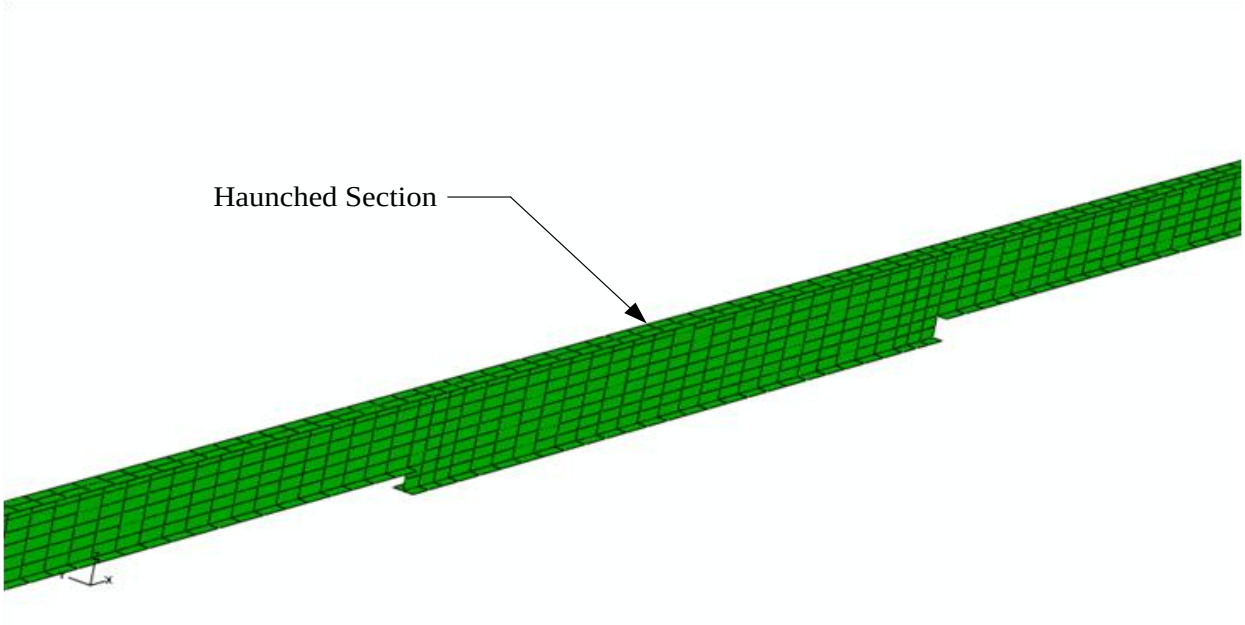

Figure 5.9: Finite Element Model of Girder Cross Section

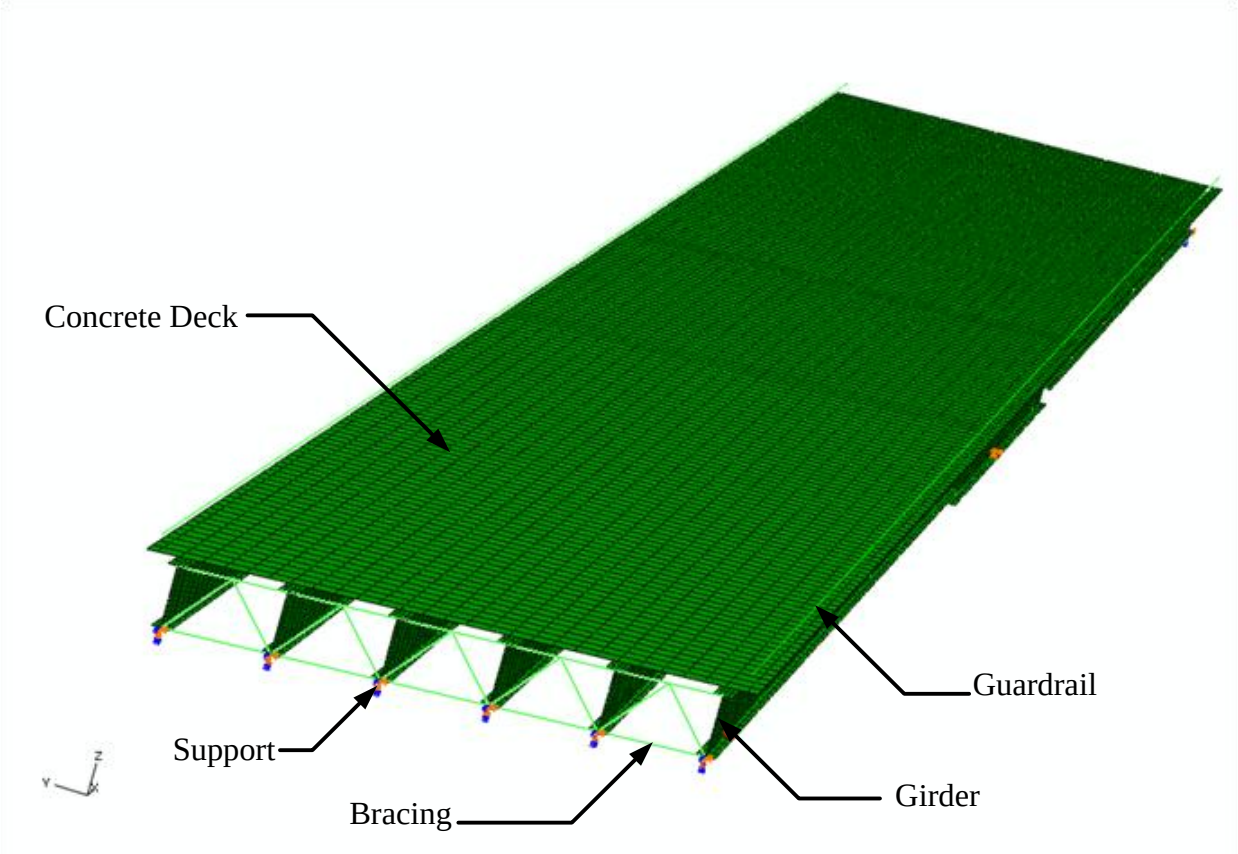

Figure 5.10: Finite Element Model of Virginia Pilot Bridge RT 15

5.4 Static Analysis of Virginia Pilot Bridge RT15

Live load testing is critical in understanding the behavior of the bridge and the change in response with time. For quasi-static test, the truckload has to be moved very slowly (2-3 mph) along the entire length of the bridge, such that response obtained for a position of the truck has no impact on the response in the subsequent truck positions. For the Virginia Pilot Bridge RT 15 two Virginia Department of Tranportation (VDOT) dump truck for which the dimensions are shown in Figure 5.11 was used for the test. For this truck the front two wheels apply a load of 8.75 kips each and the four rear wheels apply loads of 8.15 kips each.

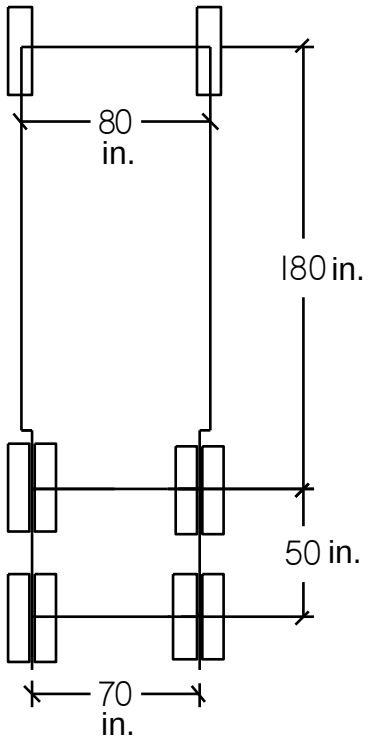

Figure 5.11: VDOT Dump Truck

Three different loading scenarios were considered in the finite element analyses. In scenario A (Figure 5.12), the truck was positioned as close to the guardrail as possible, that is at 27 in. from the deck edge. This position was considered to create maximum load on the exterior girder.

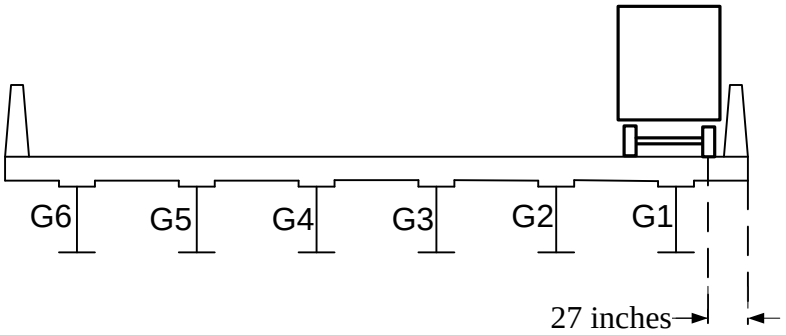

Figure 5.12: Scenario A

It was assumed that bridge has shoulder of 5ft-4in. on the left side and 9ft-4inches on the right side. For the next two loading cases Scenario D (Figure 5.13) and Scenario E (Figure 5.14), it was assumed that the truck was centered into these lanes respectively. These conditions were selected to simulate the actual traffic condition in the field.

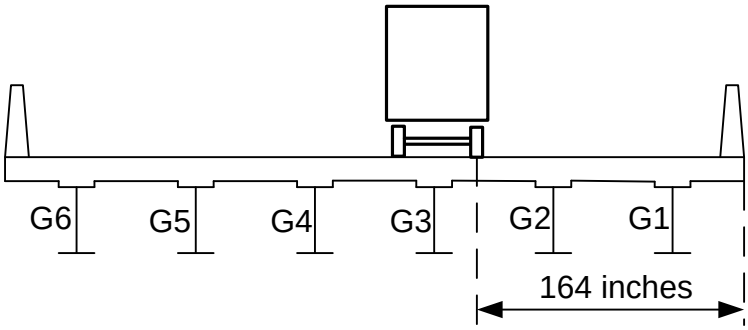

Figure 5.13: Scenario D

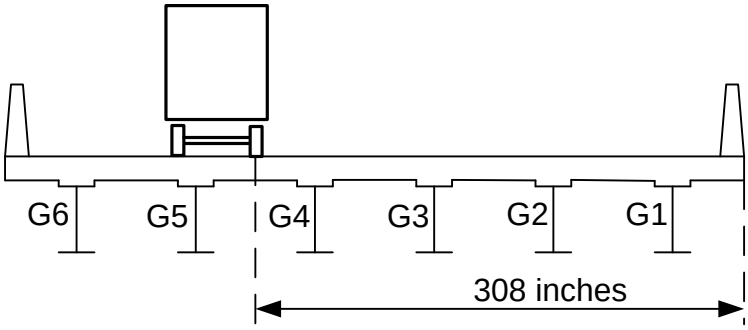

Figure 5.14: Scenario E

For static analysis, the entire truck loading was discretized into individual tire patch and each tire patch was idealized into a point load at its centroid. However, the centroid of the tire patch did not necessarily always lie at a node in the finite element model. In these cases, a point load was applied at the closest node from the centroid of the tire patch. To simulate the quasi-static moving load, each truck position was applied in different linear perturbation steps in ABAQUS (2007). In linear perturbation, results from the previous step are not transmitted to the consecutive loading position or load step. The main goal of these simulations was used understand the global response of the bridge super structure and assist in field instrumentation.

The following section discusses the results obtained from the finite element analysis of the LTBP RT15 bridge superstructure.

5.4.1 Girder Displacement Envelopes and Support Rotations

To obtain the displacements and rotations for the three loading scenarios, the exterior supports were assumed to be rollers and the interior support was assumed to be pinned. The load was applied using twenty steps to simulate the moving load for each scenario. For this analysis, the connections between the girders and bridge deck, and bridge deck and guardrail were assumed to be fully composite.

5.4.1.1 Displacement Envelopes and Support Rotations for Scenario A

Figure 5.15, shows the displacement envelope for all girders when the live load was applied as per scenario A (Figure 5.12).

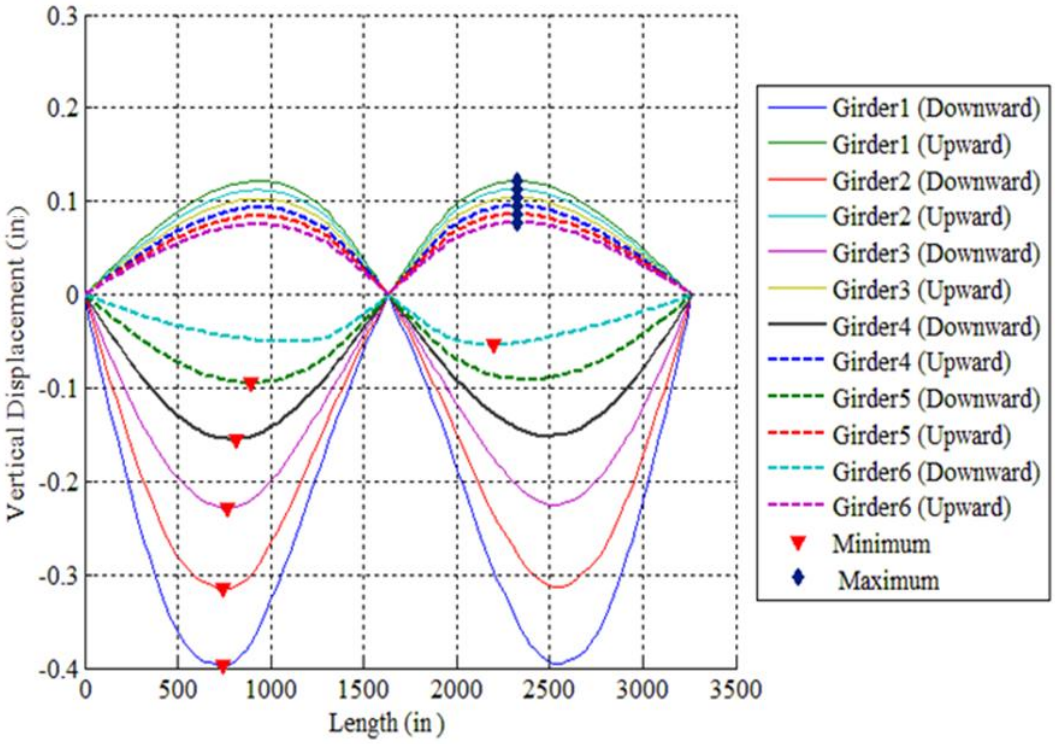

Figure 5.15: Girder Displacement Envelopes (Scenario A)

As can be seen from the maximum displacement was observed in girder-1, which was expected because of the truck location. For scenario A, Table 5.2 shows the maximum displacements, both downward and upward, and the location along the length it occurs for all girders. As can be seen from this table the maximum upward displacement for all girders occurred at the same location over the length of the bridge, while the downward displacements did not. In addition, the magnitude of the maximum downward displacement is about 45% larger than the maximum upward displacement and, as mentioned above, both maxima occur on girder-1.

Table 5.2: Maximum Girder Displacements (Scenario A)

Girder No	Distance (in.)	Maximum Downward Displacement (in.)	Distance (in.)	Maximum Upward Displacement (in.)
1	742	-0.397	2324	0.122
2	742	-0.315	2324	0.113
3	767	-0.229	2324	0.104
4	816	-0.155	2324	0.095
5	890	-0.095	2324	0.086
6	2201	-0.054	2324	0.077

Table 5.2 shows the maximum support rotations for all girders and the truck location that caused the maximum response for scenario A. The support rotations are maximum for girder-1 since the truck was placed very close to it. As can be seen they decrease as the girders are located further away from the loaded lane. Similar trend was observed for all the girders with maximum positive rotation at the left support while the maximum magnitude of negative rotation occurred at the right support.

Table 5.3: Support Rotations (Scenario A)

	Truck Position along the Length (in.)	Support Rotation (Radians)	Truck Position along the Length (in.)	Support Rotation (Radians)
Girder-1				
Left	2049	-1.95E-04	363	8.66E-04
Interior	670	-3.59E-04	2049	3.54E-04
Right	2355	-8.55E-04	670	1.88E-04
Girder-2				
Left	2049	-1.79E-04	363	6.56E-04
Interior	670	-3.22E-04	2049	3.10E-04
Right	2355	-6.67E-04	670	1.73E-04
Girder-3				
Left	2049	-1.64E-04	363	4.66E-04
Interior	670	-2.86E-04	2049	2.75E-04
Right	2355	-4.72E-04	670	1.59E-04
Girder-4				
Left	2049	-1.50E-04	516	2.97E-04
Interior	670	-2.52E-04	2049	2.43E-04
Right	2202	-3.04E-04	670	1.46E-04
Girder-5				
Left	2049	-1.35E-04	516	1.61E-04
Interior	670	-2.19E-04	2049	2.13E-04
Right	2202	-1.63E-04	670	1.33E-04
Girder-6				
Left	2049	-1.21E-04	976	7.29E-05
Interior	670	-1.83E-04	2049	1.83E-04
Right	1742	-6.78E-05	670	1.21E-04

(Positive: 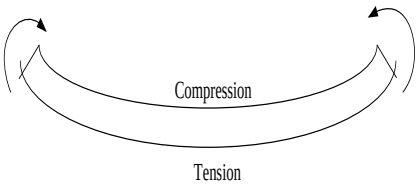

, Negative: 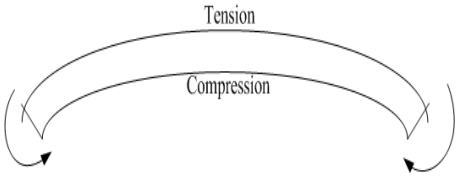

)

5.4.1.2 Displacement Envelopes and Support Rotations for Scenario D

Figure 5.16 shows the displacement envelope for all six girders when the live load was applied as per Scenario D (Figure 5.13). From the plot, it is clear that Girder-2 and Girder-3 experience the maximum downward displacements because the truck is located in between these two girders.

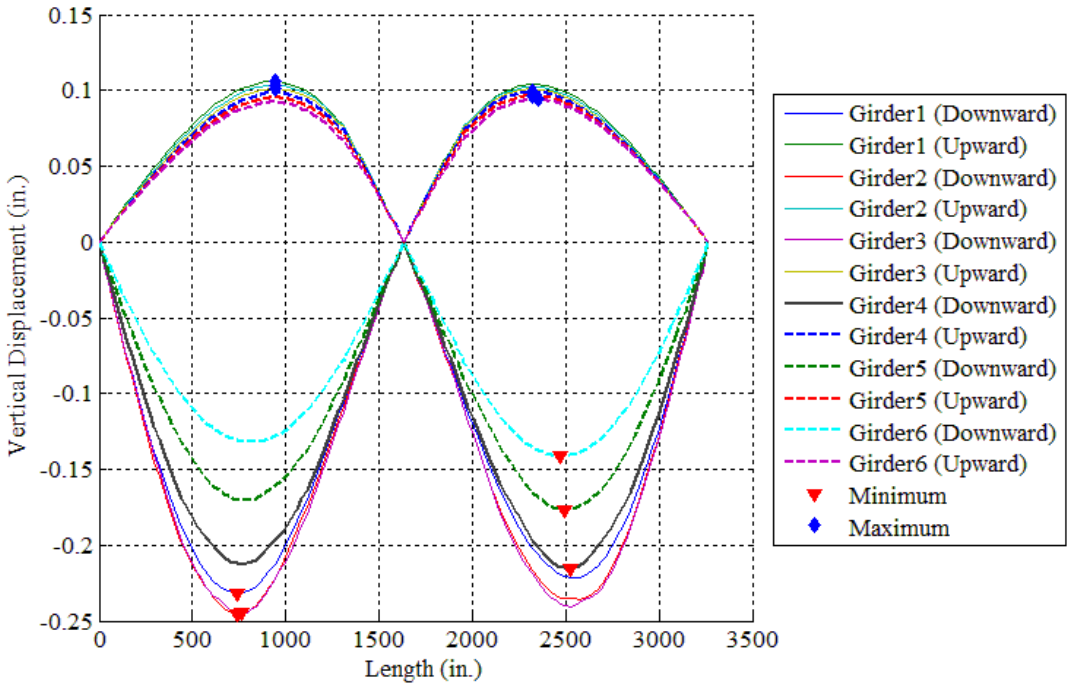

Figure 5.16: Girder Displacement Envelopes (Scenario D)

Table 5.4 shows the maximum displacement in all girders for scenario D. The maximum downward displacements for all the girders occur approximately at a distance of 0.45 of the span length from the exterior support. Also, the maximum upward displacement occurs approximately at a distance of 0.57 of the span length from the exterior support.

Table 5.4: Maximum Girder Displacements (Scenario D)

Girder No	Distance (in.)	Maximum Downward Displacement (in.)	Distance (inches)	Maximum Upward Displacement (in.)
1	742	0.232	940	0.106
2	742	0.246	940	0.104
3	767	0.245	940	0.101
4	2522	0.215	2324	0.099
5	2497	0.177	2324	0.097
6	2473	0.142	2349	0.094

Table 5.5 shows the support rotations for all six girders and the truck location that causes the maximum response for scenario D. The maximum support rotations occurred at girder-2 and girder-3 as the truck was placed between them. A similar trend can be observed in Scenario-A in this case also with the maximum positive rotation occurring at left support while maximum magnitude of negative rotation occurring at the right support.

Table 5.5: Support Rotations (Scenario D)

	Truck Position along the Length (in.)	Support Rotation (Radians)	Truck Position along the Length (in.)	Support Rotation (Radians)
Girder-1				
Left	2049	-1.69E-04	363	4.87E-04
Interior	670	-2.82E-04	2049	2.83E-04
Right	2355	-4.73E-04	670	1.63E-04
Girder-2				
Left	2049	-1.63E-04	363	5.02E-04
Interior	670	-2.83E-04	2049	2.83E-04
Right	2355	-4.88E-04	670	1.59E-04
Girder-3				
Left	2049	-1.58E-04	210	4.88E-04
Interior	670	-2.81E-04	2049	2.80E-04
Right	2509	-4.93E-04	670	1.56E-04
Girder-4				
Left	2049	-1.54E-04	363	4.22E-04
Interior	670	-2.72E-04	2049	2.69E-04
Right	2355	-4.31E-04	670	1.53E-04
Girder-5				
Left	2049	-1.50E-04	363	3.35E-04
Interior	670	-2.57E-04	2049	2.54E-04
Right	2355	-3.48E-04	670	1.51E-04
Girder-6				
Left	2049	-1.46E-04	516	2.56E-04
Interior	670	-2.39E-04	2049	2.39E-04
Right	2202	-2.79E-04	670	1.50E-04

(Positive: 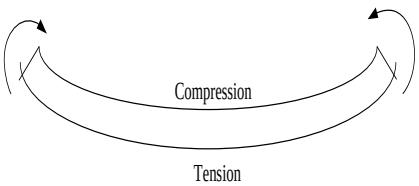

, Negative: 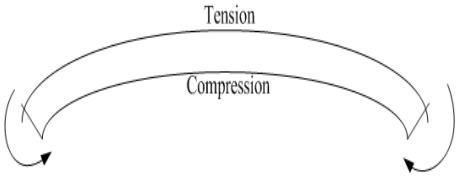

)

5.4.1.3 Displacement Envelopes and Support Rotations for Scenario E

Figure 5.17, shows the displacement envelope for all the girders when live load was applied as per Scenario E (Figure 5.14). In this loading scenario, the truck is located close to girder-5. Still, girder-6 showed the maximum downward and upward displacement responses. However, the displacement response of girder-5 was very close to the response of girder-6. The reason for this behavior could be attributed to the fact that girder-6 had a smaller effective flange width and additional mass and stiffness because of the guardrail mass sitting right above it, while girder-5 had a wider effective flange width. The upward displacement response for all six girders was not as close as that for Scenario-A and Scenario-D.

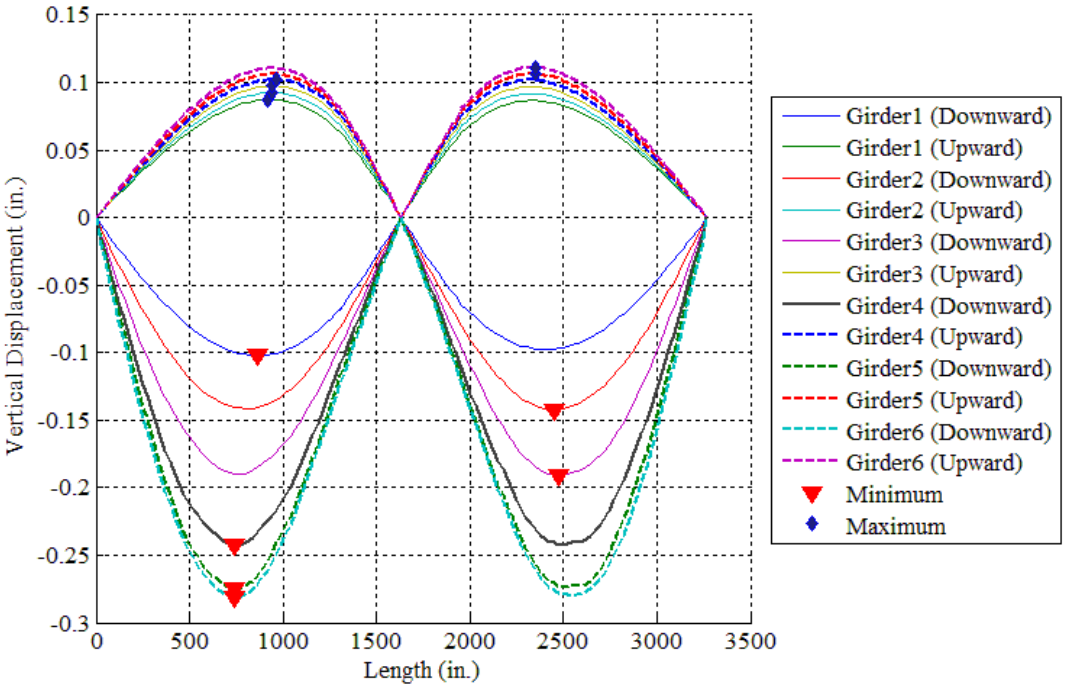

Figure 5.17: Girder Displacement Envelopes (Scenario E)

Table 5.6 shows the maximum displacement in all girders for scenario E. The maximum upward and downward displacements for all the girders occurred approximately at a distance of 0.45 to 0.6 of the span length from the exterior support.

Table 5.6: Maximum Girder Displacements (Scenario E)

Girder No	Distance (in.)	Maximum Downward Displacement (in.)	Distance (in.)	Maximum Upward Displacement (in.)
1	865	-0.102	915	0.087
2	2448	-0.143	940	0.092
3	2472	-0.191	940	0.097
4	742	-0.243	964	0.102
5	742	-0.275	2349	0.106
6	742	-0.281	2349	0.111

Table 5.7 shows the support rotations for all six girders and the truck location that causes the maximum response for scenario E. The maximum girder rotations were observed in girder-6, which was consistent with the response observed for girder displacements. Similar trends discussed previously for the other loading scenarios was observed for this loading case, i.e. maximum positive rotations occurred at the left support while the maximum magnitude of negative rotation occurred at the right support with the exception of girder-1.

Table 5.7: Support Rotations (Scenario E)

	Truck Position along the Length (in.)	Support Rotation (Radians)	Truck Position along the Length (in.)	Support Rotation (Radians)
Girder-1				
Left	2049	-1.38E-04	670	1.83E-04
Interior	670	-2.20E-04	2049	2.15E-04
Right	2202	-1.77E-04	670	1.38E-04
Girder-2				
Left	2049	-1.43E-04	516	2.76E-04
Interior	670	-2.41E-04	2049	2.41E-04
Right	2355	-2.72E-04	670	1.45E-04
Girder-3				
Left	2049	-1.50E-04	363	3.89E-04
Interior	670	-2.61E-04	2049	2.66E-04
Right	2355	-3.78E-04	670	1.53E-04
Girder-4				
Left	2049	-1.57E-04	363	4.91E-04
Interior	670	-2.78E-04	2049	2.86E-04
Right	2509	-4.88E-04	670	1.60E-04
Girder-5				
Left	2049	-1.65E-04	363	5.57E-04
Interior	670	-2.93E-04	2049	2.99E-04
Right	2509	-5.63E-04	670	1.69E-04
Girder-6				
Left	2049	-1.73E-04	363	5.94E-04
Interior	670	-3.05E-04	2049	3.09E-04
Right	2355	-6.05E-04	670	1.78E-04

(Positive: 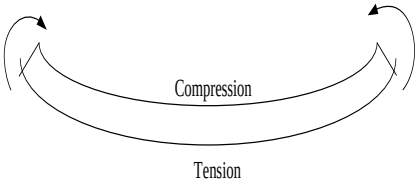

, Negative: 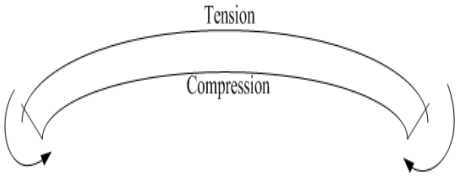

)

For all three loading scenarios, the maximum positive and negative displacement in the girders did not happen at the same location for all the girders because of the bridge skew. However, as can be seen from the results, the maximum upward response for all the girders is very closely spaced.

5.4.2 Bridge Displacement Envelopes

Displacement envelopes were obtained for all girders and all loading scenarios. As an example, Figure 5.18 and Figure 5.19 show the displacement envelopes for the three loading scenarios for Girder-3 and for the entire bridge (i.e. the largest displacement out of all the girder displacements), respectively. This analysis assumes that the bridge was supported by rollers at the exterior supports and by a pin at the interior support. For each loading scenario the loading was applied in twenty increments along the length. For girder-3, the upward displacement response was found to be very close to each other for all the loading cases. Scenario-D gives the maximum displacement in the girder because the truck is positioned over girder-3 in this scenario. The magnitude of the displacement decreases for scenarios-A through E as the applied load moves away from girder-3. Loading scenario-A gives the maximum upward and downward displacement for the entire bridge as shown in Figure 5.19

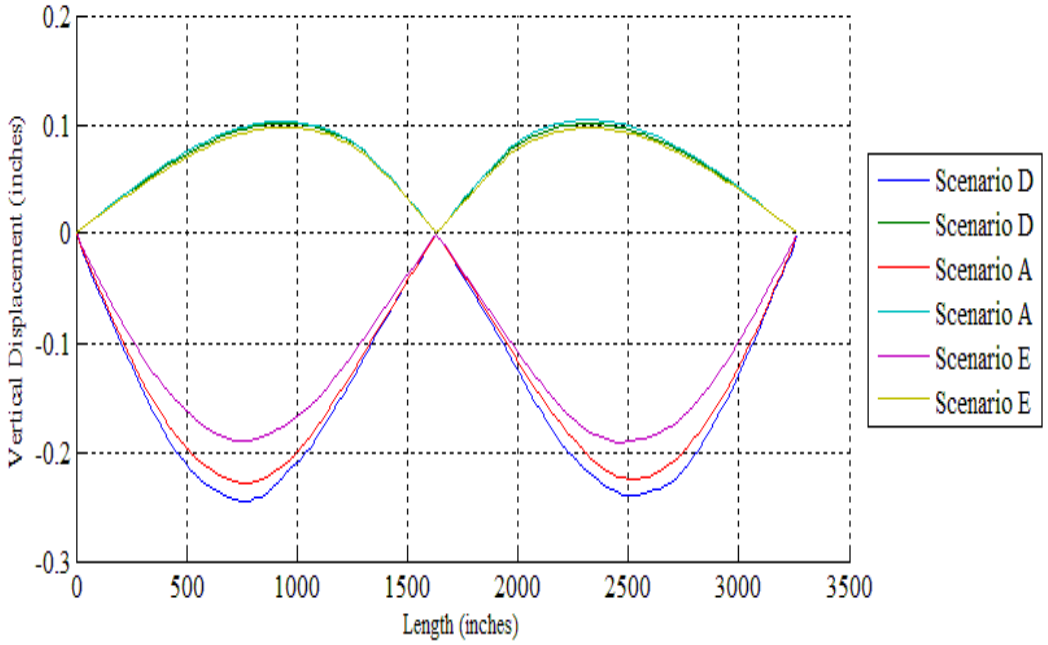

Figure 5.18: Displacement Envelope for Girder-3

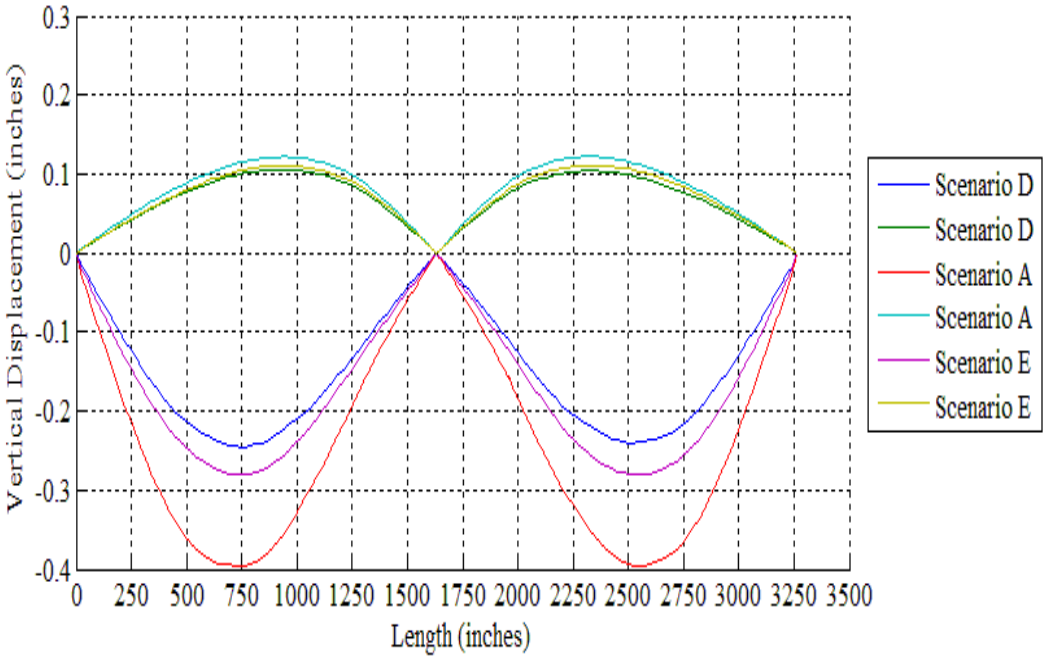

Figure 5.19: Displacement Envelope for the entire Bridge

5.4.3 Effect of Support Restraint on Girder Response and Support Rotations

To study the effect of different support restraint on the response of the girders, the truck was centered over the first lane (Scenario D) and as was done previously, it was applied using twenty load steps in the longitudinal direction. Full composite action was assumed between the girders and bridge deck, and the guardrails and bridge deck.Girder-3 was once again selected for displaying results because it had the maximum response in Scenario D (Figure 5.16). It can be concluded that the displacement response does not change much whether the pin boundary condition is modeled at the left or the interior support. Also, modeling all supports as pinned or frozen, yielded similar displacements values.

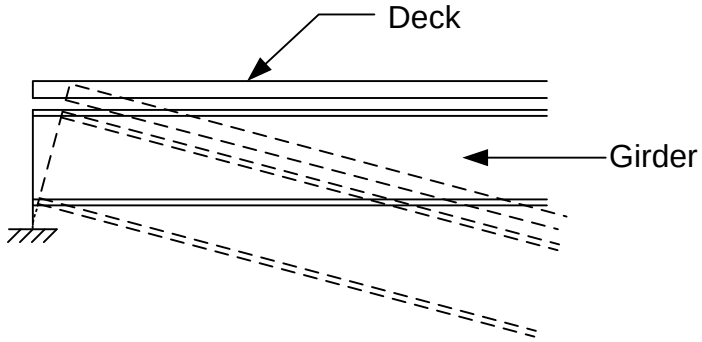

Figure 5.20: Frozen Support Condition

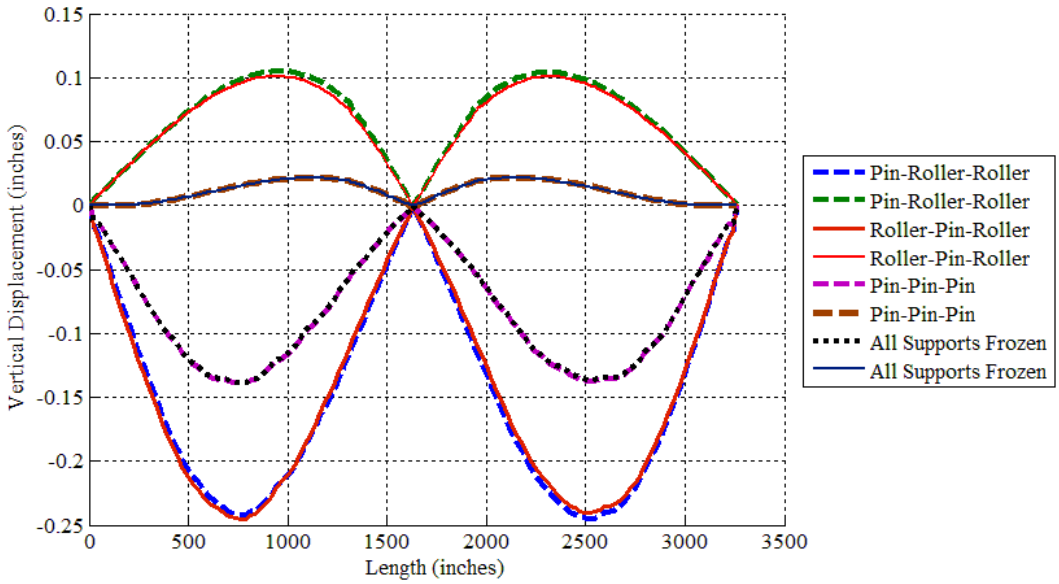

Figure 5.21: Effect of Support Restraint on Girder-3 Displacement (Scenario D)

Figure 5.22 shows the support rotations for different support conditions for girder-3. The support rotations were measured at the mid height of the girder cross-section (Figure 5.22). A similar trend to that obtained for the girder displacement was observed for support rotations. Similar rotations were observed irrespective of the where the pin condition was modeled (e.g., interior or exterior support). Effect of support restraint on support rotations was anywhere between 45% and 98%.

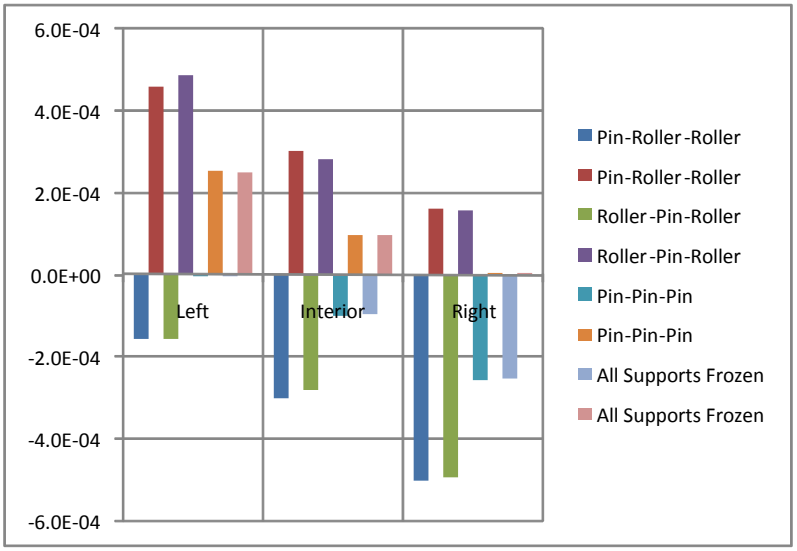

Figure 5.22: Effect of Support Restraint Conditions on Support Rotations

5.4.4 Effect of Composite Action on Girder Displacement and Support Rotations

In this section, the effect of composite action between girders and bridge deck was investigated. studying this case, the truck was positioned as per Scenario-D and the load was applied in twenty load steps in the longitudinal direction. The bridge was supported at the end supports with rollers and at the interior support as a pin. Full composite action was assumed between the bridge deck and the guardrails in all the analyses. Full composite action between bridge deck and girders was modeled using rigid links, while partial composite action was modeled using nonlinear springs. These nonlinear springs had high vertical stiffness to prevent vertical separation of the bridge deck and girders and low shear and rotational stiffness to model the non-composite action between the two structural components.

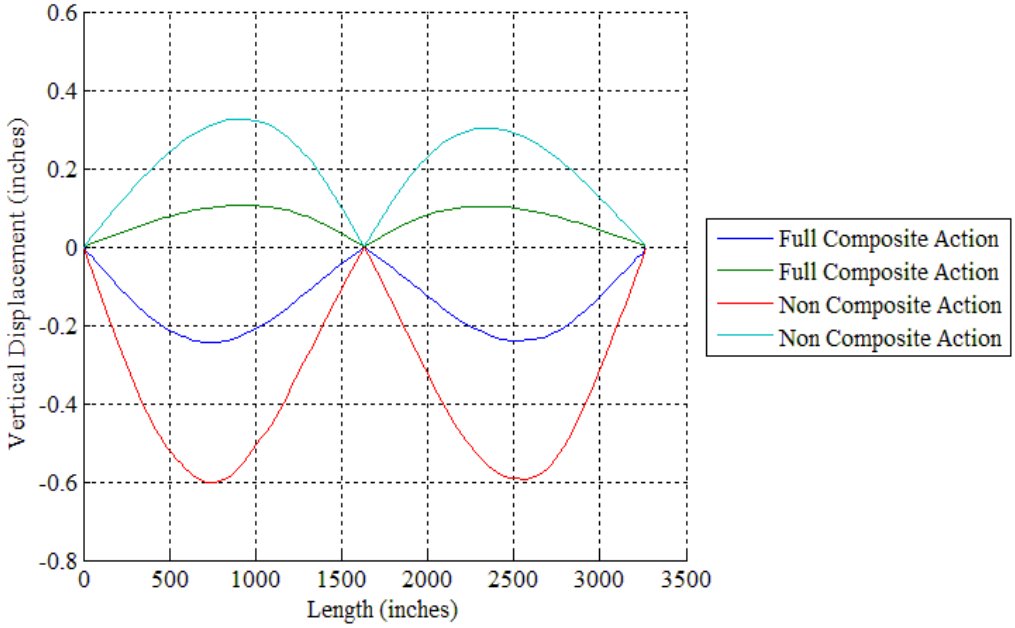

Figure 5.23: Effect of Composite Action on Girder Displacements (Scenario D)

As expected, the vertical displacement and support rotations obtained when non-composite action was assumed were higher than the values obtained when the full composite action was assumed. This is because in the former case the stiffness at the interface was zero. The maximum displacement was approximately three times higher than that obtained in case of full composite action. On average, the maximum support rotations in the former case were 50% higher than those in case of full composite action.

Table 5.8: Effect of Composite Action on Support Rotations

	Fully Composite Action		Non-Composite Action	
Girder	Support Rotation (Radians)	Support Rotation (Radians)	Support Rotation (Radians)	Support Rotation (Radians)
1	-4.73E-04	4.87E-04	-1.20E-03	1.20E-03
2	-4.88E-04	5.02E-04	-1.24E-03	1.24E-03
3	-4.93E-04	4.88E-04	-1.24E-03	1.21E-03
4	-4.31E-04	4.22E-04	-1.09E-03	1.03E-03
5	-3.48E-04	3.35E-04	-8.46E-04	7.93E-04
6	-2.79E-04	2.56E-04	-5.97E-04	5.58E-04

(Positive: 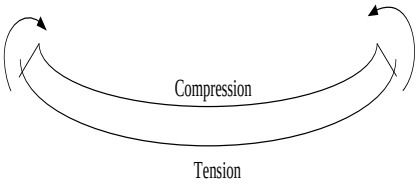

, Negative: 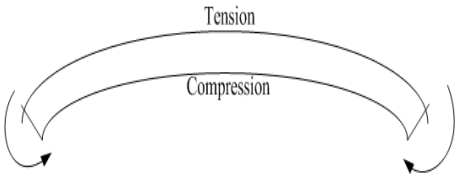

)

5.4.5 Effect of Guardrail Modeling on Displacements and Rotations of Exterior and Interior Girders

As previously discussed, three different ways of modeling the guardrails were considered in this investigation. They consisted of modeling the guardrail as: a beam element, an additional deck width as per AASHTO, and a nonstructural mass. Once again, the truck was positioned as per Scenario-D and the load was applied using twenty load steps in the longitudinal direction. The support conditions used in this investigation were such that rollers were used for the end supports and a pin was used for the interior support. Full composite action was assumed between the bridge deck and guardrail when applicable, i.e., for the first two types of models. This was accomplished via the use of rigid links. The results are plotted in Figure 5.23.

Interior girder-3 and exterior girder-1 were selected for this study to compare the impact of guardrail mass and stiffness on them. It was observed that for interior girders (such as Girder-3), modeling guardrail as a non-structural mass or as an additional width as per AASHTO had identical response while modeling guardrail using beam elements produced a stiffer response.

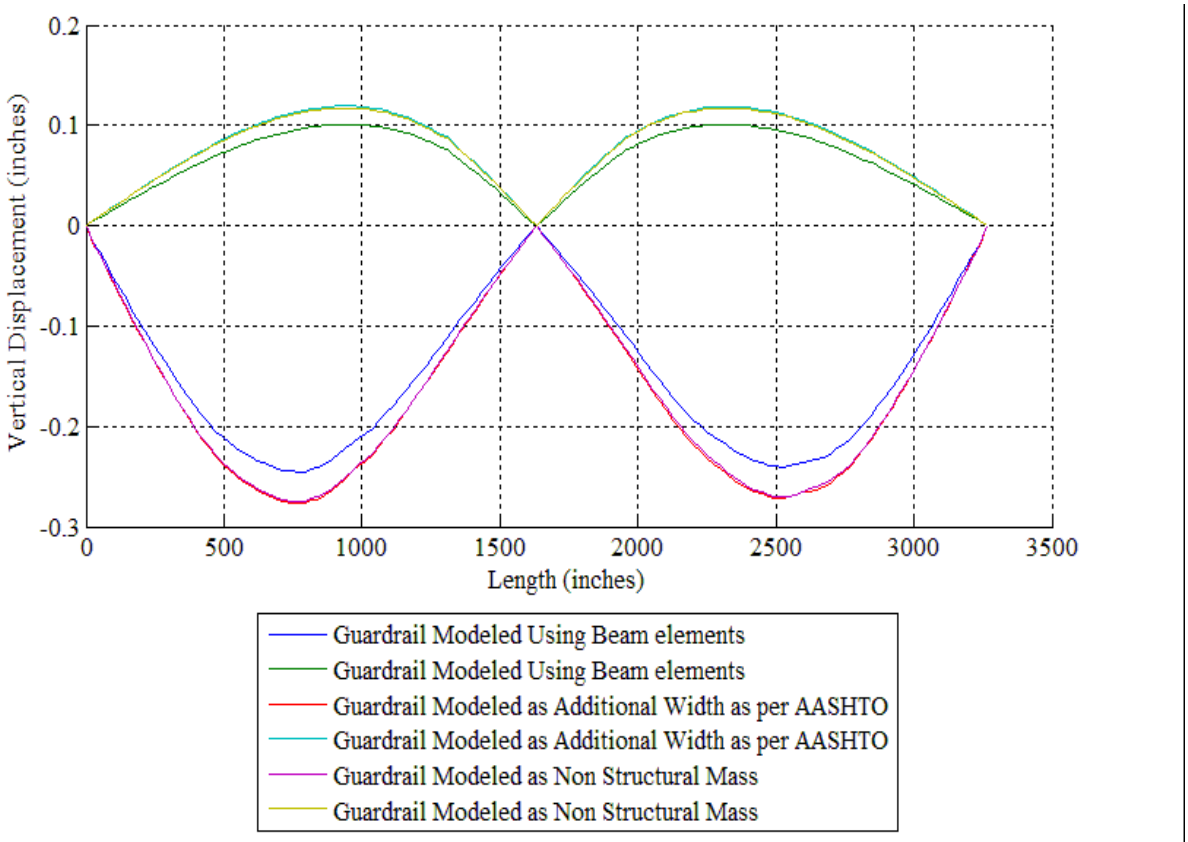

Figure 5.24: Effect of Guardrail Modeling on the Displacement Envelope of an Interior Girder (Girder-3) for Scenario D

The response of the exterior girders (such as Girder-1) was more sensitive to the guardrail modeling techniques. As before, when the guardrail was modeled using beam elements it produced a stiffer response than when the other two styles of modeling were used. However, in this case unlike before the two other modeling techniques produced slightly different results and as expected when only the mass of the guardrail was modeled it produced the most flexible response. The vertical upward displacement response of the exterior girder, though, was found to be identical in the two cases, while the vertical downward displacements were slightly different.

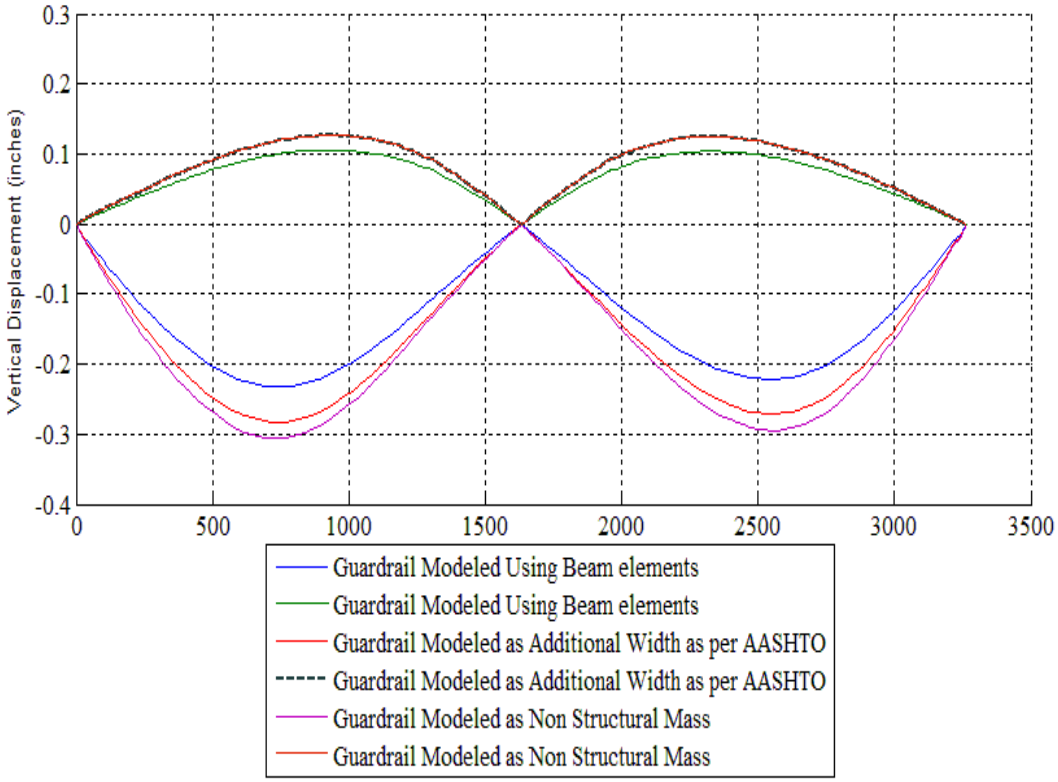

Figure 5.25: Effect of Guardrail Modeling on Displacement Envelope of Exterior Girder (Girder-1) for Scenario D

Interior and exterior girder support rotations for a bridge modeled with different guardrail models show similar trends in their responses. The exterior girders support rotations changed on an average by 22% while the interior girders support rotations changed by 15%. The exterior girder response (Table 5.9) was more sensitive to the guardrail modeling techniques than the interior girder (Table 5.10). This is reasonable since the stiffness and mass imparted by the guardrail should have more influence on the girder closer to it, e.g., the exterior girder.

Table 5.9: Effect of Guardrail modeling on Exterior Girder (Girder-1) Support Rotations

Guardrail Modeled	Support Rotation (Radians)	Support Rotation (Radians)
Using Beam Element		
Left	-1.69E-04	4.87E-04
Interior	-2.82E-04	2.83E-04
Right	-4.73E-04	1.63E-04
Additional Width as per AASHTO		
Left	-2.00E-04	5.97E-04
Interior	-3.36E-04	3.36E-04
Right	-5.84E-04	1.95E-04
Non Structural Mass		
Left	-2.01E-04	6.54E-04
Interior	-3.40E-04	3.41E-04
Right	-6.34E-04	1.94E-04

(Positive: 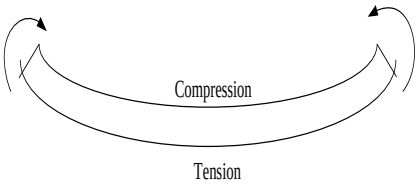

, Negative: 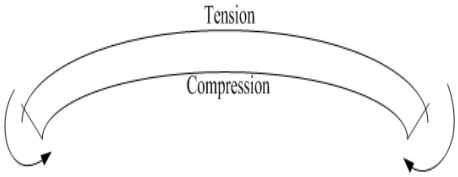

)

Table 5.10: Effect of Guardrail modeling on Interior Girder (Girder-3) Support Rotations

Guardrail Modeled	Support Rotation (Radians)	Support Rotation (Radians)
Using Beam Element		
Left	-1.58E-04	4.88E-04
Interior	-2.81E-04	2.80E-04
Right	-4.93E-04	1.56E-04
Additional Width as per AASHTO		
Left	-1.87E-04	5.48E-04
Interior	-3.26E-04	3.24E-04
Right	-5.53E-04	1.85E-04
Non Structural Mass		
Left	-1.85E-04	5.45E-04
Interior	-3.23E-04	3.19E-04
Right	-5.50E-04	1.81E-04

(Positive: 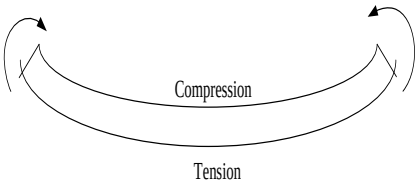

, Negative: 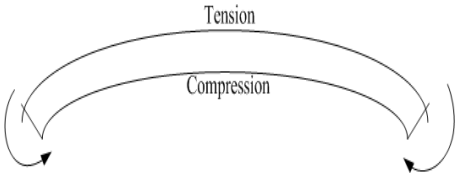

)

5.5 Dynamic Analysis of Virginia Pilot Bridge RT. 15

The dynamic analysis of Virginia Pilot Bridge RT.15 was carried out to study the effect of support condition and guardrail modeling on the natural frequencies of vibration of the bridge superstructure. Figure 5.26 shows the first five modes of vibration of the bridge obtained by the finite element model when the exterior supports were modeled as roller supports and interior support as a pin. Full composite action between the guardrail and bridge deck, and girders and bridge deck was assumed. The bridge skew of 17.45° was also included in the model so that more realistic mode shapes could be captured.

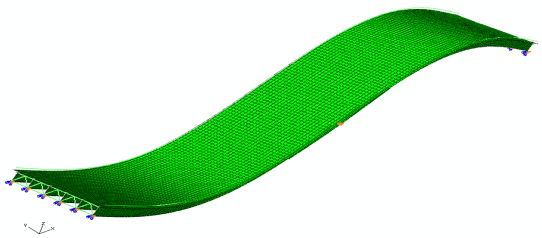

Mode-1

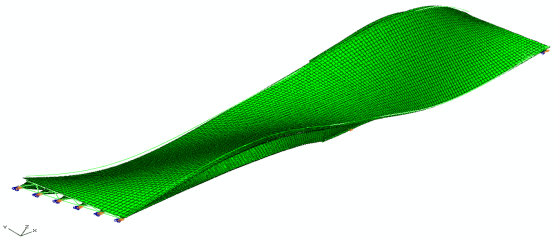

Mode-2

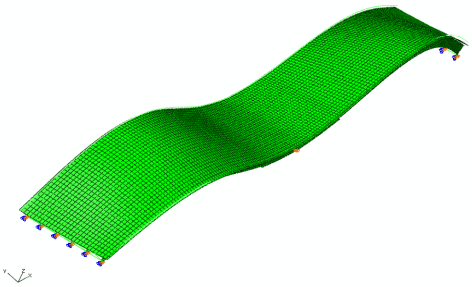

Mode-3

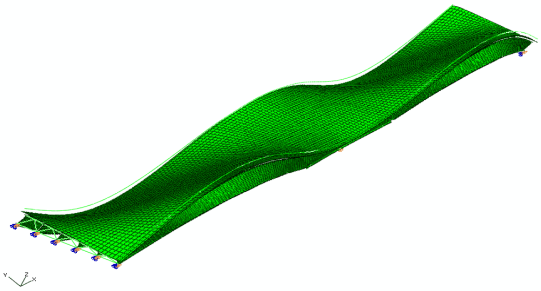

Mode-4

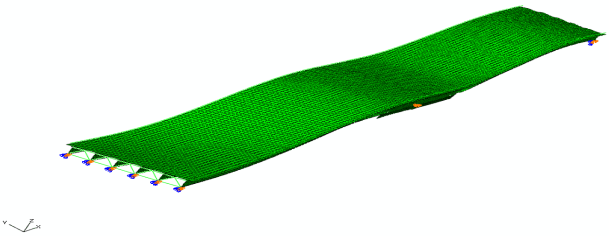

Mode-5

Figure 5.26: Mode Shapes of Virginia Pilot Bridge RT.15

Figure 5.27 shows the changes in natural frequencies for the different boundary condition. As can be seen in Table 5.11, higher frequencies were less sensitive to the support condition variation. In addition, the natural frequencies did not change significantly when the pin support was modeled at the end support from when it was modeled at the interior support. Finally, frozen support conditions with all six degrees of freedom constrained at the bottom of the flange yielded much higher values of natural frequencies.

Table 5.11: Effect of Support Restraint on Modal Response

Support Condition	1	% Error	2	% Error	3	% Error	4	% Error	5	% Error
Pin-Roller-Roller	2.04	0.00	2.73	0.00	3.45	0.00	4.46	0.00	6.42	0.00
Roller-Pin-Roller	2.03	0.56	2.70	1.27	3.54	-2.66	4.07	8.80	6.32	1.55
Pin-Pin-Pin	3.58	-75.29	3.95	-44.55	4.14	-20.21	4.70	-5.37	6.59	-2.62
All Supports Frozen	3.76	-84.07	4.16	-52.28	4.21	-21.99	4.74	-6.16	6.64	-3.44

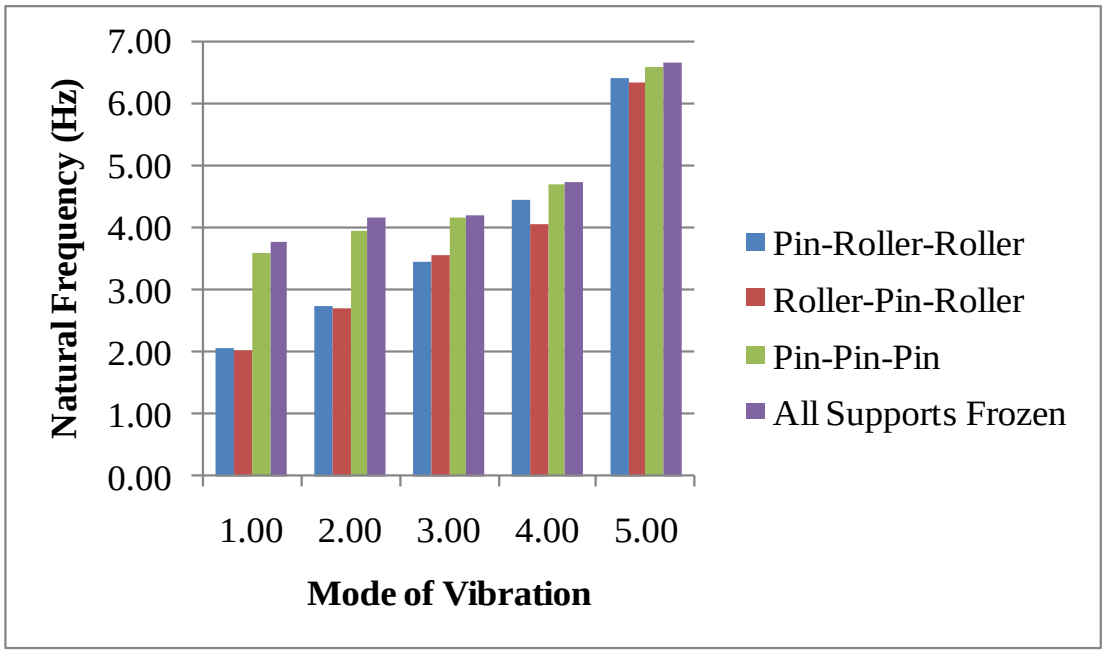

Figure 5.27: Effect of Support Restraint on Modal Response

Figure 5.28, shows change in natural frequency with guardrail modeled using the three previously discussed modeling techniques. As expected modeling the guardrail using beam elements with rigid links to model the full composite action between the guardrail and deck yielded higher natural frequencies that other methods. Conversely, modeling the guardrail mass but not its stiffness yielded the most flexible response because it increased the mass of system without increasing its stiffness. On average, this case produced natural frequencies 13.5% lower than the first method. The method suggested by increasing the deck width as per AASHTO provided intermediate results, since the additional width increased not only the mass but also the stiffness of the system. This method yielded results on an average 8.25% lower than the first method. Since the guardrails for this bridge are connected using anchors at a regular interval, the contribution of the guardrail to the mass and stiffness of the system is somewhere in between the

first two extreme cases considered for the analysis. Therefore, considering the guardrail as an additional width was able to provide a good estimate of the dynamic behavior of the bridge in this case.

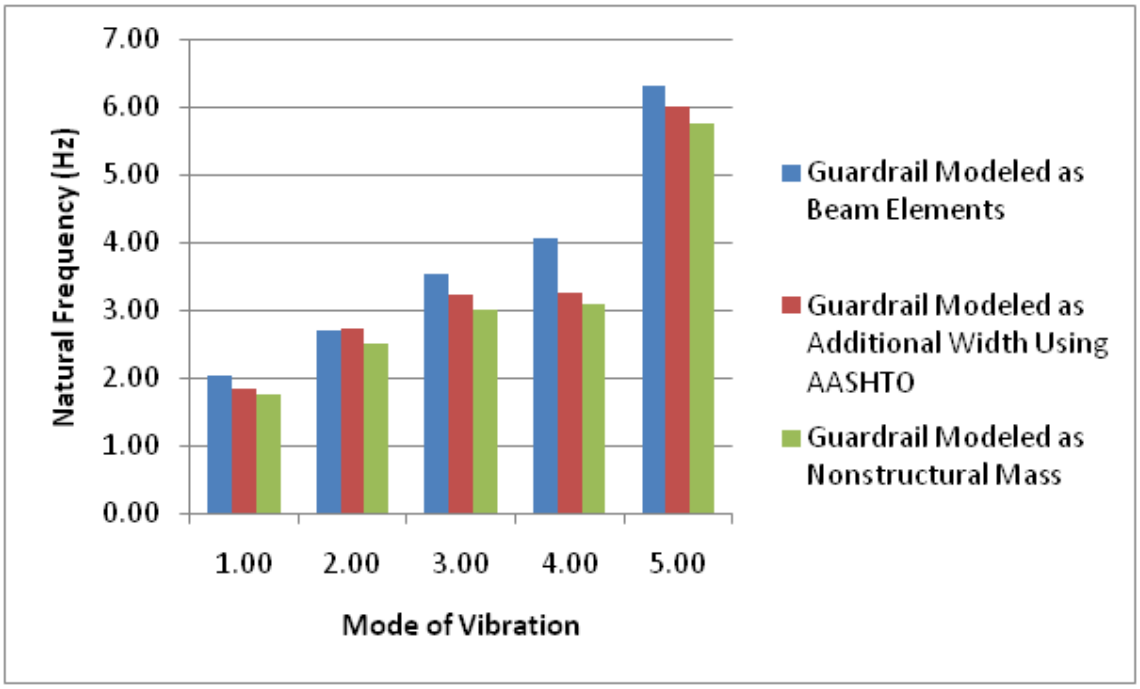

Figure 5.28: Effect of Guardrail Models on Modal Response

5.6 Summary

In this chapter, both the static and dynamic behaviors of the VA pilot bridge were investigated using finite element analysis. For these analyses, girder and deck were modeled using linear general-purpose shell elements and individual components of the bracing were modeled using linear beam elements. For the static analyses, three loading scenarios were considered and the quasi-static moving load was simulated by series of point loads. For these analyses, a similar trends was observed in displacements envelopes and support rotations of all six girders. Support restraints had a considerable impact on the displacements and support rotations. Non-composite action between the girders and bridge deck resulted in a response on an average 50% higher than the response obtained assuming full composite action. Exterior girders were found to be more sensitive to different guardrail modeling techniques as compared to interior girders. For the dynamic analyses the same model was adopted to study the effect of support restraints and guardrail models on the natural frequencies of the bridge. For first cases, it was found that higher

modes were less sensitive to the different modeling assumption than the lower modes of vibration.

6 Conclusion and Recommendations

6.1 Introduction

The present study was carried out as a part of the Long Term Bridge Performance Program (LTBP) funded by Federal Highway Administration. The first objective of this study was to develop reliable finite element models at various level of refinement and to study the effect of the inclusion of bridge parameters in the model, such as bridge skew, level of composite action, thermal gradient, and level of support restraint on the obtained bridge response. The second objective was to provide insight into the behavior of Virginia Pilot Bridge RT.15 and to assist with instrumentation decisions associated with live load and dynamic field tests.

6.2 Summary and Conclusions

To achieve these objectives, first a thorough review of three dimensional modeling techniques used by researchers over the years was carried out. In addition, a comprehensive study was performed on the different methods available in the literature that are used to model bridge parameters like composite action, live load application, support restraints, and secondary bridge elements. First, the suitability of different modeling techniques and elements used to model the primary bridge elements was accessed using simply models for which analytical solutions were available. Shell elements in ABAQUS(2007) element library were found to be adequate to model the behavior of the bridge deck. These elements were able to predict both deflection and first mode of vibration frequency within 3.5% of the analytical solution for a square plate with varying thickness and all four edges clamped subjected to a uniform pressure. Similarly, modeling the girders using either beam or shell elements was found to be adequate to predict girder response. All proposed girder models were able to predict both girder deflection and first mode of vibration frequency within 5% of the analytical solution for a simply supported beam subjected to its self-weight. Models other than eccentric beam model required significant mesh refinement to converge.

In the second part of the study, field data available in the literature for the Wildcat Creek River Bridge in Indiana, which has a 15 degrees skew, and for the Colquitz River Bridge in West Virginia were used to validate the adopted modeling techniques and to study the effect of different modeling parameters on bridge response. In the case of the Wildcat Creek River Bridge,

modeling the skew and staggered bracing softened the modal response in comparison to the response obtained when the skew and the bracing were ignored. Furthermore, the use of different guardrail models and the imposition of different support restraints had a significant effect on the modal response. However, the use of different bracing models and inclusion of thermal gradient had only a slight impact on the results. Higher modes of vibration were found to be less sensitive to variation in support restraint and to the different guardrail models. To assess the capabilities of different modeling techniques to predict the modal response, both bridges were modeled using three different techniques: Model-1 (Eccentric beam model) in which beam element at girder centroid is used to model the entire girder section, Model-2 (Three-beam model) in which beam elements are used to model girder flanges and web, Model-3 in which shell elements were used to model girder flanges and web. Model-2 predicted approximately 1.15 times higher frequencies when compared to the other two models and Model-3 predicted approximately 0.94 times the response predicted by Model-1. Therefore, it was concluded that both Model-1 and Model 3 were appropriate to model bridge response. In this study, Model-1 was used to model the global behavior and to obtain initial values of the responses for field-testing and Model-3 was adopted in the development of a more refined model, since this level of detail enables the inclusion of composite action models as well as a detailed model of the bracing.

The factors identified in these studies that affect the bridge response were considered further in the analysis of the Virginia pilot bridge for the LTBP project. In the analyses performed to investigate the behavior of this bridge, both girder and deck were modeled using linear general-purpose shell elements and the individual components of the bracing were modeled using single linear beam element. Both the static and dynamic behaviors of the bridge were studied. For static analysis, a quasi-static moving load was simulated using series of point loads for three different loading scenarios. For all three loading scenarios, the maximum positive and negative displacement in the girders did not occur at the same location for all the girders because of presence of the bridge skew. The upward response for all the girders was identical for scenario D and scenario E. Support restraints had a considerable impact on the displacements and support rotations. Non-composite action with zero stiffness at the interface yielded response 1.5 times higher than that obtained when assuming full composite action. Two extreme cases were

considered when modeling the guardrail, namely: assuming the guardrail contributes to both stiffness and mass of the bridge (full composite action between deck and guardrail), and assuming that the guardrail contributes only to the mass of the system. The response of the exterior girder was found to be more sensitive to these distinct assumptions as compared to those obtained for the interior girders. Finally, dynamic analyses were carried out using different support restraints and guardrail modeling techniques. In particular, the first fives modes of vibration were studied. It was found that higher modes are less sensitive to support condition variations than the lower modes. The frequency associated with the first mode of vibration changed by 84% when the support conditions were changed from pin-roller-roller to all frozen supports while the frequency associated with the fifth mode of vibration only changed by 3.5%. The frequencies changed by anywhere in between 4% to 24% when different guardrail modeling techniques were used.

6.3 Recommendations for Future Research

As a part of this research, three bridges were analyzed. For the first two bridges, only the dynamic response of the bridge superstructure was investigated, since only this type of data was available from field tests. For the third bridge both static and dynamic analyses were performed. More bridges with different lengths, number of spans, and skew angle should be analyzed to further validate the effects of different modeling techniques and the inclusion of the different bridge parameters in the model on the observed response.

In this investigation, it was assumed that bridge substructure had no influence on the superstructure's response. It is suggested that further analyses be carried out that study the effect of including the substructure in the model. This could be done explicitly or implicitly using springs at the support.

From the present research it was concluded that the modeling of support conditions and guardrail has a considerable impact on the obtained response. Therefore, more detailed modeling of these parameters is warranted to provide more insight into that the pilot bridge's behavior. Such a model should be based on measured responses from the field-testing. In the present study, extreme conditions were considered, e.g., girders and guardrails were assumed to be either fully composite or non-composite at all with the bridge deck. Neither of these conditions truly

represents the actual condition in the field; partial composite action could be modeled using different interaction models as discussed in Chapter 2.

For the performed static analyses, the truckload was modeled as a series of point loads. While this is sufficient to capture the global behavior of the bridge, it may not suffice for capturing localized behavior. In this case a more refined representation of the pressure applied by each tire patch is recommended. In particular, the use of work equivalent nodal loads or the approach proposed by Chung and Sotelino (2006) should be used in future analyses.

In this study, the haunch present in the girders section in the vicinity of the interior support for the Virginia Pilot Bridge RT.15 was modeled as a uniform section, which was obtained using a weighted average of the haunch section. In the future, it is recommended that a more refined representation of the haunch be used to study its impact on bridge response.

In the present finite element models, the transverse and longitudinal girder stiffeners were neglected, since their role is to prevent lateral buckling, which was not a consideration in this study. In order to investigate more localized phenomena, however, more refined models that include these stiffeners should be investigated. In addition, expansion joints at the deck level could also be modeled to study their global and local impact on the bridge's response. In this case thermal gradients may be found to have a more significant impact on the response.

During field inspection of the VA Pilot Bridge, cracks through the full depth of the concrete deck were observed at the splice location. It is recommended that a sub-model of this detail be developed to help investigate the possible reasons behind the formation of these cracks and their impact on the bridge's response. Finally, as the results from the field-testing are further evaluated, the development of more refined finite element models based on the field data can be developed which could include, for example, girder and deck deterioration, differential shrinkage between the bridge deck and girders.

References

AASHTO. (2008). "AASHTO LRFD Bridge Design Specifications (Customary U.S. Units) 4th Edition, with 2008 Interim Revisions." American Association of State Highway and Transportation Officials, Washington, DC.

ABAQUS, I. (2007). "ABAQUS/Standard User's Manual." Dassaults Systemes.

Barr, P. J., Eberhard, M. O., and Stanton, J. F. (2001). "Live-load distribution factors in prestressed concrete girder bridges." *Journal of Bridge Engineering*, 6(5), 298-306.

Baskar, K., Shanmugam, N. E., and Thevendran, V. (2002). "Finite-element analysis of steel-concrete composite plate girder." *Journal of Structural Engineering*, 128(9), 1158-1168.

Bishara, A. G., Liu, M. C., and El-Ali, N. D. (1993). "Wheel Load Distribution on Simply Supported Skew I-Beam Composite Bridges." *Journal of Structural Engineering*, 119(2), 399-419.

Buckler, J. G., Barton, F. W., Gomez, J. P., Massarelli, P. J., and McKeel, W. T. (2000). "Effect of Girder Spacing on Bridge Deck Response." United States.

Chan, T. H. T., and Chan, J. H. F. (1999). "Use of eccentric beam elements in the analysis of slab-on-girder bridges." *Structural Engineering and Mechanics*, 8(1), 85-102.

Chapman, J. C., and Balakrishnan, S. (1964). "Experiments on composite beams." *Structural Engineer*, 42(11), 369-383.

Charney, F. A., Iyer, H., and Spears, P. W. (2005). "Computation of major axis shear deformations in wide flange steel girders and columns." *Journal of Constructional Steel Research*, 61(11), 1525-58.

Chen, Y. (1995). "Refined and simplified methods of lateral load distribution for bridges with unequally spaced girders: I. Theory." *Computers and Structures*, 55(1), 1-15.

Chen, Y. (1999). "Distribution of vehicular loads on bridge girders by the FEA using ADINA: modeling, simulation, and comparison." *Computers & Structures*, 72(1-3), 127-139.

Chopra, A. K. (2001). *Dynamics of structures : theory and applications to earthquake engineering*, Prentice Hall, Upper Saddle River, NJ :.

Chung, W., and Sotelino, E. D. (2006). "Three-dimensional finite element modeling of composite girder bridges." *Engineering Structures*, 28(1), 63-71.

Cook, R. D., Malkus, D. S., Plesha, M. E., and Witt, R. J. (2001). *Concepts and applications of finite element analysis*, R. D. Cook, translator, Wiley, New York, NY :.

Eamon, C. D., and Nowak, A. S. (2004). "Effect of secondary elements on bridge structural system reliability considering moment capacity." *Structural Safety*, 26(1), 29-47.

Ebeido, T., and Kennedy, J. B. (1996). "Girder moments in simply supported skew composite bridges." *Canadian Journal of Civil Engineering*, 23(4), 904-916.

Eom, J., and Nowak, A. S. (2001). "Live load distribution for steel girder bridges." *Journal of Bridge Engineering*, 6(6), 489-497.

Fahmy, E. H., and Abu-Amra, T. F. (2008). "Longitudinal cracking of concrete slabs in composite beams with ribbed metal deck." *Journal of Constructional Steel Research*, 64(6), 670-9.

Fertis, D. G. (1995). *Mechanical and structural vibrations*, Wiley, New York :.

FHWA. (2009). "Long Term Bridge Performance Program." Federal Highway Administration

Fu, K.-C., and Lu, F. (2003). "Nonlinear finite-element analysis for highway bridge superstructures." *Journal of Bridge Engineering*, 8(3), 173-179.

Gupta, A. K., and Ma, P. S. (1977). "Error in eccentric beam formulation." *International Journal for Numerical Methods in Engineering*, 11(9), 1473-7.

Hays Jr., C., Sessions, L. M., and Berry, A. J. (1986). "Further studies on lateral load distribution using a finite element method." *Transportation Research Record*, 6-14.

Issa, M. A., Yousif, A. A., and Issa, M. A. (2000). "Effect of construction loads and vibrations on new concrete bridge decks." *Journal of Bridge Engineering*, 5(3), 249-258.

Liang, Q. Q., Uy, B., Bradford, M. A., and Ronagh, H. R. (2005). "Strength analysis of steel-concrete composite beams in combined bending and shear." *Journal of Structural Engineering*, 131(10), 1593-1600.

Mabsout, M., Jabakhanji, R., Tarhini, K., and Frederick, G. R. (2000). "Finite element analysis of concrete slab bridges." Stanford, CA, United states, 1045-1050.

Mabsout, M. E., Tarhini, K. M., Frederick, G. R., and Tayar, C. (1997). "Finite-element analysis of steel girder highway bridges." *Journal of Bridge Engineering*, 2(3), 83-87.

Machado, M. A. d. S. (2006). "Alternative acceleration-based serviceability criterion for fiber reinforced polymer deck-on-steel girder bridges," Ph D

Purdue University.

MacHado, M. A. S., Sotelino, E. D., and Liu, J. (2008). "Modeling technique for honeycomb FRP deck bridges via finite elements." *Journal of Structural Engineering*, 134(4), 572-580.

Miller, R. E. (1980). "Reduction of the error in eccentric beam modelling." *International Journal for Numerical Methods in Engineering*, 15(4), 575-82.

Oehlers, D. J., and Johnson, R. P. (1987). "STRENGTH OF STUD SHEAR CONNECTIONS IN COMPOSITE BEAMS." *Structural Engineer, Part B: R&D Quarterly*, 65 B(2), 44-48.

Oehlers, D. J., Seracino, R., and Yeo, M. F. (2000). "Effect of friction on shear connection in composite bridge beams." *Journal of Bridge Engineering*, 5(2), 91-98.

Queiroz, F. D., Vellasco, P. C. G. S., and Nethercot, D. A. (2007). "Finite element modelling of composite beams with full and partial shear connection." *Journal of Constructional Steel Research*, 63(4), 505-21.

Sebastian, W. M., and McConnel, R. E. (2000). "Nonlinear FE analysis of steel-concrete composite structures." *Journal of Structural Engineering*, 126(6), 662-674.

Tabsh, S. W., and Tabatabai, M. (2001). "Live load distribution in girder bridges subject to oversized trucks." *Journal of Bridge Engineering*, 6(1), 9-16.

Tarhini, K. M., and Frederick, G. R. (1992). "Wheel load distribution in I-girder highway bridges." *Journal of Structural Engineering*, 118(5), 1285-1294.

Ugural, A. C. (1999). *Stresses in plates and shells*, WCB/McGraw Hill, Boston :.

Ventura, C. E., Felber, A. J., and Stiemer, S. F. (1996). "Determination of the dynamic characteristics of the Colquitz River Bridge by full-scale testing." *Canadian Journal of Civil Engineering*, 23(2), [d]536-548.

Wolek, A. L., Barton, F. W., Baber, T. T., and McKeel, W. T. (1996). "Dynamic Field Testing of the Route 58 Meherrin River Bridge." United States.

Wu, H. (2003). "Influence of live-load deflections on superstructure performance of slab on steel stringer bridges," West Virginia University, Morgantown, West Virginia.

Appendix A

A.1 Preprocessor

'*preprocessor1.m'* is a MATLAB function used to generate ABAQUS input data file (*.inp) using the keyword capabilities of ABAQUS and series of user inputs. '*preprocessor1.m'* can be used to generate three types of bridge superstructure idealizations Model-1, Model-2, Model-3 as discussed in Chapter 3.

The assumptions made while developing the preprocessor are as follows (Figure A.1)

- Origin (0, 0, 0) of the bridge is assumed to be at the extreme lower left corner of the bridge deck.
- Elements are numbered in order from left to right along x-axis and from bottom to top along y-axis.
- Bridge skew is measured from the positive direction of the x-axis in the counter clockwise direction in the plan view (X-Y plane).
- Different support conditions like pin, roller, frozen or partially frozen are supported by the pre-processor and can be used to model the supports in bridge longitudinal direction. However, the support conditions in the transverse direction for a row of supports is assumed to be same.
- Bracing at the support, if present, is assumed to be at the same skew as the bridge.
- The deck slab thickness is taken to be constant over the entire bridge and the slab reinforcement is neglected in the model.
- Guardrail dimensions and properties are assumed to be constant over the entire length of the bridge.
- In case of staggered bracing the line passing through the start and the end of the bracings in the transverse direction is at the same angle that of the bridge.

- The temperature gradient is assumed to vary linearly between the temperature points defined by the user through the thickness of the slab. Constant temperature is assumed throughout the entire depth of the girders.

- In the static analyses when the truck loading is applied to the bridge, the entire loading is assumed to lie on the bridge deck and point loads are used to model the each tire patch.

- In model-2 and model-3, when each girder component is modeled separately, the top flange is assumed to be at a constant offset from the bridge deck. While in model-1, which models each girder as a beam element, the girders are at a constant offset from the deck slab along the entire length of the bridge.

- In the case of model-1, the girder spacing can be varied. But, for model-2 and model-3 uniform girder spacing is assumed. Assuming uniform girder spacing allows the generation of input data only for a single girder and the "Instance" option from ABAQUS (2007) is used to generate the girders in the transverse direction. This considerably reduces the size of input file.

In order to effectively use the developed preprocessor the user should begin by defining the critical nodes representing position of the supports, bracing along x-axis, and the position of girders and guardrails along y-axis as shown in Figure A.1. The distance between two successive critical nodes and the angle made by line passing through a series of critical node in transverse direction with positive direction of x-axis should also be defined. All transverse nodes generated across the critical node are adjusted as per bridge skew.

In the next step, the user defines the approximate element size along each axis. Using the approximate element size, the number of elements between two successive critical nodes is determined so that no element will be larger than the user-defined approximate element size. To allow for local refinement the user must also define the number of elements between two successive critical nodes along x-axis and y-axis. These numbers are stored in the *elemx1* and *elemy1* vectors. The maximum of number of elements between two consecutive critical points is calculated using the approximate element size and inputted by the user above and are used in the development of the model.

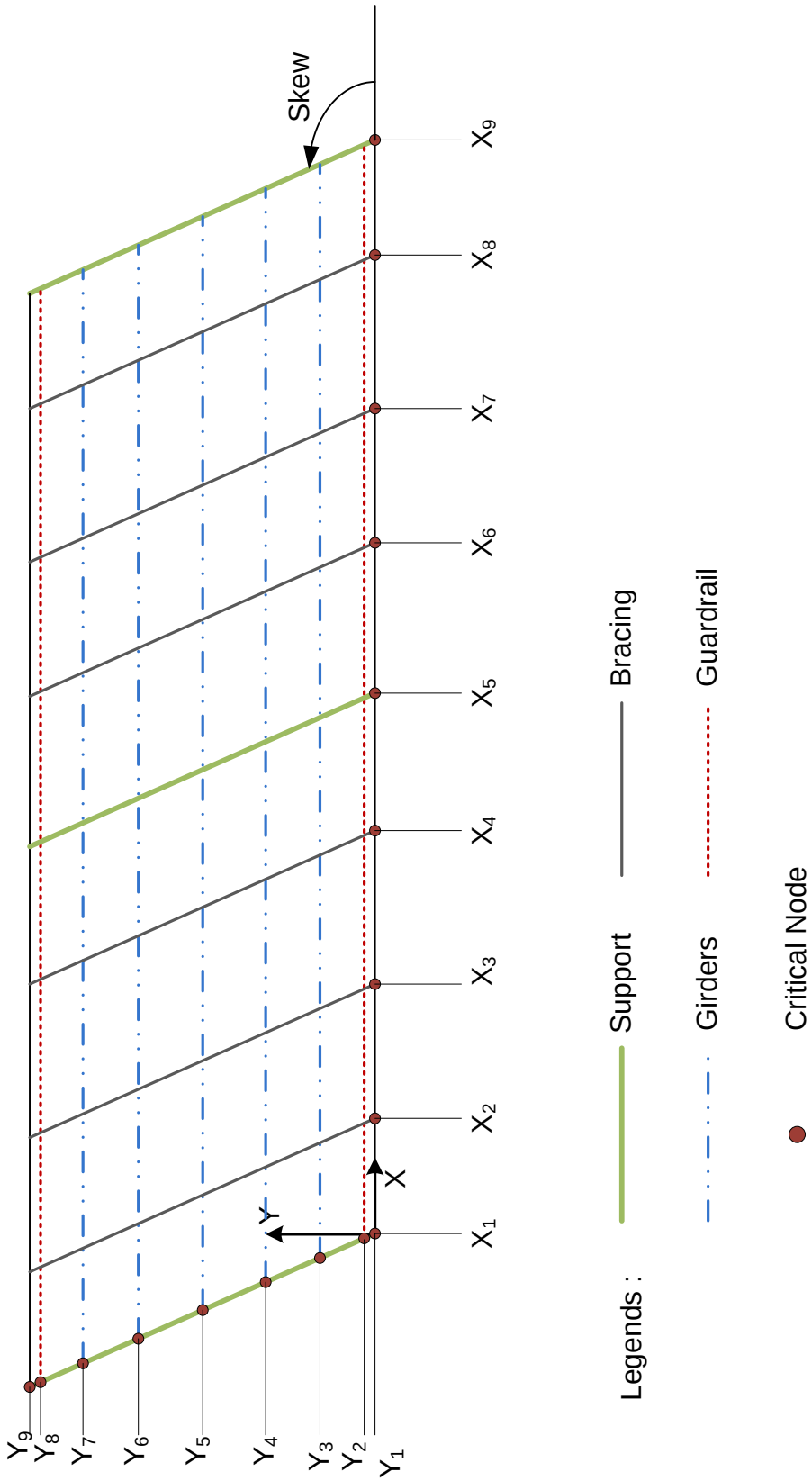

Figure A.1: Bridge Layout

The critical nodes along each axis along with the number of elements between them and the type of elements (linear or quadratic) are used to generate a matrix, referred to as *girder* matrix, which contains the node numbering for all critical nodes of the entire model. This matrix is used later in the generation of all bridge elements as explained below.

A.1.1 Deck

To model the deck with or without skew the *girder* matrix generated previously is used. Two consecutive rows and columns in the *girder* matrix represent a quadrilateral on the bridge deck. The node numbers in two consecutive rows and columns were used to write element data to *shell.inp* file. The thermal gradient is applied by defining initial temperature at temperature points across the deck thickness using the initial condition option in ABAQUS(2007).

A.1.2 Girder

Using the *girder* matrix, appropriate columns containing nodes for the bridge girders are filtered out. These nodes are then used to generate beam elements to model girders at an offset equal to the distance between centroid of the deck and centroid of the girder for model-1. In the case of model-2, these nodes are copied three times to model the top flange, web and the bottom flange and rigid links are used to connect the girder parts. For model-1 and model-2, the change in girder cross-section along the length is incorporated by shifting the centroid of the girder section in the case of predefined I section in ABAQUS (2007) or modifying the moment of inertia using parallel axis theorem in case of general beam section in ABAQUS (2007).

For model-3, similarly to the generation of the deck mesh, the number of elements in the girder flanges and web are calculated using the approximate element size inputted by the user. The number of elements calculated along with the nodes filtered from girder matrix is used to generate girder input data. To allow for the smooth transition between girder sections with varying depths, additional critical nodes are added as shown in Figure A.2. The same approach is used for the flange width transition.

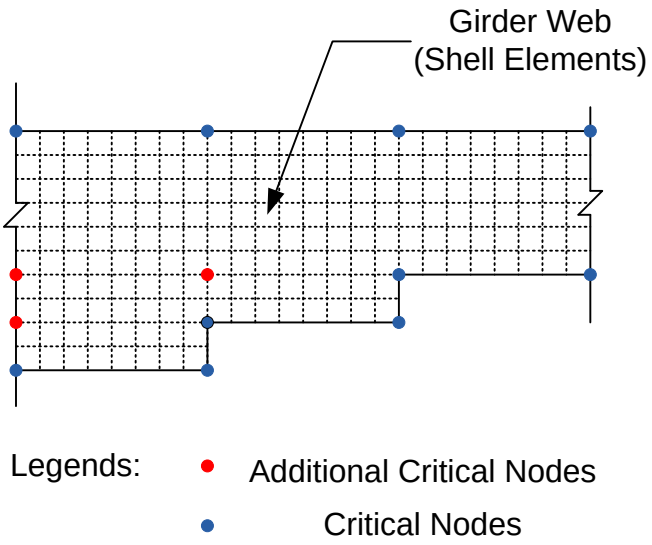

Figure A.2: Varying Girder Cross Section

A.1.3 Guardrail

'*preprocessor1.m'* supports three different ways of modeling the guardrails, namely:

1. Fully composite guardrail with bridge deck.
2. Partially composite guardrail with bridge deck.
3. Guardrail modeled as a non-structural mass per unit area.

From the girder matrix, appropriate columns containing nodes for the guardrails are filtered out and are used to generate beam elements to model guardrails at an offset equal to the distance between mid-surface of the deck and centroid of the guardrail. When the guardrail is modeled as a non structural mass then the elements in the area of the deck that would be occupied by the guardrail are filtered out and the non structural mass option in ABAQUS(2007) is used so that these elements have mass, but no structural stiffness.

A.1.4 Bracing

'*preprocessor1.m'* supports three different ways of modeling the bracing scenarios, e.g:

1. Both non-skewed and skewed bracing for non-skewed and skewed bridges, respectively, using a single beam element representing the entire bracing assembly as discussed previously in 3.2.3.1
2. Both non-skewed and skewed bracing for non-skewed and skewed bridges, respectively, with each part of the bracing assembly modeled using single linear beam element as discussed in 3.2.3.1

3. Skewed bracing at the supports with staggered intermediate bracing for skewed bridge with a single beam line representing the entire bracing assembly as shown in Figure A.3

In case of staggered bracing, each row of the transverse bracing is assumed to be at the same distance from the skewed edge of the bridge. Therefore, each brace row is confined within two parallel lines at the same angle as that of the skew. Therefore, the user needs to define two critical nodes for each row of the staggered bracing as shown in Figure A.3. To model non-skewed or skewed brace in model-1and model-3, the same numbers of elements used to model the deck are used to model the bracing, while a single linear beam element is used to model the staggered bracing in model-1 and model-3. The developed functions can be easily modified to increase the number of beam elements used to model a staggered bracing. This would be necessary if an external member load where to be applied directly on the bracing, which will hardly ever happen. Rigid links are used to connect the bracing to the girder. If the connection properties are available then springs can be used to model the connection.

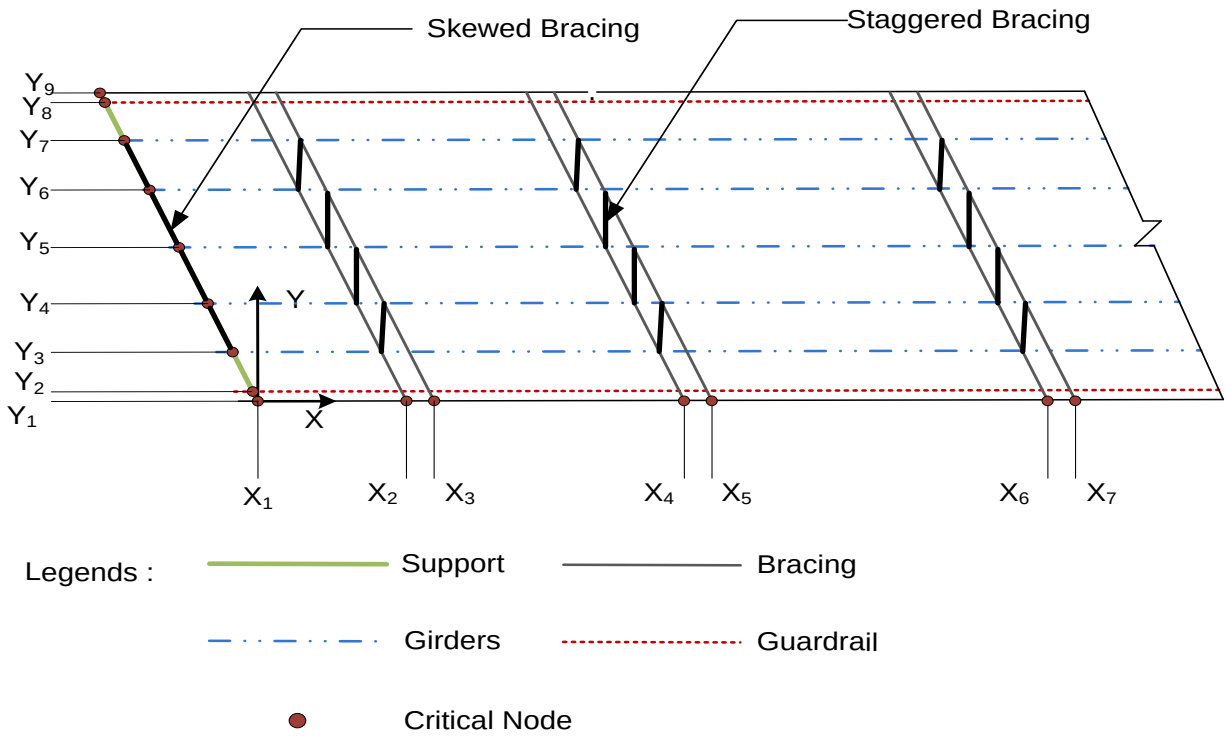

Figure A.3: Staggered Bracing Layout

A.1.5 Constraints

Rigid links are used to model full composite action between the bridge components. To model partial composite action between the girders and bridge deck, six nonlinear spring elements are used. The supports are modeled at the bottom of the girders using zero dimensional elements. Partial fixity at the supports is incorporated using linear springs.

A.1.6 Loading

Truck loading is applied by series of point loads each representing a tire patch. First the region in which truck loading is applied is located and the distance of each point load from the nodes present in that region is calculated. The point load is applied at the closest nodes. (Figure A.4)

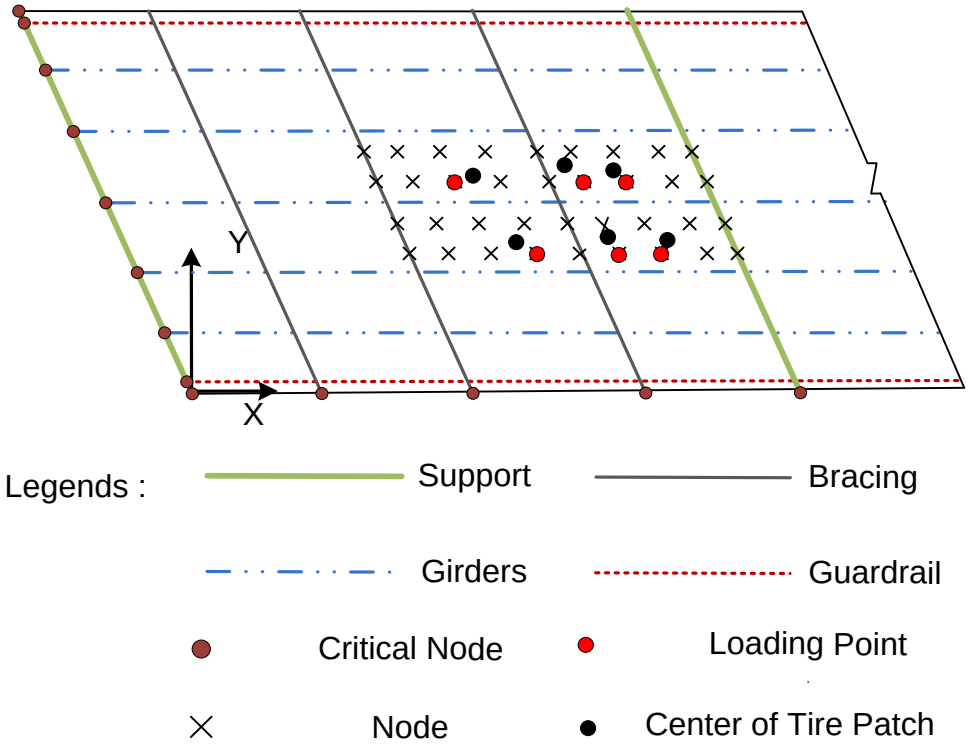

Figure A.4: Truck Loading on Bridge Deck

To simulate the quasi-static live load test, the truck loading is applied in different independent steps equal to number of steps specified by the user. The truck positions for each loading scenario are calculated by diving the total length of the bridge into number segments equal to number of steps. The first and the last positions of the truck for any loading scenario are fixed at

the start and the end of the bridge. To move the truck loading in the transverse direction is done manually by inputting the position of truck in transverse direction.

A.1.7 Input File Generation

All bridge elements, such as deck, girder, bracing, guardrails are written into separate input data files and are referenced in the main input data file (bridge.inp) which makes it easier to debug. All the output requests like displacements and stresses along the length of the girder and support rotations are written into the main input file. After running the analysis all the requested outputs are written to the output database file (bridge.dat) which is used later to post-process the results.

A.1.8 List of Functions

Some of the important functions that are called during the generation of the input files are described next.

a. preprocessor1.m

This is the main function that is called during generation of the input file for ABAQUS, which is called 'bridge.inp' file. This function calls the other functions, which generate input for different parts of the bridge superstructure and selects the analysis parameters depending on the type of analysis selected.

b. nodegenX2.m

This sub-function generates the nodes for the different parts of the bridge superstructure and writes them to the corresponding input file. The NGEN keyword in ABAQUS(2007) is used to generate the intermediate nodes between two successive critical nodes by dividing the distance between them by a number of elements between them.

c. shellgen.m

This function generates the input for the generation of the mesh of the bridge deck. In particular, it specifies the type of shell element to be used, i.e., linear or quadratic shell elements with full or reduced integration, and writes this data to 'shell.inp' file. It begins by defining single element and then it uses the ELGEN keyword from ABAQUS(2007) to generate the remaining elements incrementally.

d. girdergen.m

This sub-function generates the necessary input syntax for the use of linear or quadratic beam elements to model the girders. For the eccentric beam model, it writes this data to 'girder.inp'. For the "three–beam" model, it writes the data to three files: 'girder_top_flange.inp', 'girder_web.inp', and 'girder_bottom_flange.inp'. As done in the functions previously discussed, the ELGEN keyword is used for the generation of the beam elements.

e. girdershellgen.m

This sub-function is used to generate the mesh for the girders, when shell elements are used to model the web and flanges. It define whether linear or quadratic shell elements and writes this data to 'girder.inp' file.

f. guardrailgen.m

This sub-function is similar to *girdergen.m*, but for the guardrails. It writes the generated data to the file 'guardrail.inp'. Once again, the ELGEN keyword is used to generate beam elements that are used to simulate the guardrails.

g. bracinggen2.m

This sub-function generates input for non-staggered bracing, which can be modeled with either linear or quadratic beam elements. Then it writes this data to 'bracing.inp' file. As before, the ELGEN keyword is used to generate the beam elements that represent the bracing components.

h. bracinggen_s.m

This sub-function is similar to *girdergen.m*, but it generates input for staggered. In this case the data is written to 'bracing.inp' file.

i. multipoint2.m

This sub-function generates rigid beam elements or spring elements to model the composite action between different parts of the bridge superstructure. This sub-function writes the input to the 'bridge.inp' file.

j. loading.m

This sub-function generates a matrix that contains information required for the application of the truck loading for static analysis that mimics a live-load field test. This sub-function writes the input to 'bridge.inp' file.

k. generate_history.m

This sub-function generates the necessary data for instructing ABAQUS the appropriate analysis type it should use. Depending upon the type of analysis selected by the user, this function writes the necessary data to the 'bridge.inp' file. This function is capable of generating input data required for both static analysis and free vibration analysis.

A.2 Postprocessor

After the input file is generated by *'preprocessor1.m'* and submitted to ABAQUS (2007) , the output results specified by the user are written to the output database (bridge.dat) file. This file is read line by line using Matlab to generate several plots including, envelopes for girder displacements, support rotations and stresses at the bottom flange of the girders. Some of the main functions used for the postprocessing task are described next.

a. plot12.m

'plot12.m' is the main file that calls all other Matlab functions. This file calls the functions discussed below multiple times to generate envelopes of the various quantities for the entire bridge.

b. global_local.m

When ABAQUS (2007) runs the job it assigns different node numbering to all the nodes and outputs both the modified and original node numbering to the output database file. This node numbering is read using the function *'global_local.m'* and stored into a matrix called *'GL matrix'* . This matrix is used later to map the location of each node.

c. disp_envelope.m

This function extracts the displacements for all the nodes at the bottom of the girder for each load step and filters out the maximum upward and downward displacements for all the nodes. These values are the stored in a matrix called *'dispenv matrix'*.

d. support_rotation.m

This function works similar to *'disp_envelope.m'*, but it extracts support rotations at the girder mid height for each load step and filters out the maximum and minimum values. These values are then stored it in a matrix referred to as *'rotenv matrix'*.

e. getstress.m

This function extracts the stress values at the centroid of the bottom flange of the girder where it is connected to the girder web. ABAQUS evaluates stresses across the thickness of the shell and reports them at the integration points. Only the top and bottom points are extracted here for each step and maximum tensile and compression stresses are stored in the matrix *'S_env matrix'*.

f. displacement_allgirder

This function filters out the maximum and minimum vertical displacement for the entire bridge from the response obtained for each girder. The following plot illustrates a sample displacement envelope obtained using this function.

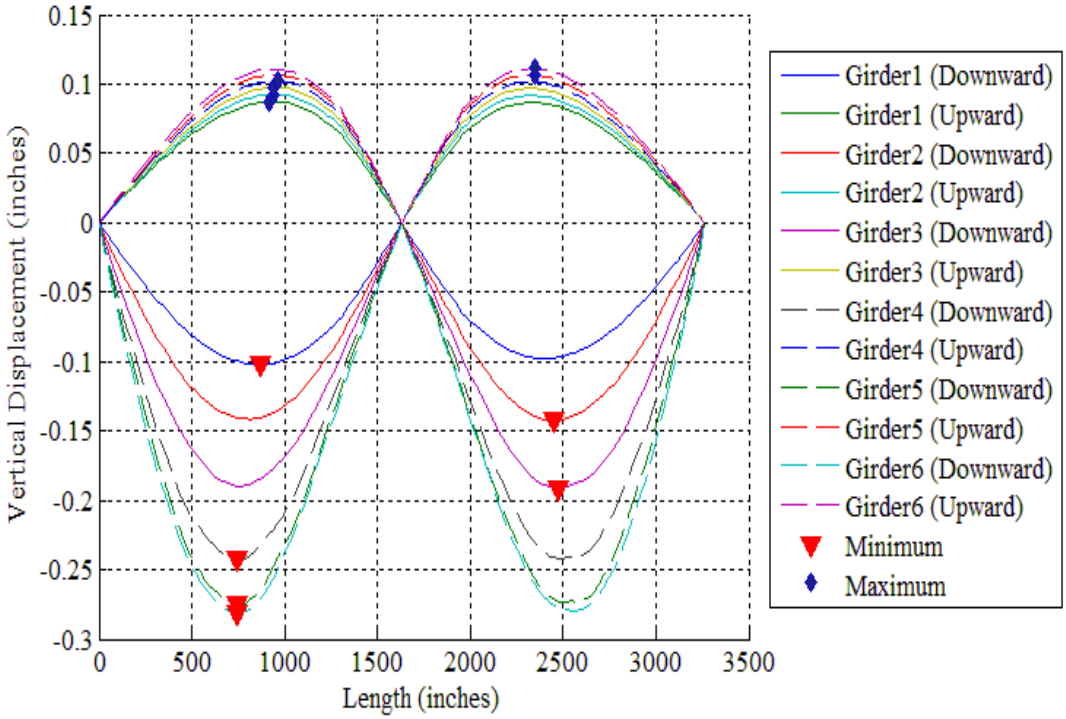

Figure A.5: Girder Displacement Envelopes

A.3 User Inputs

Following is the list of user inputs required for preprocessor and postprocessor.

x	Column vector containing distance between two successive critical nodes along x-axis.
y	Column vector containing distance between two successive critical nodes along y-axis.
angle	Column vector containing the angle made between the line passing through series of critical nodes in transverse direction with the positive direction of x-axis measured in the counter clockwise direction.
staggered	Flag that is set to ‘yes’ or ‘no’, depending upon whether bracing is staggered or not.
staggered_data	Column vector that for each critical node along x-axis contains the entry 1 for staggered bracing, 0 for non-staggered bracing, and 2 for bracing at the same angle as that of the bridge skew.
gap	Column vector containing a 1 to indicate the presence of a gap between two successive critical nodes along x-axis and a 0 for the absence of such a gap.
esizex	Approximate element size along x-axis.
esizey	Approximate element size along y-axis.
esizez	Approximate element size in the web along the z-axis.
esize_top_flange	Approximate element size in the top flange along the y-axis.
esize_bottom_flange	Approximate element size in the bottom flange along the y-axis.

elem_x1	Column vector containing the number of elements between two successive critical nodes along x-axis.
elem_y1	Column vector containing the number of elements between two successive critical nodes along y-axis.
elem_type	Shell element used to model the reinforced concrete bridge deck (S4, S4R, S4R5, S8R, S8R5).
elem_type1	Beam or shell element used to model the girders (B31, B32, S4, S4R, S4R5, S8R, S8R5).
girder_modeling	Set to‘1’ when beam elements are used to model the entire girder (model-1).
	Set to ‘2’ when shell elements are used to model the girder flanges and web (model-2).
	Set to ‘3’ when beam elements are used to model the top, bottom flange and girder web separately (model-3).
spring_or_rigid	Set to ‘spring’ to model partial composite action between the girder top flange and deck slab (model-2 and model-3).
	Set to ‘rigid’ to model full composite action between the girder top flange and deck slab (model-2 and model-3).
springtype	Set to ‘linear’ or ‘nonlinear’ depending upon whether the shear studs are modeled using linear or nonlinear springs.
elem_type11	Beam element used to model the bracing
	For staggered bracing – Linear beam element (B31).
	For non-staggered bracing – Linear and Quadratic beam elements (B31/B32).

springK	Column vector containing shear connector stiffness for all six degrees of freedom starting with three displacements and then three rotations.
elem_type2	Beam element used to model the guardrail (B31/B32).
angle1	Skew angle measured from the positive direction of x-axis in counter clockwise direction (plan view).
partialcomposite	'yes' or 'no' flag to input whether guardrail is fully or partially composite with the bridge deck, respectively.
pcomposite	Column vector containing the position of connector element relative to the previous connector element. This is used to model partial composite action between guardrail and deck.
sg	Distance between the mid-surface of the bridge deck and the centroid of the girder for model-1(eccentric beam model). If the girder cross-section varies along the length, the girder is still modeled at the same level, but its moment of inertia is modified to account for that.
sb	Distance between the mid-surface of the bridge deck and the centroid of bracing.
ss	Column vector containing distance between the centroid of bridge deck and the supports.
sgr	Distance between the centroid of bridge deck and the centroid of the guardrail.
stf	Distance between the deck mid-surface and the bottom of the top flange for model-2 and model-3.
sr	Column vector containing row numbers extracted from the *x* vector along with their corresponding boundary conditions.

sr2	Column vector containing boundary conditions like pin, roller ,fix for the each row corresponding to the *sr* matrix.
spring_support	Matrix containing the input required to model partial fixity at any of the supports defined in the *sr* matrix. 1st column = support row number from the *sr* matrix. 2nd column = Degree of freedom constrained using a spring element. 3rd column = Spring stiffness. User needs to enter '0' in the first row and first column element if no partial constraints are applied at any of the bridge supports.
bracing_startend	Column vector containing the row numbers extracted from the *x* vector where bracing is present.
savename	Main input data file that makes reference to the other input data files.
savename1	Input data file that stores the data required in the generation of the bridge deck mesh.
savename2	Input data file that stores the data required in the generation of of bridge girders mesh.
savename3	Input data file that stores the data required in the generation of the bracing mesh. It is set to 'bracing' or 'zero' depending upon whether bracing is considered in the model.
savename4	Input data file that stores the data required in the generation of the guardrail mesh. It is set to 'guardrail' or 'zero' depending upon whether guardrail is considered in the model.

savename5	Input data file that stores the data required to run different types of analysis.
guardrail_mass	Set to ‘yes’ if the guardrail is modeled as a nonstructural mass.
	Set to ‘no’ if the guardrail is not considered in the model.
gmass	Guardrail mass acting per unit area.
mat1	Column vector containing different materials used in the model.
mat2	Column vector containing material properties for each material in *mat1*.
girderX	Column vector containing girder section variation in the longitudinal direction.
gsectiontype	Matrix containing girder section types used in the model for model-1,.
gsection	Girder section properties for the girder sections in ‘*gsectiontype’* matrix.
	It should be set to ‘99999’ in the first column when the girder is modeled using model-2. The second column is set to the section number corresponding to *Ibreak* matrix (see below).
Ibreak	Matrix containing data required to model top flange, web and bottom flange separately for model-2,.
Icg	Column vector containing distance between the centroid of bridge deck and centroid of girder parts starting with top flange, web and then bottom flange for three beam model.
bracingX	Column vector containing the bracing section variation in the longitudinal direction.
bsectiontype	Matrix containing bracing sections used in model-1.
bsection	Section properties for the bracing sections in ‘*bsectiontype’* matrix.

bracingXtype	Bracing data matrix 1st column = Type of bracing (e.g., Kbracing, Inverted Kbracing, and X bracing). 2nd column = Row number corresponding to the bracing details in the bracing data matrix for each type of bracing. 3rd column = Distance measured from the top of web to the top most point on the bracing assembly 4th column = Distance measured from the top of web to the bottom most point on the bracing assembly.
guardrail_sectiontype	Matrix containing a list of guardrail sections used in the model.
guardrailX	Column vector containing guardrail section variation in the longitudinal direction. 1st column = Section number from the *guardrail_sectiontype* matrix 2nd column = Material number from the *mat1* matrix.
guardrail_section	Guardrail section properties corresponding to each section in the *guardrail_sectiontype* matrix
initialtemp	Set to 'yes' if the effect of initial temperature is considered. Set to 'no' if the effect of initial temperature is not considered.
temppoints	Number of temperature points across the thickness of bridge deck at which the temperature is defined.
decktemp	Column vector containing temperature at *tmppoints*.
girdertemp	Uniform temperature assumed throughout the girder section.

analysis_type Set to ‘static’ for static analysis.

Set to ‘hz’ for free vibration analysis.

no_step Number of load steps in which the live load is applied along the bridge length.

truck_location Location of the centroid of the left most tire patch for each truck.

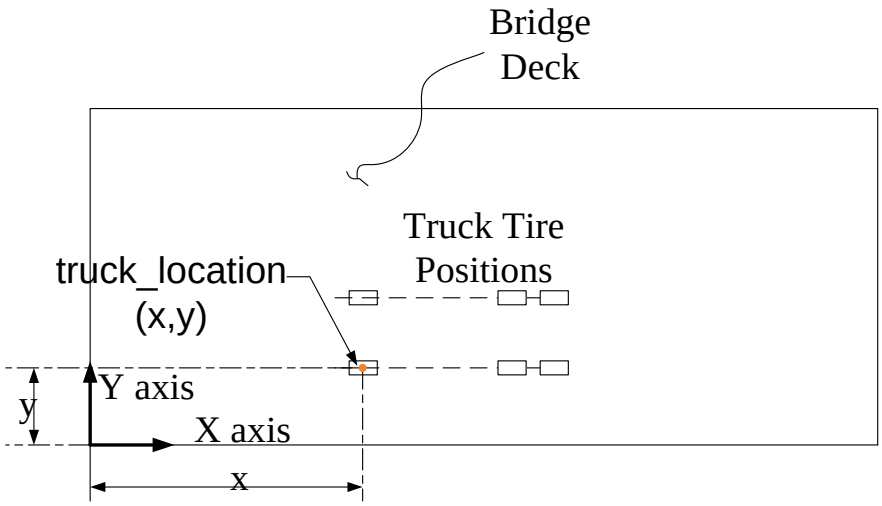

truck_def Truck loading definition.

1st column = Tire patch number.

2nd column = Magnitude of the load applied by each tire patch in the direction of z-axis.

3rd column = x co-ordinate of the centroid of the tire patch.

4th column = y co-ordinate of the centroid of the tire patch.